# Rate and Power Adaptation Techniques for Wireless Communication Systems

Thesis submitted to the University of Cardiff in candidature for the degree of Doctor of Philosophy

Lay Teen Ong

Centre of Digital Signal Processing

Cardiff University

2007

UMI Number: U584941

All rights reserved

INFORMATION TO ALL USERS
The quality of this reproduction is dependent upon the quality of the copy submitted.

In the unlikely event that the author did not send a complete manuscript
and there are missing pages, these will be noted. Also, if material had to be removed,
a note will indicate the deletion.


UMI U584941
Published by ProQuest LLC 2013. Copyright in the Dissertation held by the Author.
Microform Edition © ProQuest LLC.
All rights reserved. This work is protected against
unauthorized copying under Title 17, United States Code.


ProQuest LLC
789 East Eisenhower Parkway
P.O. Box 1346
Ann Arbor, MI 48106-1346

# Abstract

Attaining the most spectrally efficient form of data transmission over a time-varying channel remains as fundamentally important target in wireless systems. Link adaptation (LA) is a promising approach to increase spectral efficiency. In general, the transmitter adjusts its parameter such as rate, power and coding in accordance with the channel state information (CSI) fed back from the receiver. Consequently, the accuracy of the CSI is prevalent in LA design. In this thesis, an investigation of the performance of a variable rate variable power (VRVP) multi-level quadrature amplitude modulation (MQAM) scheme is performed for a single antenna system. Then, a novel VRVP-MQAM system is proposed that employs a rate and power adaptation algorithm based on the statistical characterization of CSI imperfection. Instead of using the conventional signal-to-noise ratio (SNR) estimate as a CSI parameter, the proposed system is based on both an SNR estimate and a bit error rate (BER) estimate, as BER is a more direct representation for quality of service (QoS) of a communication system. The proposed rate and power adaptation algorithm is then generalized to incorporate a pilot symbol assisted modulation (PSAM) based channel predictor. The BER and SNR estimates are then employed within a code division multiple access (CDMA) based rate and power adaptation system. Finally, the performances of the proposed systems are shown to achieve higher spectral efficiency when compared to

the alternative systems derived based on conventional approach.

Another requirement in today's wireless digital communication systems is to provide services for integrated voice and data traffic. The QoS requirement for voice and data can be application specific. For example, real-time traffic is delay-constrained, whereas non-real time traffic has a relaxed requirement on delay but may be capacity-constrained. With this motivation, a rate and power adaptation technique is proposed for a multiple-input multiple-output (MIMO) based integrated voice and data service. On the basis of analytical and simulation results, the performance of the proposed scheme is assessed for a Rayleigh fading environment. Finally, the results demonstrated that the MIMO based system is suitable for integrate voice and data traffic with different requirements and specification.

# Acknowledgements

I would like to thank my supervisors Dr. Sangarapillai Lambotharan and Professor Jonathon A. Chambers at Cardiff University, and Dr. Mohammad Shikh-Bahaei at King's College London. Without their continuous support and guidance, I would not have completed my thesis.

I also wish to thank all my friends at King's College London and Cardiff University. Their presence has brightened up the research environments. A special thank also goes to Ms Theresa Burnette of King's College London. Her professional advice has made my journey so much easier.

Finally, I want to send my most heartfelt gratitude to my family. My husband, Yew Fei Tang, for his endless love, support, trust,..., a list without bound that is impossible to complete here. I also thank my parents Sem Yam and See An, for their understanding and bravery. This thesis is dedicated to them.

# Contents

# List of Figures

# List of Tables

# List of Abbreviations

| | |
|---|---|
| **ACM** | Adaptive coded modulation |
| **ASE** | Average spectral efficiency |
| **AST** | Adaptive SNR target |
| **AWGN** | Additive white Gaussian noise |
| **BPSK** | Binary phase shift keying |
| **BER** | Bit error rate |
| **BERT** | Bit error rate target |
| **bps/Hz** | Bits per second per Hertz |
| **CDF** | Cumulative distribution function |
| **CDMA** | Code division multiple access |
| **CSI** | Channel state information |
| **FST** | Fixed SNR target |
| **LA** | Link adaptation |
| **LOS** | Line-of-sight |
| **LSVV** | Largest singular value for voice |
| **MAC** | Media access control |
| **MAP** | Maximum a posteriori |
| **max** | Maximum |

| | |
|---|---|
| **min** | Minimum |
| **MIMO** | Multiple-input multiple-output |
| **ML** | Maximum-likelihood |
| **MMSE** | Minimum mean-square error |
| **MQAM** | Multi-level quadrature amplitude modulation |
| **MPSK** | Multi-level phase shift keying |
| **OFDM** | Orthogonal frequency-division multiplexing |
| **PDF** | Probability density function |
| **PSAM** | Pilot symbol assisted modulation |
| **QAM** | Quadrature amplitude modulation |
| **QoS** | Quality of Service |
| **RRM** | Radio resource management |
| **RV** | Random variable |
| **SIMO** | Single-input multiple-output |
| **SISO** | Single-input single-output |
| **SNR** | Signal-to-noise ratio |
| **SVD** | Singular value decomposition |
| **SSVV** | Smallest singular value for voice |
| **USVV** | Unordered singular value for voice |
| **VRVP** | Variable rate variable power |
| **W-CDMA** | Wideband CDMA |
| **ZMCSCG** | Zero-mean circularly symmetric complex Gaussian |

# Mathematical Notation and Symbols

The following symbols and notations are used commonly throughout the thesis.

Vectors are usually written in bold lowercase letters (e.g. $\mathbf{x}$), whereas matrices are written in bold uppercase letters (e.g. $\mathbf{X}$).

It is noted that the conventional way to represent random variables (RVs) from the corresponding realization is by using uppercase letters for RVs and lowercase for the corresponding realization. However, due to the constant use of Greek letters in this thesis, the conventional approach would result in complication in the expressions. To avoid this difficulty, the same Greek letter is used to represent a random variable and its realization, but the difference should be evident in the context.

| | |
|---|---|
| $(.)^*$ | Complex conjugate |
| $\approx$ | Approximately equal to |
| $(.)!$ | Factorial |
| $\mathbb{Z}$ | The set of integers {...,-2,-1,0,1,2,...} |
| $\mathbb{Z}^+$ | The set of positive integers {1,2,...} |
| $\min\{x_1, ..., x_m\}$ | Minimum of $x_1, ..., x_m$ |

| | |
|---|---|
| $\max\{x_1, ..., x_m\}$ | Maximum of $x_1, ..., x_m$ |
| $\|x\|$ | Magnitude of the scalar $x$ |
| $\|\mathbf{x}\|$ | Euclidean norm of a vector with complex elements, $\sqrt{\mathbf{x}^{\mathrm{H}}\mathbf{x}}$ |
| $\|\mathbf{X}\|$ | Determinant of matrix $\mathbf{X}$ |
| $\mathrm{Re}\{z\}$ | The real part of the complex argument $z = x + jy$ |
| $E[.]$ | Statistical expectation |
| $f_x(x)$ | PDF of the random variable X |
| $\mathbf{x}^{\mathrm{H}}, \mathbf{X}^{\mathrm{H}}$ | Hermitian transpose of vector $\mathbf{x}$ and matrix $\mathbf{X}$ |
| $\mathbf{x}^{\mathrm{T}}, \mathbf{X}^{\mathrm{T}}$ | Transpose of vector $\mathbf{x}$ and matrix $\mathbf{X}$ |
| $\mathbf{I}_m$ | Identity matrix of dimensions $m \times m$ |
| $\mathrm{Cov}(.,.)$ | Covariance |
| $\mathrm{Var}(.)$ | Variance |
| $f_d$ | Maximum Doppler frequency in Hz |
| $v_t$ | Vehicular speed in meters/second (m/s) |
| $f$ | Carrier frequency in Hz |
| $c$ | Speed of light ($3 \times 10^8$ m/s) |
| $i, t$ | Time index |
| $j$ | $\sqrt{-1}$, in the context of Chapter 2 |
| $I$ | $\sqrt{-1}$, in the context of Chapters 4 and 6 |
| $j$ | Symbol instant, in the context of Chapters 4 and 6 |
| $L$ | PSAM period in symbol length, in the context of Chapters 4 and 6 |
| $L$ | Number of subchannels of a MIMO channel, in the context of Chapter 8 |
| $\gamma(.)$ | Instantaneous received SNR |

| | |
|---|---|
| $\mu$ | Lagrangian multiplier |
| $\hat{\gamma}(.)$ | Instantaneous received SNR estimate |
| $\breve{\gamma}(.)$ | Instantaneous received SNR estimate based on prediction method |
| $N_o$ | Noise power spectral density in watts/Hz (W/Hz) |
| $B$ | Signal Bandwidth |
| $\bar{S}$ | Average transmit signal power |
| $K_o$ | Length of channel predictor |
| $\int_x g(x)\, dx$ | The integral of a function $g(x)$ of a variable $x$, and the range of $x$, unless otherwise specified, is from zero to infinity |

The symbols $\Gamma$ and $\sigma$ have been conventionally used for several definitions. In order to adhere to the conventional approach, but to avoid confusion, subscripts are used to differentiate these notations:

| | |
|---|---|
| $\sigma_\tau$ | root mean square (rms) delay |
| $\sigma_n^2$ | noise variance |
| $\sigma_{\hat{p}_B}^2$ | variance of BER estimate ($\hat{p}_B$) |
| $\sigma_{\text{CI}}$ | SNR target for total channel inversion (CI) type power control |
| $\sigma_{\text{TCI}}$ | SNR target for truncated channel inversion (TCI) type power control |
| $\sigma(.)$ | Adaptive SNR target |
| $\Gamma$ | Average received SNR, where $\Gamma \triangleq E[\gamma(i)]$ |
| $\hat{\Gamma}$ | Average received SNR estimate, where $\hat{\Gamma} \triangleq E[\hat{\gamma}(i)]$ |
| $\breve{\Gamma}$ | Average received SNR estimate based on prediction method, where $\breve{\Gamma} \triangleq E[\breve{\gamma}(i)]$ |
| $\Gamma(.)$ | Gamma function |

| | |
|---|---|
| $\Gamma_L(.)$ | Lower incomplete Gamma function |
| $\Gamma_U(.)$ | Upper incomplete Gamma function |

# Statement of Originality

Chapters 5 to 8 of this thesis contain the work which to the author's best knowledge is original except where referenced and stated. The novelty of the thesis stems from the following contributions:

**Chapter 5: VRVP-MQAM System under Imperfect CSI Knowledge**

- Derivation of the rate and power adaptation algorithms based on SNR and BER estimates for a VRVP-MQAM system.
- Derivation of a Bayesian BER estimator based on the proposed SNR-estimate and BER-estimate VRVP-MQAM system.

**Chapter 6: VRVP-MQAM System with PSAM-Based Channel Prediction**

- Extension of the Bayesian estimation based VRVP-MQAM system proposed in Chapter 5 to incorporate a MAP-optimal channel predictor and a discrete MQAM scheme.

**Chapter 7: VRVP-MQAM System with Adaptive SNR Target**

- Derivation of the rate and power adaptation algorithm for a joint SNR target and rate adaptation MQAM system.
- Derivation of an ML BER estimator based on the proposed scheme.

**Chapter 8: MIMO Based VRVP-MQAM System**

- The rate and power adaptation algorithms for integrated voice and data services in a MIMO system.
- Derivation of the statistical functions for the related eigenvalues in the above proposed scheme.

and the associated simulation studies in each chapter.

# Publications

The originality of this thesis is partially supported by the following publications:

### Journal Papers

1) L.T. Ong, and S. Lambotharan, "Adaptive rate and power allocation for integrated voice and data services in MIMO systems" submitted to *IEEE Transactions on Communications,* Feb. 2007.

2) L.T. Ong, M. Shikh-Bahaei, and J.A. Chambers, "Variable rate and variable power MQAM system based on Bayesian Bit Error Rate and channel estimation techniques," accepted for publication in *IEEE Transactions on Communications,* Sep. 2006.

### Conference Papers

1) L.T. Ong, and S. Lambotharan, "On rate and power allocation for MIMO based integrated voice and data transmission," accepted for *IEEE Vehicular Technology Conference,* VTC2007, Baltimore Oct. 2007.

2) L.T. Ong, and S. Lambotharan, "Variable rate variable power MIMO system for integrated voice and data services," *IEEE Int. Conference on Communications Systems,* ICCS, Singapore, Oct. 2006.

3) L.T. Ong, S. Lambotharan, J.A. Chambers, and M. Shikh-Bahaei, "Perfor-

mance of Bayesian Estimation based Variable Rate Variable Power MQAM System," *IEEE Int. Symp. on Personal, Indoor and Mobile Radio Communications,* PIMRC2006, Finland, Sep. 2006.

4) L.T. Ong, M. Shikh-Bahaei, S. Lambotharan, and J.A. Chambers, "Performance of Variable Rate Variable Power MQAM System Based on Bit Error Rate and Channel Estimates," *Int. Conference on Communications, Circuits and Systems,* ICCCAS 2006, China, Jun. 2006.

5) L.T. Ong, A. Olfat, and M. Shikh-Bahaei, "Joint SNR target and rate adaptation based on bit error rate estimation," *IEEE Int. Symp. Wireless Communication System,* Italy, pp. 470-474, Sep. 2005.

# Chapter 1

# Introduction

Demand for robust and spectrally efficient communication over time-varying fading channels for high-speed digital wireless data transmission has motivated a great deal of research interest, see [1] and the references therein. Among the numerous works, link adaptation (LA) is one of the promising solutions to increase spectral efficiency in a wireless system [1–7]. In general, LA techniques adapt transmission parameters such as modulation, coding level, and signal power with the channel variation. LA techniques use channel state information (CSI) feedback from the receiver to dynamically adapt appropriate transmitter parameters over the fading channel. In [2] the capacity of a single-user channel is examined when optimal and suboptimal rate and power adaptation are used over a flat-fading channel. In [3], the work in [2] has been extended to the capacity of Rayleigh fading channels under different adaptive transmission and diversity-combining techniques. The work in [4,5] examined the rate and power adaptation for maximum spectral efficiency within a multi-level quadrature amplitude modulation (MQAM) scheme. Also, [4] extends the analysis to include a multi-level phase shift keying (MPSK) scheme. In [4] and [5] maximum spectral efficiency is achieved subject to an average power constraint and a bit error rate (BER)

requirement.

An important premise that detracts from the practical performance of such adaptive techniques is the availability of accurate CSI. In a practical situation, the transmitter and the receiver rarely have the ability to measure or estimate perfectly the channel state. Imperfect CSI such as inaccurate channel estimates at the receiver and the delay in the feedback of CSI to the transmitter may degrade the performance of a wireless system. Several papers have addressed these issues, [4, 6, 7] and [8–10]. In [4], a variable rate and variable power MQAM (VRVP-MQAM) system is proposed with optimal solutions derived assuming an ideal CSI scenario. The effect of channel estimation error and delay on the BER performance of the VRVP-MQAM system is also analyzed in [4]. The effect of imperfect channel estimation on a VRVP-MQAM system is studied in [6] through a new set of system formulas embedding imperfect channel estimates and feedback delay parameters. An instantaneous signal-to-noise ratio (SNR) estimate obtained at the receiver based on the minimum mean-square error (MMSE) criterion was considered. Most works, such as [4,6], have employed rate and power adaptation algorithms assuming perfect knowledge of the channel fading values after which the effect of channel imperfections on the performance of the adaptive system is characterized. These adaptive designs based on perfect CSI assumption are known to work well only for a small CSI estimation error and a limited feedback delay [4,6]. Alternatively, the use of channel prediction has been shown to relax the constraint on delay and estimation error [7–10]. In these work, optimum rate and power algorithms are derived based on the predicted SNR and the statistical properties of the channel predictor. Most of the adaptive designs consider SNR as a system performance indicator. However, SNR measurements may not be a direct measure of quality for a mobile system with time-varying channel characteristics due to fading. Therefore a power adaptation scheme based

on BER, which is considered to be a more direct representation of the measure of quality was proposed in [11] and [12]. Outer-loop power control based upon BER or FER (frame erasure rate) in wideband-code division multiple access (W-CDMA) systems is a practical example of this kind of power adaptation [13]. Joint optimization of BER-based adaptive modulation and outer loop SNR target was considered in [14,15]. Besides BER based power adaptation, an adaptive coding scheme that is based on BER was proposed in [16] for a GSM (Global System for Mobile Communication) system.

In recent years, a higher demand for capacity has resulted in substantial interest in the study of multiple-antenna systems, see for example the books [17,18] and research work in [19–22]. Based on the singular value decomposition (SVD) approach, the multiple-input multiple-output (MIMO) channel can be decomposed into parallel single-input single-output (SISO) subchannels with nonequal gains [20]. For a deterministic MIMO channel, when CSI is available at the transmitter and receiver, a water-filling power allocation among the parallel subchannels has been shown to maximize channel capacity [17, 20]. On the other hand, when CSI is only available at the receiver, maximum capacity can be obtained by equal power distribution among the subchannels [17, 20]. In a time-varying MIMO channel, LA techniques for a multiple-antenna system can be inferred from the techniques used for a single antenna system. For example, the VRVP-MQAM scheme of the SISO system [4] has been extended to a MIMO system in [23], and the channel prediction method has been extended to adaptive systems with multiple-antenna system in [24, 25]. Similar to a single antenna system, the degradation of the performance of a multi-antenna system due to inaccurate channel estimation (and imperfect CSI) has also attracted a great deal of attention [23, 25–28]. In the case of channel estimation based on a training signal, additional training effort is required for a multiple antenna adaptive sys-

tem, because more parameters (due to multiple antennas) have to be estimated. Considering that full CSI is fed back to the transmitters, this implies an increased in the amount of feedback information as compared to a single antenna system and increased requirement for quasi-stationarity on the channel. In [27], a signal processing architecture at the receiver was proposed using outdated CSI in combination with linear filtering. The proposed design reduces the effect of incorrect CSI at the transmitter without increasing overhead in feedback. Another approach to reduce feedback overhead is to send only partial CSI based upon channel statistics rather than precise channel parameters. For instance, an adaptive modulation with channel mean feedback for multi-antenna transmission was proposed in [28, 29].

Beside higher capacity transmission, another demand in today's digital wireless communication systems is to provide a wide variety of services for voice, video and data traffic. The performance of such systems will be application specific and is likely to have different QoS (quality of service) requirements, see [30] and the references therein. Among several requirements, delay constraint is one of the QoS parameters that varies dependent upon whether the traffic is real-time or non real-time. Real-time traffic such as a conversational voice service demands stringent delay requirement whereas non real-time traffic such as streaming audio or web browsing and database access traffic has a relaxed requirement on delay. Therefore, the need to support multi-class services has attracted recent research interests in exploring LA techniques for integrated voice and data services. These include the research work based on single-antenna [31] to the very recent research work on MIMO and Orthogonal frequency-division multiplexing (OFDM) systems [32, 33].

## 1.1 Aims and Objectives

The aims of this research are to study radio resource allocation and management for digital wireless communication systems, identify practical limitations from a communication theory and signal processing perspective and to propose novel solutions. To achieve these goals, the objectives of research have been categorized as follows:

i) Review existing research on radio resource allocation and management for digital wireless communications.

ii) Identify transmission parameters that would impact the performance of a digital wireless communication system over a time-varying channel.

iii) Design rate and power adaptation algorithms considering practical implementation aspects.

iv) Implement the proposed algorithms taking into consideration the practical constraints of digital wireless communication systems.

v) Extend the rate and power adaptation techniques to a MIMO system incorporating various QoS targets.

## 1.2 Thesis Outline

The thesis is organized as follows: An overview on radio channel characteristics is given in Chapter 2.

Optimal adaptation techniques for maximum spectral efficiency of a wireless communication system over time-varying channels are discussed in Chapter 3. This chapter includes a summary of the framework for the VRVP-MQAM scheme [4] under perfect channel assumption. The chapter provides the necessary background materials that will be used in the subsequent contribution chapters.

Chapter 4 provides an overview of a pilot symbol assisted modulation (PSAM) scheme and the PSAM-based channel prediction method. The chapter gives the background materials that will be used in the subsequent chapters.

In Chapter 5, a rate and power adaptation technique based on the SNR and BER estimate is proposed. This chapter presents the derivation of the BER estimator and formulates a new set of rate and power algorithms. The spectral efficiency of the proposed system is evaluated under perfect and partial CSI scenarios.

The solutions derived in Chapter 5 are extended to a VRVP-MQAM system that incorporates a maximum a posteriori (MAP) channel predictor in Chapter 6.

A joint SNR target and rate adaptation scheme based on BER estimation is proposed in Chapter 7. The control policy is similar to a truncated channel inversion type power control algorithm that is commonly used in a CDMA/WCDMA system.

In Chapter 8, a MIMO based VRVP-MQAM system is introduced. The chapter starts with a brief discussion on a MIMO channel model and presents discussion in the context of a VRVP-MQAM system. The chapter finally presents another contribution work, where rate and power adaptation schemes for integrated voice and data services for a MIMO system are proposed.

Finally, conclusions are drawn together with suggestions for future work in Chapter 9.

# Chapter 2

# Channel Model

## 2.1 Fading

Radio signal propagation between wireless communication devices is known to experience both large scale and small scale fading. Large scale fading is due to the motion of a transmitter and/or receiver over prominent terrain contours such as hills and buildings. Some of the popular large scale models are Okumura [34] and Hata [34, 35] models, which relate parameters such as antenna height, distance between transmitter and receiver, and signal mean-path loss and standard deviation. In contrast, small scale fading refers to the rapid fluctuation of the radio signal over a short distance and over relatively short time duration. Throughout this thesis, small scale fading will be the main fading phenomena to be considered.

## 2.2 Small Scale Fading and Multipath Effect

In a wireless mobile communication system, a signal can travel from the transmitter to the receiver over multiple reflective paths. The constructive and destruc-

tive additions of the signal through different paths with different delays result in fluctuations in the amplitude and phase within the signal which arrives at the receiver. This phenomenon is known as the multipath effect and is commonly related to small scale fading. Small-scale fading can manifest itself as time dispersion and frequency dispersion mechanisms. Depending on the characteristics of the transmitted signal and the transmission channel, each mechanism can imply that the transmission channel is flat/frequency selective fading based on the multipath time delay spread parameter; or fast/slow fading based on the Doppler spread parameter.

## 2.3 Multipath Time Delay Spread: Flat/Frequency Selective Fading

### 2.3.1 Flat-Fading

A flat-fading channel refers to the situation where the coherence bandwidth $B_c$ of the channel is much greater than the transmitted signal bandwidth $B_s$. In general, coherence bandwidth refers to the bandwidth of the channel which passes all spectral components of the transmitted signal with approximately equal gain and linear phase. In [34], a relaxed definition for $B_c$ is defined as the bandwidth over which the frequency correlation function is above 0.5, and is written as

$$B_c \approx \frac{1}{5\sigma_\tau}, \tag{2.1}$$

where $\sigma_\tau$ is the root mean square (rms) delay spread [34]. Therefore the following relationship could characterize a flat-fading channel

$$B_s << B_c, \tag{2.2}$$

or equivalently,

$$T_s >> \sigma_\tau, \tag{2.3}$$

where $T_s$ denotes the symbol period of the baseband transmitted signal.

For the flat-fading situation, the spectral characteristics of the transmitted signal are preserved at the receiver, but the amplitude of the signal will change in accordance to the time variations of the channel gain. The two common distribution functions defining the instantaneous gain of flat-fading channels are Ricean and Rayleigh distributions. In physical implementation, when the received signal is made up of a dominant line-of-sight (LOS) signal and multiple reflective signals, the envelope amplitude has a Ricean distribution [34]. When the LOS signal becomes faded and approaches zero, the Ricean distribution approaches a Rayleigh distribution. Throughout this thesis, the Rayleigh distribution function is adopted to simulate a scattering rich wireless environment.

## Statistical model for Rayleigh fading

This section summaries the statistical Clark's model as detailed in [34,36]. Consider a scattering rich environment within which $N$ paths of waves arrive at the receiver from a fixed transmitting antenna. Let $\varphi_n$ denotes each angle of arrival, which is measured in the direction of receiver motion. Due to the Doppler effect, the frequency of each wave incident on the receiver is shifted by

$$f_n = f_d \cos \varphi_n \,, \tag{2.4}$$

where $f_d$ denotes the maximum Doppler frequency and is defined as $f_d \triangleq \frac{v_t f}{c}$, where $v_t$ defines the vehicular speed in m/s, $c$ is the speed of light ($3 \times 10^8$ m/s) and $f$ is the carrier frequency in Hz.

Assume that $a_n$ and $\theta_n \triangleq 2\pi f_n t + \phi_n$ denote respectively the amplitude and random phase of the $n^{th}$ path. The transmitted signal can be expressed as

$$s(t) = \mathrm{Re}\{m(t)\exp(j2\pi f t)\}, \tag{2.5}$$

where $m(t)$ denotes the complex envelope of the transmitted signal and Re{.} denotes the real part of a complex argument. The received signal is then expressed as

$$\begin{aligned} r(t) &= \mathrm{Re}\{m(t)\sum_{n=1}^{N} a_n \exp(j2\pi f t + \theta_n)\} && (2.6)\\ &= \mathrm{Re}\{m(t)c(t)\exp(j2\pi f t)\}, && (2.7) \end{aligned}$$

where

$$c(t) = c_I(t) + j\, c_Q(t), \tag{2.8}$$

$$c_I(t) = \sum_{n=1}^{N} a_n \cos(\theta_n), \tag{2.9}$$

$$c_Q(t) = \sum_{n=1}^{N} a_n \sin(\theta_n). \tag{2.10}$$

For sufficiently large $N$, $c_I(t)$ and $c_Q(t)$ can be considered as Gaussian random variables as a consequence of the central limit theorem [37]. Let us assume the average received power is normalized to $A^2$, that is,

$$E[|r(t)|^2] = A^2, \tag{2.11}$$

where $E[.]$ denotes the ensemble average over all possible value of $a_n$ and $\theta_n$, and $|.|$ denotes amplitude. With the phase angles $\theta_n$ assumed to be uniformly distributed within the interval $(0, 2\pi]$, and $c_I$ and $c_Q$ are uncorrelated zero-mean Gaussian random variables with equal variance, then

$$E[c_I^2] = E[c_Q^2] = \frac{A^2}{2}. \tag{2.12}$$

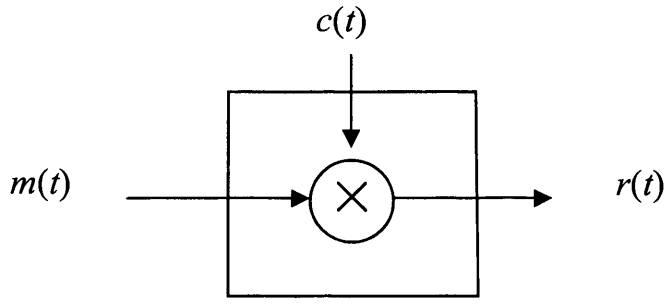


Figure 2.1: Block diagram of a fading channel model.

The envelope of the fading component $\alpha(t)$ is represented as

$$\alpha(t) = \sqrt{c_I^2(t) + c_Q^2(t)}. \tag{2.13}$$

Since $c_I$ and $c_Q$ are random variables, the received signal envelope is also a random variable. Through random variable transformation [37], the received envelope random variable $r$ therefore has a Rayleigh distribution written as

$$f_r(r) = \frac{2r}{A^2} \exp\left(-\frac{r^2}{A^2}\right). \tag{2.14}$$

Finally, the equivalent Rayleigh fading channel model, represented as shown in Figure 2.1, will be used in the subsequent chapters.

## Other flat-fading distributions

The Rayleigh distribution is well suited for modelling a flat-fading channel that is rich in scattering and has no dominant LOS signal component. If the channel has a fixed LOS signal component, the random multipath components arriving at different angels are superimposed on the dominant signal. That means the received signal is equal to the superposition of a complex Gaussian component and an LOS component. The resulting signal envelope has a Ricean distribution [34,38], given by

$$f_r(r) = \frac{2r}{A^2} \exp\left(-\frac{(r^2 + d_o^2)}{A^2}\right) I_0\left(\frac{2d_o r}{A^2}\right), \tag{2.15}$$

for $d_o \geq 0$ and $r \geq 0$. $I_0$ is the zero order modified Bessel function [39]. The parameter $d_o^2$ denotes the power of the dominant signal. The Ricean distribution is often described in terms of a fading parameter, $W$, which is given by

$$W = \frac{d_o^2}{A^2}. \tag{2.16}$$

The parameter $W$ is also known as the Ricean factor and characterizes the Ricean distribution. For instance, as $d_o \rightarrow 0$, and $W \rightarrow 0$, the Ricean distribution approaches a Rayleigh distribution. On the other hand, as $W \rightarrow \infty$, the Ricean distribution approaches a no fading channel model with only an LOS component.

Another fading distribution that is commonly used, due to its flexibility to adjust its parameters to fit to a variety of empirical measurements is the Nakagami fading distribution [40], given by

$$f_r(r) = 2\left(\frac{m}{\Omega}\right)^2 \frac{r^{2m-1}}{\Gamma(m)} \exp\left(\frac{-mr^2}{\Omega}\right), \quad m \geq 0.5, \tag{2.17}$$

where $\Omega = E[r^2]$ is the average received power, $\Gamma(.)$ is the Gamma function [39] and $m$ is the Nakagami fading parameter. The parameter $m$ characterizes the Nakagami distribution. For instance, when $m = 1$, (2.17) reduces to a Rayleigh distribution. When $m = (W+1)^2/(2W+1)$, (2.17) approaches the Ricean distribution with parameter $W$. When $m = \infty$, (2.17) represents a channel with no multi-path fading, but with an LOS component.

### 2.3.2 Frequency Selective Fading

If the coherence bandwidth of the channel is smaller than the bandwidth of the transmitted signal [34],

$$B_s >> B_c\,, \tag{2.18}$$

or equivalently,

$$T_s << \sigma_\tau\,, \tag{2.19}$$

the received signal could experience frequency selective fading. That is, the spectral frequency components of the transmitted signal experience different spectral gains when passing through a frequency selective channel. Physically, multiple versions of the transmitted waveform will be attenuated and delayed in time, and this is the familiar intersymbol interference (ISI) effect. This is commonly experienced in wideband transmission and is not a topic to be explored within this thesis. However, for related interest, details on frequency selective channel modelling can be obtained from text books such as [34].

## 2.4 Doppler Spread: Fast/Slow Fading

In general, fast/slow fading defines a time-varying channel whose channel impulse response changes faster/slower than the transmitted baseband signal. Statistically the time variation can be related to Doppler effect through Doppler spread $B_d$ and coherence time $T_c$ parameters, as detailed in [34]. In summary, a signal undergoes fast fading if

$$T_s > T_c\,, \tag{2.20}$$

or equivalently,

$$B_s < B_d\,. \tag{2.21}$$

In contrast, a signal undergoes slow fading if

$$T_s << T_c\,, \tag{2.22}$$

or equivalently,

$$B_s >> B_d\,. \tag{2.23}$$

Doppler spread $B_d$ is a measure of the spectral broadening which is related to the Doppler shift effect. Coherence time $T_c$ defines the time duration over which the impulse response of the channel is essentially invariant, or alternatively is the time duration over which a strong correlation occurs between the amplitude of two received signals. $T_c$ can be expressed as [34]

$$T_c \approx \frac{1}{f_d}. \tag{2.24}$$

In [34,41], the coherence time is defined as the time over which the time correlation function is above 0.5, and is expressed as

$$T_c \approx \frac{9}{16\pi f_d}. \tag{2.25}$$

Alternatively, based on the geometric mean of expressions (2.24) and (2.25), $T_c$ can be expressed as

$$T_c = \sqrt{\frac{9}{16\pi f_d^2}}. \tag{2.26}$$

Using any one of the expressions (2.24-2.26) in (2.20) and (2.22), fast and slow fading can also be characterized by the spread factor $f_d T_s > 1$ and $f_d T_s << 1$ respectively.

## 2.5 Summary

This chapter provided an overview on radio channel characteristics. In particular, the properties of the multipath radio channel due to small scale fading phenomenon have been described. The statistical model of a flat-fading channel in a scattering rich environment (with no LOS signal) has been shown to be Rayleigh distributed, and is modelled as a zero mean complex-valued Gaussian random process. For comparison, two commonly known flat-fading channel distributions that model a scattering rich environment with LOS signal component

were provided. These are the Ricean distribution and the Nakagami distribution. The time-varying nature of a radio channel in terms of fast/slow fading based on the Doppler spread parameter was discussed. In brief, the fast and slow fading channel can be characterized in terms of Doppler spread factor $f_d T_s$.

In the subsequent chapters, a flat-fading channel with Rayleigh distribution will be mainly considered.

# Chapter 3

# Link Adaptation Techniques under Perfect CSI Knowledge

## 3.1 Introduction

This chapter outlines existing link adaptation techniques for wireless communication systems over time-varying channels. Perfect CSI is assumed available at the transmitter and the receiver. The maximum spectral efficiency of an adaptive code, rate and power scheme is first summarized in terms of Shannon capacity. Next, the maximum spectral efficiency of a variable rate variable power MQAM (VRVP-MQAM) system is presented. This chapter provides the necessary background required for designing the imperfect CSI based VRVP-MQAM system and a VRVP-MQAM MIMO system to be presented in the subsequent chapters.

## 3.2 Capacity of a Time-Varying Channel

The capacity of a time-invariant bandwidth limited transmission over an additive white Gaussian noise (AWGN) channel was originally derived by Shannon in [42], and also well explained in [43]. The well known capacity formula, in bits per second (bps), is written as

$$C = B \log_2 \left( 1 + \frac{\bar{S}}{N_o B} \right), \tag{3.1}$$

where $\frac{\bar{S}}{N_o B}$ is the received average SNR, denoted as $\Gamma$, and $\bar{S}$ represents the average transmit power. The parameter $B$ denotes the bandwidth and $N_o$ denotes the noise power spectral density.

### 3.2.1 Optimal Rate and Power Adaptation

Based on (3.1), Goldsmith *et al.* derived the optimal adaptive scheme which maximizes the spectral efficiency of a narrow band transmission system over a fading channel [2]. The framework of [2] is summarized here. Consider the system model shown in Figure 3.1. The channel is modelled in discrete-time, denoted by index $i$, with statistically stationary and ergodic time-varying gain $\alpha(i) = |c(i)|$, where $c(i)$ denotes the complex fading, and zero mean AWGN $n(i)$. For a constant average transmit power $\bar{S}$, the instantaneous received SNR $\gamma(i)$ is defined as

$$\gamma(i) = \frac{\bar{S}[\alpha(i)]^2}{N_o B}, \tag{3.2}$$

and the average received SNR is

$$\Gamma \triangleq \frac{\bar{S} E\left[\alpha(i)^2\right]}{N_o B}. \tag{3.3}$$

Perfect CSI is assumed available at the receiver, and the CSI is fed back to the transmitter error-free and with negligible delay. That is, at time $i$ the channel

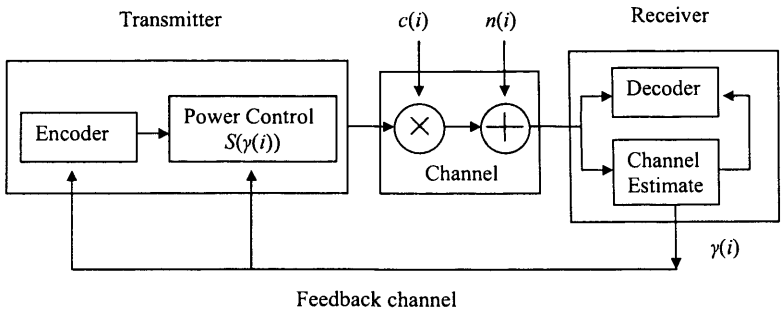


Figure 3.1: Block diagram of an adaptive system.

gain estimate $\hat{\alpha}(i)$ at the receiver is equal to its true channel gain $\alpha(i)$, and its equivalent SNR, $\gamma(i)$, is fed back to the transmitter with negligible delay. Subsequently, the transmitter will adapt the transmit power $S(\gamma(i))$ based on $\gamma(i)$, and the corresponding instantaneous received SNR will be

$$\sigma(\gamma(i)) = \gamma(i)\frac{S(\gamma(i))}{\bar{S}}. \tag{3.4}$$

Having clarified the definitions, the discrete time reference $i$ will be omitted in the remaining sections for brevity.

The transmitter will adapt its power $S(\gamma)$ and code according to the instantaneous SNR $\gamma$. The transmit power is also subject to an average power constraint

$$\int_{\gamma} S(\gamma) f_{\gamma}(\gamma)\, d\gamma = \bar{S}, \tag{3.5}$$

where $f_{\gamma}(\gamma)$ denotes the probability density function (PDF) of $\gamma$. The notation $\int_x g(x)\, dx$ denotes the integral of a function $g(x)$ of a variable $x$, and the range of $x$, unless otherwise specified, is from zero to infinity. For an average power constraint (3.5), the time-varying channel capacity (in bits/sec/Hz) can be written as [2]

$$C/B = \max_{S(\gamma)} \int_{\gamma} \log_2\left(1 + \frac{S(\gamma)\gamma}{\bar{S}}\right) f_{\gamma}(\gamma)\, d\gamma. \tag{3.6}$$

The optimisation problem can then be formulated as

$$F\left(S\left(\gamma\right)\right)=\int_{\gamma}\log_2\left(1+\frac{S\left(\gamma\right)\gamma}{\bar{S}}\right)f_{\gamma}\left(\gamma\right)d\gamma+\mu\left(\int_{\gamma}S\left(\gamma\right)f_{\gamma}\left(\gamma\right)d\gamma-\bar{S}\right), \quad (3.7)$$

where $\mu$ denotes the Lagrangian multiplier. The optimal power adaptation can be obtained from the solution of $\frac{\partial F}{\partial S(.)}=0$. The resulting power adaptation is [2]

$$\frac{S(\gamma)}{\bar{S}}=\begin{cases}\frac{1}{\gamma_0}-\frac{1}{\gamma}\,, & \gamma\geq\gamma_0,\\ 0, & \text{otherwise},\end{cases} \quad (3.8)$$

where $\gamma_0$ denotes the cutoff value for positive power transmission. The parameter $\gamma_0$ is also dictated by the average power constraint $\bar{S}$, and can be determined numerically from

$$\int_{\gamma_0}^{\infty}\left(\frac{1}{\gamma_0}-\frac{1}{\gamma}\right)f_{\gamma}\left(\gamma\right)d\gamma=1, \quad (3.9)$$

where $\infty$ denotes infinity. The power algorithm in (3.8) is commonly known as the 'water-filling' type power control, and is represented pictorially in Figure 3.2 where the inverse SNR $\frac{1}{\gamma}$ is plotted as a function of time unit $i$. The power allocation $S\left(\gamma\right)$ is analogy to water-filling with the threshold level of $\frac{1}{\gamma_0}$.

Finally, substituting (3.8) into (3.6), the maximum spectral efficiency is obtained as [2]

$$C/B=\int_{\gamma_0}^{\infty}\log_2\left(\frac{\gamma}{\gamma_0}\right)f_{\gamma}\left(\gamma\right)d\gamma. \quad (3.10)$$

### 3.2.2 Sub-Optimal Transmitter Adaptations

A simpler form of transmitter adaptation used in current digital wireless communication systems (such as a CDMA/WCDMA-based systems) to combat channel variations is the 'total channel inversion' (CI) type power control. This is a sub-optimal adaptation technique where the transmitter adjusts its power to maintain

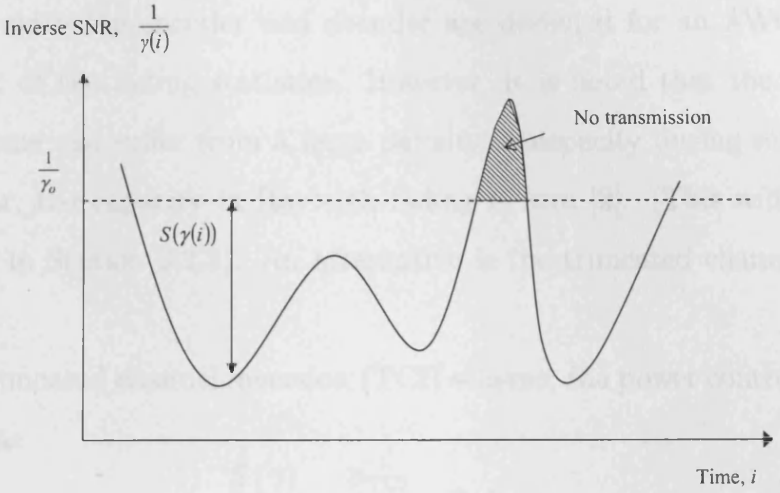


Figure 3.2: Water-filling type power control.

a constant received power. [1] The power control algorithm [2] is given by

$$\frac{S(\gamma)}{\bar{S}} = \frac{\sigma_{\mathrm{CI}}}{\gamma}, \tag{3.11}$$

where $\sigma_{\mathrm{CI}}$ denotes the received SNR that can be maintained subject to the average power constraint $\bar{S}$. That is,

$$\int_{\gamma} \left(\frac{\sigma_{\mathrm{CI}}}{\gamma}\right) f_{\gamma}(\gamma)\, d\gamma = 1, \tag{3.12}$$

and

$$\sigma_{\mathrm{CI}} = 1/E[1/\gamma], \tag{3.13}$$

$$E[1/\gamma] \triangleq \int_0^{\infty} \frac{1}{\gamma} f_{\gamma}(\gamma)\, d\gamma. \tag{3.14}$$

Subsequently, the channel capacity with the channel inversion adaptation [2] is written as

$$C/B = \log_2(1 + \sigma_{\mathrm{CI}}). \tag{3.15}$$

Note that the derived capacity (3.15) is actually the capacity of an AWGN channel with SNR $\sigma_{\mathrm{CI}}$ (3.1). Therefore the channel inversion scheme is simple to

[1] The intention is not to maximise capacity, but to mitigate the near-far effect at the receiver.

implement, since the encoder and decoder are designed for an AWGN channel independent of the fading statistics. However, it is noted that the channel inversion scheme can suffer from a large penalty in capacity during severe fading. In particular, the capacity in Rayleigh fading is zero [2]. (This will be verified numerically in Section 3.2.3). An alternative is the truncated channel inversion scheme.

In the truncated channel inversion (TCI) scheme, the power control algorithm [2] is given as

$$\frac{S(\gamma)}{\bar{S}} = \frac{\sigma_{\text{TCI}}}{\gamma}, \quad \gamma > \gamma_0, \tag{3.16}$$

and no transmission is allowed below the cutoff fade depth $\gamma_0$. To satisfy the power constraint $\bar{S}$,

$$\sigma_{\text{TCI}} = 1/E_{\gamma_0}[1/\gamma], \tag{3.17}$$

$$E_{\gamma_0}[1/\gamma] \triangleq \int_{\gamma_0}^{\infty} \frac{1}{\gamma} f_\gamma(\gamma)\, d\gamma. \tag{3.18}$$

Subsequently, the capacity is given by

$$C/B = \log_2(1 + \sigma_{\text{CTI}})\, p(\gamma \geq \gamma_0), \tag{3.19}$$

where $p(\gamma \geq \gamma_0)$ denotes the probability of transmission.

Figure 3.3 summaries the channel inversion type power control policy $S(\gamma)$ plotted as a function of time unit $i$.

### 3.2.3 Numerical Results

This section compares the capacity between optimal rate and power adaptation scheme (3.10), total channel inversion scheme of (3.15) and the truncated channel inversion scheme of (3.19). The plots for capacity per unit bandwidth as a function of average received SNR, $\Gamma$, for a Rayleigh and Nakagami ($m$=2) fading

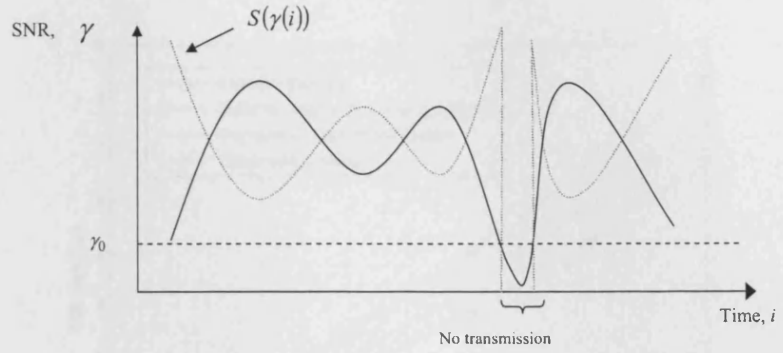


Figure 3.3: Channel inversion type power control.

channel are shown respectively in Figure 3.4 and Figure 3.5. The plot for AWGN channel capacity is also included for comparison.

For a Rayleigh fading channel, the PDF of $\gamma$ is given by

$$f_\gamma(\gamma) \triangleq \frac{1}{\Gamma} \exp\left(-\frac{\gamma}{\Gamma}\right). \tag{3.20}$$

For a Nakagami fading channel, the PDF is given by [44],

$$f_\gamma(\gamma) \triangleq \left(\frac{m}{\Gamma}\right)^m \frac{\gamma^{m-1}}{\Gamma(m)} \exp\left(\frac{-m\gamma}{\Gamma}\right). \tag{3.21}$$

Recall (from Section 2.3.1) that a Rayleigh fading can be represented through a Nakagami fading formula with the parameter $m = 1$, and that a channel with Rayleigh distribution experiences a more severe fading condition as compared to a channel having Nakagami distribution with parameter $m > 1$. Closed-form expressions for the capacities based on the Nakagami fading distribution have been derived in [44]. For the optimal rate and power adaptation scheme, the capacity for a Nakagami fading channel is given by [44]

$$C/B = \frac{1}{\ln 2} \sum_{k=0}^{m-1} \frac{\Gamma_U(k, m\gamma_0/\Gamma)}{k!}, \tag{3.22}$$

where $\Gamma_U(a, u) \triangleq \int_u^\infty x^{(a-1)} e^{-x} dx$ is the upper incomplete Gamma function [45].

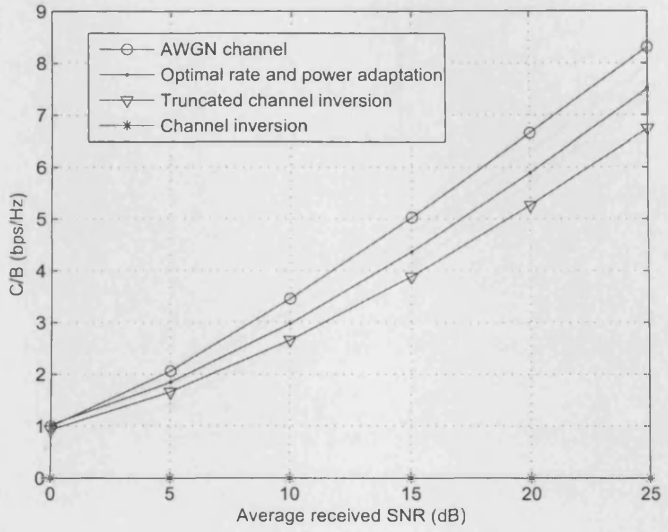


Figure 3.4: Capacity comparison for a Rayleigh fading channel.

For the total channel inversion scheme, the capacity is given by [44]

$$C/B = \log_2\left(1 + \frac{m-1}{m}\Gamma\right). \tag{3.23}$$

For the truncated channel inversion scheme, the capacity is given by [44]

$$C/B = \log_2\left(1 + \frac{\Gamma\Gamma(m)}{m\Gamma_U(m-1, m\gamma_0/\Gamma)}\right)\frac{\Gamma_U(m, m\gamma_0/\Gamma)}{\Gamma(m)}. \tag{3.24}$$

These formulae (3.22-3.24) are used to compute the numerical results shown in Figure 3.4 and Figure 3.5. At a higher SNR, the capacity for rate and power adaptation scheme outperforms the truncated channel inversion scheme, but both converge to the same performance as AWGN channel capacity at a lower SNR. Note that the capacity for channel inversion is zero. For the Nakagami fading channel ($m = 2$), a small increase in capacity can be observed in all three schemes as compared to the Rayleigh fading environment. Moreover, the difference between the respective capacities reduces in a less severe fading environment. It is expected that as $m$ increases, the respective capacities approach to that of AWGN channel.

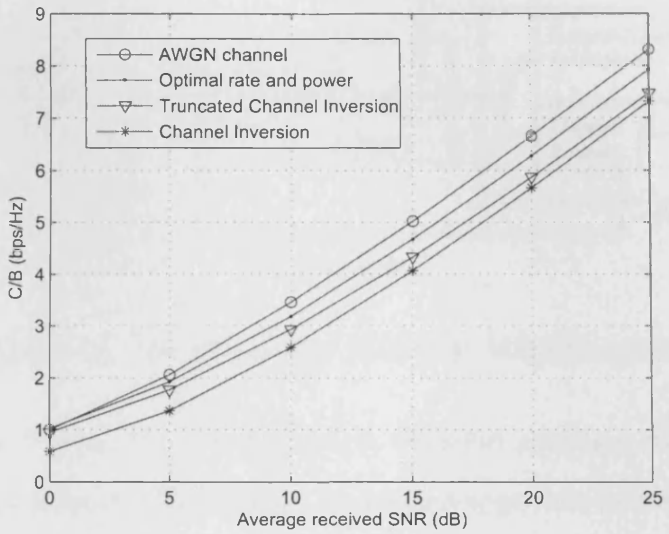


Figure 3.5: Capacity comparison for Nakagami fading channel with parameter $m = 2$.

These results summarise the performance of the transmitter adaptation schemes in terms of Shannon capacity. Though this is not an exact representative for a real system, these results can serve as a good upper bound approximation for the design of a real adaptive system. An example of a real adaptive system employing rate and power adaptation for an MQAM scheme [4, 5] shall be discussed in the next section.

## 3.3 VRVP-MQAM System

The rate and power optimisation for maximum spectral efficiency of a practical adaptive modulation system is discussed in this section. An adaptive MQAM scheme is considered for maximising spectral efficiency. Figure 3.6 shows the block diagram of the system over a single user flat-fading channel. The variable rate variable power (VRVP) MQAM system model follows the descriptions of the

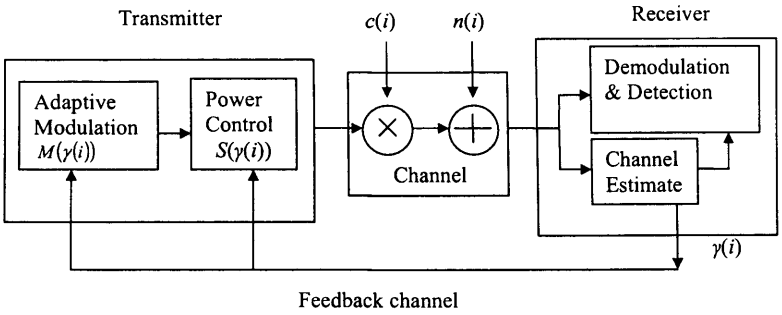


Figure 3.6: Block diagram of VRVP-MQAM system.

system model in Figure 3.1 except that an uncoded adaptive modulator control module is used in place of the encoder. A similar approach to the rate and power optimization discussed in Section 3.2 will be applicable to the adaptive system.

### 3.3.1 BER for MQAM

The BER expression of a square Gray-encoded MQAM scheme with AWGN channel has been derived in several works [43,46]. For example, in [43] the exact BER expression of a square QAM transmission with ideal coherent phase detection in an AWGN channel has been provided as

$$\text{BER} = \left[1 - \left[(1 - 2\left(1 - \frac{1}{\sqrt{M}}\right) Q\left(\sqrt{\frac{3}{M-1}\Gamma}\right)\right]^2\right] \frac{1}{\log_2(M)}, \tag{3.25}$$

where $M$ is the constellation size and $Q(.)$ is the Q-function,

$$Q(x) = \frac{1}{\sqrt{2\pi}} \int_x^\infty \exp(\frac{-t^2}{2}) dt, x \geq 0. \tag{3.26}$$

On the other hand, the BER expression for a non-square QAM scheme is tightly upper-bounded as

$$\text{BER} \leq \left(1 - \left[1 - 2Q\left(\sqrt{\frac{3}{M-1}\Gamma}\right)\right]^2\right) \frac{1}{\log_2(M)}. \tag{3.27}$$

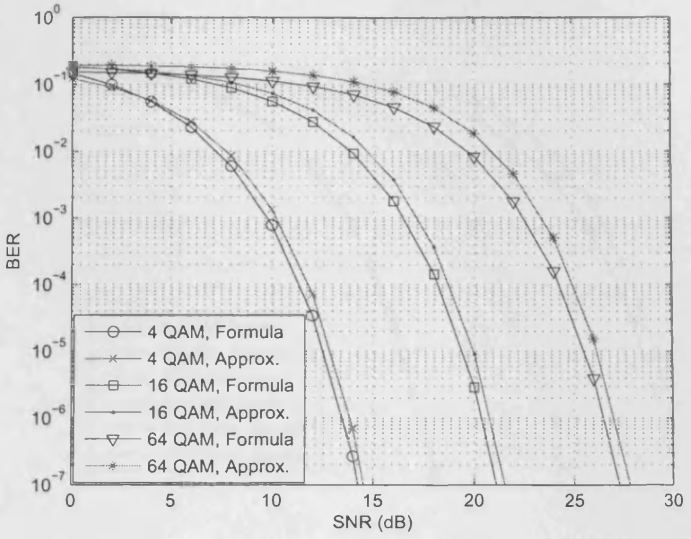


Figure 3.7: BER of a square MQAM scheme. Legend 'Formula' refers to exact BER expression (3.25) and 'Approx.' refers to the approximate BER expression (3.28).

Note that for an MQAM signal with a fixed symbol rate $T_s$ and ideal Nyquist data pulses ($B = 1/T_s$), the average received SNR $\Gamma$ is also equal to $E_s/N_o$, where $E_s$ is the average energy per symbol. For a given BER and $\Gamma$ value, the required $M$ level can be determined numerically from expressions (3.25) or (3.27). However, a closed-form expression for $M$ in terms of BER and $\Gamma$ is not easily obtainable from (3.25) or (3.27). Therefore Goldsmith *et al.* [4, 5] derived an approximate BER expression as,

$$\text{BER} = c_1 \exp\left(\frac{-c_2\,\Gamma}{M-1}\right), \tag{3.28}$$

where $c_1$ and $c_2$ are positive real numbers.

To validate the approximation for the BER expression, in Figure 3.7 and Figure 3.8, the exact BER expressions (3.25),(3.27) and the approximate BER expression (3.28) are compared for square and non-square MQAM schemes. Nu-

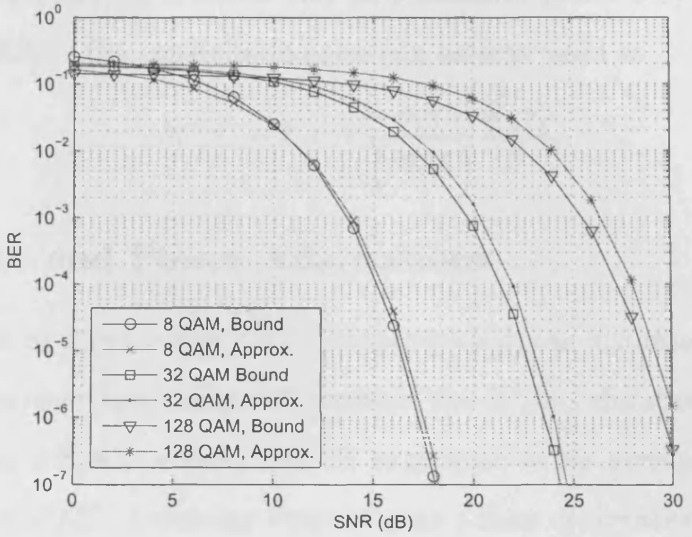


Figure 3.8: BER of a non-square MQAM scheme. Legend 'Bound' refers to the upper bounded non-square QAM BER expression (3.27) and 'Approx.' refers to the approximate BER expression (3.28).

merical values from [4] are used, i.e. $c_1 = 0.2$, $c_2 = 1.5$. For all the cases, the results show that the approximate BER expression upper bounds the exact BER expressions to within 1 dB for $M \geq 4$ and BER $\leq 10^{-2}$, which is a suitable BER range for practical applications.

In the VRVP-MQAM scheme, rate and power at the transmitter will vary in accordance with the time-variations of the channel. Consider a family of uncoded MQAM signal constellation. The transmitter adapts to channel variations by adjusting the constellation size $M(\gamma)$ and the transmit power $S(\gamma)$ in accordance with the variations in $\gamma$. At the receiver, the corresponding received SNR is $\gamma \frac{S(\gamma)}{\bar{S}}$. Consequently, based on (3.28), the instantaneous BER at the receiver can be expressed as

$$\mathrm{BER}(\gamma) = c_1 \exp\left(-\frac{c_2 \gamma}{M(\gamma) - 1} \frac{S(\gamma)}{\bar{S}}\right). \tag{3.29}$$

By re-arranging (3.29), it is noted that for a transmit power $S(\gamma)$ and a required BER target BERT, the constellation size can be expressed as

$$M(\gamma) = 1 + \frac{-c_2\gamma}{\ln\left(\frac{\text{BERT}}{c_1}\right)}\frac{S(\gamma)}{\bar{S}}. \tag{3.30}$$

### 3.3.2 Rate and Power Adaptations

With data sent at $k(\gamma) = \log_2(M(\gamma))$ bits/symbol, the instantaneous data rate is $k(\gamma)/T_s$ bits/sec (bps), where $T_s$ denotes the symbol duration. The spectral efficiency of an MQAM scheme can be expressed as its average data rate per unit bandwidth $R/B$. Assuming Nyquist data pulses of duration $T_s = 1/B$, the spectral efficiency (in bps/Hz) for continuous rate is

$$\frac{R}{B} = \int_\gamma k(\gamma) f_\gamma(\gamma)\, d\gamma, \tag{3.31}$$

where $f_\gamma(\gamma)$ denotes the PDF of $\gamma$. Subsequently, substituting (3.30) into (3.31), the final form for the spectral efficiency of an MQAM system is expressed as

$$\frac{R}{B} = \int_\gamma \log_2\left(1 + \frac{-c_2\gamma}{\ln(\text{BERT}/c_1)}\frac{S(\gamma)}{\bar{S}}\right) f_\gamma(\gamma)\, d\gamma. \tag{3.32}$$

The power adaptation for maximum spectral efficiency (3.32) subject to a power constraint $\bar{S}$ can be obtained using the method of Lagrangian optimization. The formulation becomes

$$F(S(\gamma)) = \int_\gamma \log_2\left(1 + \frac{KS(\gamma)\gamma}{\bar{S}}\right) f_\gamma(\gamma)\, d\gamma + \mu\left(\int_\gamma S(\gamma) f_\gamma(\gamma)\, d\gamma - \bar{S}\right), \tag{3.33}$$

where $\mu$ denotes the Lagrangian multiplier and $K \triangleq \frac{-c_2}{\ln(\text{BERT}/c_1)}$. The optimal power adaptation can be obtained from the solution of $\frac{\partial F}{\partial S(.)} = 0$ and is obtained as

$$\frac{S(\gamma)}{\bar{S}} = \begin{cases} \frac{1}{\gamma_o} - \frac{1}{\gamma K}, & \gamma \geq \gamma_0/K, \\ 0, & \text{otherwise,} \end{cases} \tag{3.34}$$

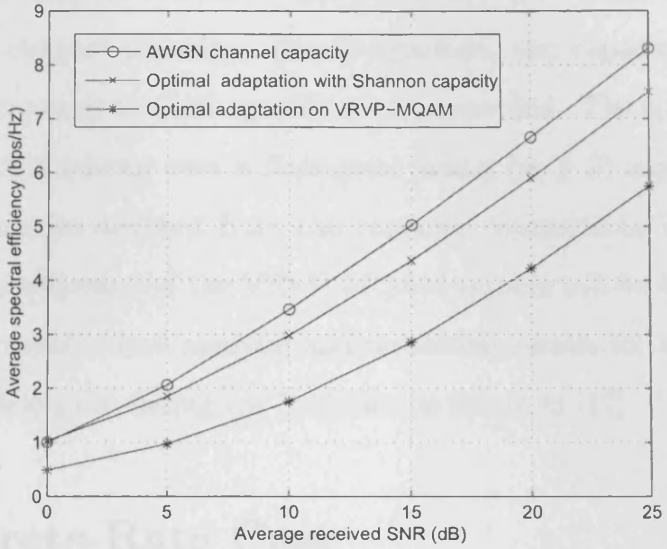


Figure 3.9: Spectral efficiency for a Rayleigh fading channel.

where $\gamma_0/K$ is the optimized cutoff value below which no transmission is allowed. The parameter $\gamma_0/K$ can be obtained numerically through

$$\int_{\gamma_0/K}^{\infty} \left( \frac{1}{\gamma_0} - \frac{1}{\gamma K} \right) f_\gamma(\gamma)\, d\gamma = 1. \tag{3.35}$$

Finally, substituting (3.34) into (3.32), the maximum spectral efficiency is simplified to

$$\frac{R}{B} = \int_{\gamma_0/k}^{\infty} \log_2 \left( \frac{\gamma K}{\gamma_0} \right) f_\gamma(\gamma)\, d\gamma. \tag{3.36}$$

### 3.3.3 Numerical Results

The numerical results in Figure 3.9 compare the spectral efficiency of the adaptive transmission scheme for the VRVP-MQAM system (3.36) to the channel capacity (3.10) of a Rayleigh flat-fading channel. No restriction on the constellation size of the MQAM system is assumed, that is, $M$ can be a non-integer value. The BER target is set to $10^{-3}$, $c_1 = 0.2$ and $c_2 = 1.5$. The figure illustrates a power

loss in the VRVP-MQAM scheme of approximately equal to the $K$ factor relative to the optimal channel capacity. For comparison, the capacity of an AWGN channel (3.1) expressed in $C/B$ bps/Hz is also provided. The spectral efficiency of a VRVP-MQAM scheme over a Nakagami fading ($m \geq 2$) is not shown in the figure since it can be deduced from the capacity comparisons in Section 3.2.3, that the spectral efficiency of the VRVP-MQAM system will be better over a less severe fading channel. More analysis and numerical results for a VRVP-MQAM scheme over a Nakagami fading ($m \geq 2$) can be found in [47].

## 3.4 Discrete-Rate Case

Previous sections (3.3.2 and 3.3.3) discussed a continuous rate adaptation scheme where signal constellation sizes are assumed unrestricted, that is, $M$ can be a non-integer number. However, for practical implementation of instantaneous symbol level, the constellation size of a modulation scheme should be an integer value and it should also be restricted to a maximum value. For a discrete-rate VRVP-MQAM system, the analysis follows closely to that of the continuous rate VRVP-MQAM system. In [5], a detailed analysis of the discrete rate and power adaptation scheme for an instantaneous BER requirement and an average BER requirement has been provided. Since we are based on instantaneous BER requirement, we shall outline in this section the problem formation for the discrete rate and power adaptation with instantaneous BER requirement [5]. We will conclude this section by comparing the numerical results from selected references relating to discrete-rate VRVP-MQAM systems.

### 3.4.1 Problem Formation

For a finite set of $N$ constellations, the corresponding discrete boundaries in SNR are defined as $\{\gamma_i\}_{i=0}^{N-1}$, and $\gamma_N = \infty$. Each SNR region, $\gamma_i$, defines the range of $\gamma$ over which the different constellations are transmitted. Let $M_i$ denote the assigned constellation size for the region $\gamma_i \leq \gamma < \gamma_{i+1}$, and $k_i = \log_2(M_i)$ denote the corresponding transmission rate. The spectral efficiency for the discrete case can be written as [5]

$$\frac{R}{B}_{\text{discrete}} = \sum_{i=0}^{N-1} \log_2(M_i) \int_{\gamma_i}^{\gamma_{i+1}} f_\gamma(\gamma)\, d\gamma, \tag{3.37}$$

and the power constraint is

$$\sum_{i=0}^{N-1} \int_{\gamma_i}^{\gamma_{i+1}} \frac{S(\gamma)}{\bar{S}} f_\gamma(\gamma)\, d\gamma = 1. \tag{3.38}$$

For a BER target BERT, the transmit power control under each region is given as

$$\frac{S(\gamma)}{\bar{S}} = \frac{\ln\left(\frac{\text{BERT}}{c_1}\right)\left(\frac{M_i - 1}{-c_2}\right)}{\gamma}. \tag{3.39}$$

Finally, the Lagrange formulation is expressed as

$$F(\gamma_1, \gamma_2, ..., \gamma_N) = \sum_{i=0}^{N-1} k_i \int_{\gamma_i}^{\gamma_{i+1}} f_\gamma(\gamma)\, d\gamma + \mu \left[ \sum_{i=0}^{N-1} \int_{\gamma_i}^{\gamma_{i+1}} \frac{S_i(\gamma)}{\bar{S}} f_\gamma(\gamma)\, d\gamma - 1 \right]. \tag{3.40}$$

Solving for $\frac{\partial F}{\partial \gamma_i} = 0$, the optimal rate region boundaries are obtained as [5]

$$\gamma_0 = \frac{h(k_0)}{k_0} u, \tag{3.41}$$

$$\gamma_i = \frac{h(k_i) - h(k_{i-1})}{k_i - k_{i-1}} u, \tag{3.42}$$

where $h(k_i) = -\frac{\ln(\text{BERT}/c_1)}{c_2}(M_i - 1)$ and $u$ is determined by the average power constraint (3.38). Similar to the continuous rate case, $\gamma_0$ is the cutoff SNR below which no transmission is allowed.

### 3.4.2 Numerical Results

The discrete rate VRVP-MQAM system performance is summarised through the following case study.

1) For a VRVP-MQAM system over a Rayleigh fading channel, Goldsmith *et al.* [4] showed that a discrete rate continuous power (DRCP) scheme using five different signal constellations ($M_i = 0, 2, 4, 16, 64$) results in a lower spectral efficiency that is within 1 dB of that of a continuous rate continuous power (CRCP) scheme.

2) In [23], Zhou *et al.* have made comparison between a DRCP and CRCP scheme for a VRVP-MQAM multi-antenna system. For $N = 5$ discrete-regions, the DRCP scheme results in a small SNR penalty of less than 0.5 dB as compared to the CRCP counterpart.

3) In [48], Lim *et al.* have also made comparison between a discrete rate and a continues rate MQAM system, but they have incorporated a suboptimal power adaptation approach (an on/off power control). Their numerical results showed around 1.3 dB penalty when the discrete rate MQAM scheme is used.

In summary, these results illustrate that the continuous rate provides a good upper bound limit to their discrete rate counterparts.

## 3.5 Summary

Link adaptation techniques for wireless communication systems over time-varying flat-fading channels were investigated.

The chapter started with the introduction of the Shannon capacity of a time-invariant narrow band transmission system over an AWGN channel in Section 3.2. The capacity of a narrow band transmission system over a time-varying channel

with perfect CSI was then discussed. When perfect CSI knowledge was assumed at the receiver and the transmitter, the optimal power adaptation was shown to be a water-filling scheme. A simpler form of transmitter adaptation scheme, known as the (total/truncated) channel inversion type power control, was further discussed. This is a sub-optimal adaptation technique where the transmitter adjusts its power to maintain a constant receive power, and is commonly used in CDMA/WCDMA-based systems. Using numerical results, the capacities for the optimal and suboptimal schemes were compared for Rayleigh and Nakagami ($m = 2$) fading channels. The capacity of an AWGN channel was included for comparison. The results verified that fading reduces channel capacity, and that the optimal adaptation scheme is superior than the sub-optimal schemes. However at a lower SNR, all schemes (except the total channel inversion scheme) converge to the same performance as the AWGN channel capacity. The capacity of the total channel inversion scheme was shown to be zero in a severe fading environment (based on the Rayleigh fading channel). In this circumstance, the truncated channel inversion scheme is considered. That is, the transmitter only compensates for fading above a cutoff fade level.

In Section 3.3, an adaptive system employing rate and power adaptation for an MQAM scheme (denoted as the VRVP-MQAM system) was considered. The rate and power adaptation techniques discussed in Section 3.2 are applicable to the VRVP-MQAM system. A continuous rate with an uncoded MQAM scheme was considered. Numerical results confirmed that an MQAM based optimal adaptation scheme resulted in a power loss of approximately $\frac{-1.5}{\ln(5\ \mathrm{BERT})}$ factor relative to the optimal channel capacity.

For comparison, a discrete rate adaptation scheme was discussed in Section 3.4. The problem formation was outlined and a case study for VRVP-MQAM systems based on discrete rate and continuous rate adaptation was provided. In

summary, the discrete rate VRVP-MQAM system could result into approximately 1 dB penalty as compared to the continuous rate VRVP-MQAM system. The continuous rate VRVP-MQAM design, which provides a good upper bound limit to its discrete rate counterpart, will be considered in the subsequent chapters.

# Chapter 4

# Pilot Symbol Assisted Modulation Based Channel Predictor

## 4.1 Introduction

Chapter 3 discussed a VRVP system where perfect CSI is available at the receiver and the transmitter. A more practical scenario would be when CSI is imperfectly estimated at the receiver, which then arrives at the transmitter with a delay. The delay might be from the processing time of the channel estimation and prediction at the receiver, and also due to the time required for CSI to be fed back to the transmitter. The impact of the uncertainty in channel estimates has been studied in several works, for example [4, 6–9, 24], wherein results confirmed that the performance of the LA system is dependent on the accuracy of the CSI at the receiver and the transmitter. In particular, depending on the estimation technique, system parameters such as the BER performance and spectral efficiency can be

affected considerably. A channel estimate for signal detection at the receiver can be obtained non-causally as the receiver can wait until the end of a transmitted sequence before decoding. On the other hand, a channel estimate for LA is obtained causally since the transmitter is adapting to the channel variations based on sequential CSI that is obtained at the receiver. A good example is in the power control policy of a CDMA/WCDMA cellular network where the measurements of the instantaneous fading level are fed back sequentially to the transmitter via a feedback link [13].

Several approaches to incorporate channel estimation for an LA system over a fading channel have been investigated. These include a single outdated fading estimate approach used in [7] and a long-range CSI predictor that assumes the use of perfect channel estimates in [49]. An alternate approach to mitigate the effects of fading that is commonly used in digital wireless communication systems is the pilot symbol assisted modulation (PSAM) method [50]. PSAM is commonly used to improve the reliability of signal detection at the receiver. For example, Tang *et al.* [51] investigated the impact of imperfect channel estimates on the BER performance of a PSAM-based MQAM transmission system over a Rayleigh fading channel, wherein the channel gain estimate at the receiver is a linear combination of preceding and subsequent known pilot symbols. In addition to estimation for signal detection, PSAM can be useful in channel estimation for link adaptation. For instance, Oien *et al.* [24] exploited the PSAM scheme and incorporated a channel predictor to estimate the channel gain of an ACM system over a Rayleigh fading channel.

In one of my thesis contributions, I have incorporated the PSAM-based channel predictor [24] into a proposed rate and power algorithm. The channel PSAM-based prediction method is adopted because the PSAM scheme has been a feasible method commonly employed in a digital wireless communication system. To

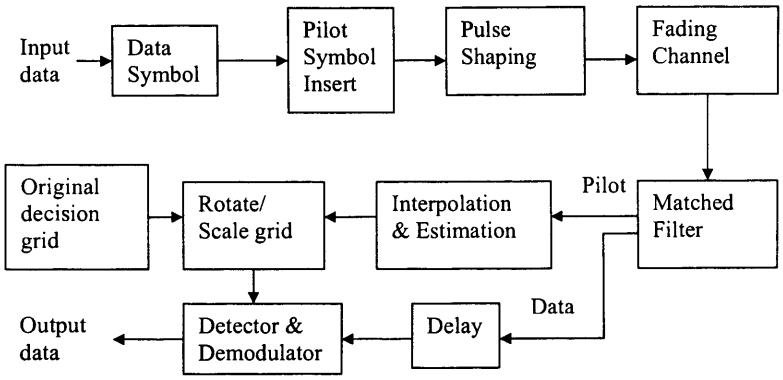


Figure 4.1: Block diagram of a PSAM system.

provide the necessary background material that will be used in the subsequent contribution chapters, the PSAM scheme is introduced in this chapter and the framework of the PSAM-based optimal-MAP channel predictor [24, 52] will be summarized.

## 4.2 PSAM

This section provides an overview of the PSAM scheme. A detailed description of the PSAM scheme can be found in [50] and [53, ch.9]. Figure 4.1 shows the block diagram of a PSAM based system. At the transmitter, pilot symbols are periodically inserted (at $L$ symbols interval) into the data symbols prior to pulse shaping. At the receiver, after matched filtering, sequences of data and pilot symbols are extracted separately. The extracted pilot symbols are then interpolated and used to form an estimate of the channel state. Decision is then carried out against a decision level reference grid, scaled and rotated according to the estimated channel. Since delay is incurred in the interpolation process, the data sequence must be delayed accordingly.

CSI estimation for detection can be accomplished based on several novel inter-

polator filter designs. An example of an optimal design is the non-causal Wiener interpolator filter [50], which smooths the noise and allows for coherent detection to be used. Alternatively, Tang *et al.* in [51] used a simpler but a near-optimal *sinc* interpolator that was proposed in [54].

## 4.3 PSAM-Based Channel Prediction for an LA System

In [24], a PSAM-based channel prediction method was proposed for an adaptive coded modulation (ACM) multi-antenna system. Discrete rate adaptation is performed by switching between $N$ transmitter-receiver pairs over a Rayleigh fading channel. The adapted rate at the transmitter is based on the (causal) CSI which is periodically fed back from the receiver. In practice, the performance of the ACM scheme depends mainly on two factors: 1) the accuracy of the CSI, estimated and/or predicted at the receiver at time $i$ when the signal is received, 2) the update rate of the transmitter (i.e. how frequent the transmitter updates its modulation level and power level). The update time is written as $(i+\tau)$, where $\tau$ denotes the total time for estimation and/or prediction processing together with the delay in the feedback path. Therefore in a practical scenario, the transmitter may adapt to an inaccurate CSI, and result in degradation of BER performance and spectral efficiency. For a coherent detection, Oien *et al.* have proposed a scheme based on the optimal Wiener estimation, and also they assumed that the CSI used for detection is perfect. They investigated the BER performance and spectral efficiency of their proposed MAP-optimal prediction based ACM system, and concluded that the proposed channel prediction is feasible for practical feedback delays for a Rayleigh fading channel.

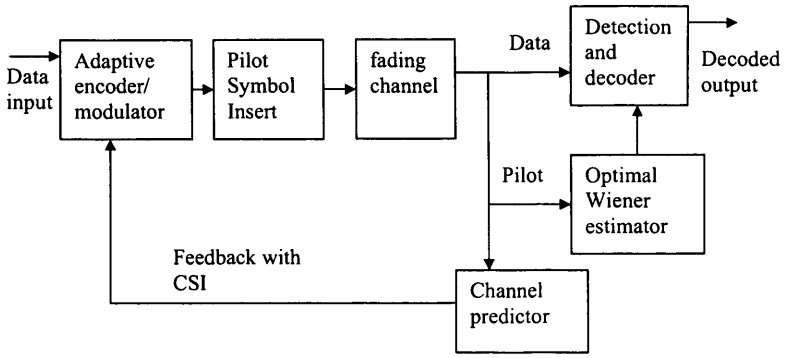


Figure 4.2: Adaptive system with PSAM-based channel estimation and channel prediction.

Due to the feasibility of the PSAM-based channel prediction method for an LA system, the proposed rate and power algorithms are generalized to incorporate the MAP-optimal predictor. The proposed adaptive rate and power algorithms are based on the BER and SNR estimate of a single antenna system over a Rayleigh fading channel. In this context, and without loss of generality, the framework of the multi-antenna system in [24] is reduced to a single antenna system and discussed here.

Figure 4.2 shows the block diagram of the channel prediction scheme for a single antenna system [24]. An optimal channel predictor with minimum error variance, which is a MAP based Rayleigh fading envelope predictor, is adopted. A perfect signal detection based on the optimal Wiener estimator [50] is considered. Let $x(i)$ denote the transmitted complex baseband signal at time index $i$. At the receiver, after matched filtering and sampling with perfect symbol timing at a rate of $1/Ts$, where $T_s$ is the symbol duration, the received complex-valued signal over a flat-fading channel can be written as

$$y(i) = z(i)\,x(i) + n(i), \tag{4.1}$$

where $z(i)$ denotes the complex fading and $n(i)$ is complex circularly symmetric

AWGN component. The noise variance is defined as $\sigma_n^2 = N_o B$, where $N_o$ denotes the noise power spectral density and $B$ denotes the received signal bandwidth.

Assume that all pilot symbols have the same absolute value $a_p$, and that the pilot symbol is perfectly known to the receiver. The estimated fading channel at any pilot-symbol time instant $v - kL$ can be represented as

$$\hat{z}(v - kL) = \frac{y(v - kL)}{x(v - kL)} \tag{4.2}$$

$$= z(v - kL) + \frac{n(v - kL)}{a_p}, \tag{4.3}$$

where $v = pL$ ($p \in \mathbb{Z}, L \in \mathbb{Z}^+$) and $k = 0, 1, ..., K_o - 1$. $K_o$ defines the number of fading observations used in the channel predictor. Note that (4.3) is the result of a maximum-likelihood (ML) estimation based on one received observation, and the proof will be shown in Section 4.3.1. The two terms in (4.3) are statistically independent and they are distributed according to a zero-mean complex Gaussian function. Therefore their sum is also a complex Gaussian variable with variance equal to the sum of the individual variances.

Oien *et al.* [24] have considered the channel predictor as a linear combination of $K_o$ memoryless estimates $\hat{z}(v - kL)$. That is, the predicted fading at $(v+j)^{th}$ symbol-instant can be written as

$$\breve{z}(v + j) = \sum_{k=0}^{K_o - 1} f_j^*(k)\, \hat{z}(v - kL) \tag{4.4}$$

$$= \mathbf{f}_j^{\mathrm{H}} \hat{\mathbf{z}}, \tag{4.5}$$

where $j$ relates to the update rate at $j$ symbol-instants ahead of the $v^{th}$ symbol-instant (i.e. $j = qL$ and $q \in \{1, 2, ...\}$). $\mathbf{f}_j^{\mathrm{H}} = [f_j^*(0), f_j^*(1), ..., f_j^*(K_o - 1)]$ is the predictor filter coefficient vector and $\hat{\mathbf{z}} = [\hat{z}(v), \hat{z}(v - L), ..., \hat{z}(v - (K_o - 1)L)]^{\mathrm{T}}$ is the vector of the estimates of the complex fading amplitude in the last $K_o$ pilot-symbol instants. The superscripts '*' and 'H' denote complex conjugate

and Hermitian transpose respectively. The superscript 'T' denotes transpose. The method to determine $\mathbf{f}_j^{\mathrm{H}}$ shall be explained in the next section.

### 4.3.1 Optimal-MAP Channel Predictor

The optimal-MAP channel predictor developed by Holm *et al.* [52] is summarized in this section. Consider the case when all the pilot symbols are equal, that is $x(pL) = a_p$, where $p \in \mathbb{Z}$. Next, let $\mathbf{A}$ denote the diagonal matrix,

$$\mathbf{A} = \begin{pmatrix} x(v) & & & \\ & x(v-L) & & \\ & & \ddots & \\ & & & x(v-(K_o-1)L) \end{pmatrix}, \tag{4.6}$$

where the diagonal elements are the transmitted pilot symbols. Therefore, $\mathbf{A} = a_p \mathbf{I}_{K_o}$, where $\mathbf{I}_{K_o}$ is an identity matrix of dimension $K_o \times K_o$. Let $\mathbf{n}$ denote the noise elements at the pilot-symbol time instants, the corresponding covariance matrix is, $\mathbf{C}_n = N_o B \mathbf{I}_{K_o}$, where $B$ denotes the signal bandwidth. Subsequently, the received signal corresponding to the pilot-symbol time instants can be written as

$$\mathbf{y} = \mathbf{A}\mathbf{z} + \mathbf{n} \tag{4.7}$$

$$= a_p \mathbf{z} + \mathbf{n}, \tag{4.8}$$

where $\mathbf{z} = [z(v), z(v-L), ..., z(v-(K_o-1)L)]^{\mathrm{T}}$ is the vector of the fading values at the pilot-symbol time instants.

The ML-optimal estimate of $\mathbf{z}$ based on the observations $\mathbf{y}$ is obtained by determining $\hat{\mathbf{z}}$ that maximizes the likelihood function $f_{y|z}(\mathbf{y}|\mathbf{z})$. It has been shown

that the solution for such a Gaussian likelihood function is [55, ch.12] [56, ch.4]

$$\hat{\mathbf{z}} = \left[\mathbf{A}^{\mathrm{H}}\mathbf{R}_n^{-1}\mathbf{A}\right]^{-1}\left[\mathbf{A}^{\mathrm{H}}\mathbf{R}_n^{-1}\mathbf{y}\right] \tag{4.9}$$

$$= \mathbf{A}^{-1}\mathbf{y}, \tag{4.10}$$

where $\mathbf{R}_n$ is the noise correlation matrix. Since all the diagonal elements of $\mathbf{A}$ are equal to $a_p$, (4.10) is reduced to

$$\hat{\mathbf{z}} = \frac{\mathbf{y}}{a_p} = \mathbf{z} + \frac{1}{a_p}\mathbf{n}, \tag{4.11}$$

where each element of $\hat{\mathbf{z}}$ is an estimate of the fading channel at a particular pilot-symbol time instant, also represented as in (4.3).

The MAP-optimal estimate $\breve{z}$ of a channel parameter $z$ based on the observations $\mathbf{y}$ is obtained by locating $\breve{z}$ that maximizes the MAP function, $f_{z|y}(z|\mathbf{y})$. As $z$ and $\mathbf{y}$ are jointly Gaussian distributed random variables, the conditional PDF $f_{z|y}(z|\mathbf{y})$ is also Gaussian. Subsequently, the optimal MAP estimate obtained by maximising $f_{z|y}(z|\mathbf{y})$ can be shown to be the conditional mean

$$\breve{z}_{\mathrm{MAP}} = E\left[z|\mathbf{y}\right] \tag{4.12}$$

$$= \mathbf{r}_{z,y}^{\mathrm{T}}\mathbf{R}_y^{-1}\mathbf{y}. \tag{4.13}$$

where $\mathbf{r}_{z,y}$ denotes the cross correlation vector of $z$ and $\mathbf{y}$, and $\mathbf{R}_y$ denotes the covariance matrix of $\mathbf{y}$. The vector $\mathbf{r}_{z,y}$ and matrix $\mathbf{R}_y$ are given respectively as

$$\mathbf{r}_{z,y} = E\left[\mathbf{y}z^*\right] = a_p E\left[\mathbf{z}z^*\right] = a_p \Omega \mathbf{r}_j, \tag{4.14}$$

$$\mathbf{R}_y = E\left[\mathbf{y}\mathbf{y}^{\mathrm{H}}\right] = a_p^2 E\left[\mathbf{z}\mathbf{z}^{\mathrm{H}}\right] \tag{4.15}$$

$$= a_p^2 \Omega \mathbf{R} + \sigma_n^2 \mathbf{I}_{K_o}, \tag{4.16}$$

where $\Omega = E\left[|z|^2\right]$. The elements of the vector $\mathbf{r}_j$ are the correlations between the fading at pilot-symbol time instants $v - kL$ and the fading at the prediction

time instant $v+j$, and the vector is written as

$$\mathbf{r}_j = \frac{1}{\Omega} E[\mathbf{z} z^*(v+j)]. \tag{4.17}$$

The elements of $\mathbf{r}_j$ can be represented in terms of the normalized correlation function $R(.)$,

$$\begin{aligned} r_{j,k} &= \frac{1}{\Omega} E[z(v-kL) z^*(v+j)] && (4.18) \\ &= R((j+kL)T_s). && (4.19) \end{aligned}$$

$\mathbf{R}$ is a $K_o \times K_o$ covariance matrix of the fading at the pilot symbol instants, written as

$$\mathbf{R} = \frac{1}{\Omega} \mathrm{Cov}(\mathbf{z}, \mathbf{z}) = \frac{1}{\Omega} E[\mathbf{z}\mathbf{z}^{\mathrm{H}}]. \tag{4.20}$$

The elements $R_{k,l}$ are the correlations of the fading between pilot-symbol instants, and can be represented in terms of the correlation function with the time difference $(|k-l|)LT_s$, written as

$$R_{k,l} = R((|k-l|)LT_s). \tag{4.21}$$

Substituting (4.14) and (4.16) into (4.13), the MAP estimate is simplified to [52]

$$\begin{aligned} \check{z}_{\mathrm{MAP}} &= a_p \Omega \mathbf{r}_j^{\mathrm{T}} \left(a_p^2 \Omega \mathbf{R} + N_o B \mathbf{I}_{K_o}\right)^{-1} \mathbf{y} && (4.22) \\ &= \mathbf{r}_j^{\mathrm{T}} \left(\mathbf{R} + \frac{N_o B}{a_p^2 \Omega} \mathbf{I}_{K_o}\right)^{-1} \frac{\mathbf{y}}{a_p}, && (4.23) \end{aligned}$$

where $\frac{\mathbf{y}}{a_p} = \hat{\mathbf{z}}$. Thus the MAP-optimal filter coefficient vector $\mathbf{f}_j$ is determined as

$$\mathbf{f}_j^{\mathrm{T}} = \mathbf{r}_j^{\mathrm{T}} \left(\mathbf{R} + \frac{N_o B}{a_p^2 \Omega} \mathbf{I}_{K_o}\right)^{-1}. \tag{4.24}$$

## 4.4 Statistical Properties of the Predicted and the True Fading Amplitude

Since the channel is considered stationary, and for clarity of notation, the time index shall be omitted in the remaining sections.

For a Rayleigh distributed fading channel, the real and imaginary components of the envelope of the fading gain, $\alpha$, can be modelled as a zero-mean Gaussian random process with equal variance $\sigma_z$ (This was discussed in Section 2.3.1). Therefore, the PDF of $\alpha$ can be written as

$$f_{\alpha}(\alpha) = \frac{2\alpha}{\Omega} \exp\left(-\frac{\alpha}{\Omega}\right), \tag{4.25}$$

where $\Omega = E[\alpha^2]$. When $\alpha$ is Rayleigh distributed, $\alpha^2$ has a chi-square distribution with two degrees of freedom (alternatively, $\alpha^2$ is also known to be exponentially-distributed), and the PDF is written as [37]

$$f_{\alpha^2}(\alpha^2) = \frac{1}{2\sigma_z^2} \exp\left(-\frac{\alpha^2}{2\sigma_z^2}\right) \tag{4.26}$$

$$= \frac{1}{\Omega} \exp\left(-\frac{\alpha^2}{\Omega}\right). \tag{4.27}$$

The predicted linear fading $\breve{z}$ is also a complex Gaussian variable because it is a linear function of zero-mean complex Gaussian variables. Subsequently, the equivalent predicted channel gain, $\breve{\alpha} = |\breve{z}|$, is clearly Rayleigh distributed, with PDF

$$f_{\breve{\alpha}}(\breve{\alpha}) = \frac{2\breve{\alpha}}{\breve{\Omega}} \exp\left(-\frac{\breve{\alpha}}{\breve{\Omega}}\right), \tag{4.28}$$

where $\breve{\Omega} = E[\breve{\alpha}^2]$. Since $\breve{\alpha}$ is Rayleigh distributed, $\hat{\alpha}^2$ is therefore exponentially distributed, with PDF

$$f_{\breve{\alpha}^2}(\breve{\alpha}^2) = \frac{1}{\breve{\Omega}} \exp\left(-\frac{\breve{\alpha}^2}{\breve{\Omega}}\right). \tag{4.29}$$

### 4.4.1 The Ratio $r = \breve{\Omega}/\Omega$

The ratio $r = \breve{\Omega}/\Omega$ is a convenient term that relates the expectation of the estimated channel gain, $\breve{\Omega}$, to the expectation of the actual channel gain, $\Omega = E[\alpha^2]$.

In the case of channel prediction, $\breve{\alpha}^2 = |\breve{z}|^2$, where $\breve{z}$ is the predicted channel gain in complex components. Thus the expectation of $\breve{\alpha}^2$ can be expressed as [24]

$$\begin{aligned}
\breve{\Omega} &= E\left[\breve{\alpha}^2\right] = E\left[|\breve{z}|^2\right] && (4.30)\\
&= E\left[|\mathbf{f}_j^{\mathrm{H}}\,\hat{\mathbf{z}}|^2\right] = \mathbf{f}_j^{\mathrm{H}} E\left[\hat{\mathbf{z}}\hat{\mathbf{z}}^{\mathrm{H}}\right]\mathbf{f}_j && (4.31)\\
&= \mathbf{f}_j^{\mathrm{H}} E\left[\left(\mathbf{z}+\frac{\mathbf{n}}{a_p}\right)\left(\mathbf{z}+\frac{\mathbf{n}}{a_p}\right)^{\mathrm{H}}\right]\mathbf{f}_j && (4.32)\\
&= \mathbf{f}_j^{\mathrm{H}}\left(E\left[\mathbf{z}\mathbf{z}^{\mathrm{H}}\right]+\frac{1}{a_p^2}E\left[\mathbf{n}\mathbf{n}^{\mathrm{H}}\right]\right)\mathbf{f}_j\,, && (4.33)
\end{aligned}$$

where $\mathbf{n} = [n(v), n(v-L), ..., n(v-(K_o-1)L)]^{\mathrm{T}}$ is the noise vector component. Since $n(i)$ is assumed to be white, its covariance matrix is $E[\mathbf{n}\mathbf{n}^{\mathrm{H}}] = (N_o B)\mathbf{I}_{K_o}$. The covariance matrix of the fading components is $E\left[\mathbf{z}\mathbf{z}^{\mathrm{H}}\right] = \Omega\mathbf{R}$. Subsequently, (4.33) is simplified to

$$\breve{\Omega} = \Omega\mathbf{f}_j^{\mathrm{H}}\mathbf{R}\mathbf{f}_j + \frac{N_o B}{a_p^2}\|\mathbf{f}_j\|^2. \tag{4.34}$$

Consider that the power of the pilot signal $a_p^2$ is equal to the average data signal power $\bar{S}$, and the average SNR $\Gamma = E[|\alpha|^2]\bar{S}/(N_o B) = \Omega\bar{S}/(N_o B)$, thus

$$\frac{N_o B}{a_p^2} = \frac{\Omega}{\Gamma}. \tag{4.35}$$

The ratio, $r$, is therefore simplified to

$$r = \frac{\breve{\Omega}}{\Omega} = \mathbf{f}_j^{\mathrm{H}}\mathbf{R}\mathbf{f}_j + \frac{\|\mathbf{f}_j\|^2}{\Gamma}. \tag{4.36}$$

### 4.4.2 Correlation Coefficient

The correlation coefficient between the predicted instantaneous SNR, $\breve{\gamma} = \frac{\breve{\alpha}^2 \bar{S}}{N_o B}$, and the true instantaneous SNR, $\gamma = \frac{\alpha^2 \bar{S}}{N_o B}$, is defined as [24]

$$\rho = \frac{\mathrm{Cov}(\breve{\gamma}, \gamma)}{\sqrt{\mathrm{Var}(\breve{\gamma})\mathrm{Var}(\gamma)}}, \tag{4.37}$$

where

$$\begin{aligned}
\mathrm{Cov}(\breve{\gamma}, \gamma) &= \frac{\bar{S}}{N_o B}\left(E\left[\breve{\alpha}^2\alpha^2\right] - E\left[\breve{\alpha}^2\right]E\left[\alpha^2\right]\right) && (4.38)\\
&= \left(\frac{\bar{S}}{N_o B}\right)\mathrm{Cov}(\breve{\alpha}^2, \alpha^2), && (4.39)\\
\mathrm{Var}(\gamma) &= \frac{\bar{S}}{N_o B}\left(E\left[\alpha^2\alpha^2\right] - E\left[\alpha^2\right]E\left[\alpha^2\right]\right) && (4.40)\\
&= \left(\frac{\bar{S}}{N_o B}\right)\mathrm{Var}(\alpha^2), && (4.41)\\
\mathrm{Var}(\breve{\gamma}) &= \frac{\bar{S}}{N_o B}\left(E\left[\breve{\alpha}^2\breve{\alpha}^2\right] - E\left[\breve{\alpha}^2\right]E\left[\breve{\alpha}^2\right]\right) && (4.42)\\
&= \left(\frac{\bar{S}}{N_o B}\right)\mathrm{Var}(\breve{\alpha}^2). && (4.43)
\end{aligned}$$

Thus $\rho$ in (4.37) can be written in terms of the statistics of the channel gain $\alpha$ and the predicted channel gain $\breve{\alpha}$ as

$$\rho = \frac{\mathrm{Cov}(\breve{\alpha}^2, \alpha^2)}{\sqrt{\mathrm{Var}(\breve{\alpha}^2)\mathrm{Var}(\alpha^2)}}. \tag{4.44}$$

With $\alpha^2$ and $\breve{\alpha}^2$ being exponentially-distributed, the respective first two moments can be written as [43, ch.2]

$$\begin{aligned}
E\left[\alpha^2\right] &= \Omega, && (4.45)\\
\mathrm{Var}(\alpha^2) &= \Omega^2, && (4.46)\\
E\left[\breve{\alpha}^2\right] &= \breve{\Omega}, && (4.47)\\
\mathrm{Var}(\breve{\alpha}^2) &= \breve{\Omega}^2. && (4.48)
\end{aligned}$$

Using (4.45)-(4.48) in (4.44), the correlation coefficient can be written as

$$\rho = \frac{E\left[\alpha^2\breve{\alpha}^2\right] - \Omega^2 r}{\Omega^2 r}, \tag{4.49}$$

where the ratio $r$ is shown in (4.36). With the term $E\left[\alpha^2\breve{\alpha}^2\right] = \Omega^2|\mathbf{f}_j^{\mathrm{H}}|^2 + \Omega^2 r$ derived in [24], the expression for $\rho$ can be simplified to

$$\rho = \frac{|\mathbf{f}_j^{\mathrm{H}}|^2}{r} = \frac{|\mathbf{f}_j^{\mathrm{H}}|^2}{\mathbf{f}_j^{\mathrm{H}}\mathbf{R}\mathbf{f}_j + \frac{\|\mathbf{f}_j\|^2}{\Gamma}}. \tag{4.50}$$

### 4.4.3 Relationship between $r$ and $\rho$

It has been proven in [52] that by substituting the filter coefficients $\mathbf{f}_j$ (4.24) into the expression in (4.36), $r$ is simplified to

$$r = \mathbf{f}_j^{\mathrm{T}}\left(\mathbf{R} + \frac{1}{\Gamma}\mathbf{I}_{K_o}\right)^{-1}\mathbf{r}_j. \tag{4.51}$$

Similarly, based on the filter coefficients $\mathbf{f}_j$ (4.24), $\rho$ in (4.50) can be simplified to

$$\rho = \mathbf{f}_j^{\mathrm{T}}\left(\mathbf{R} + \frac{1}{\Gamma}\mathbf{I}_{K_o}\right)^{-1}\mathbf{r}_j. \tag{4.52}$$

Therefore, in the MAP-optimal predictor scheme, the ratio $r$ and the correlation coefficient $\rho$ are equal.

### 4.4.4 Selection of $(L, K_o)$ and its impact on $\rho$

It is clear that the correlation coefficient $\rho$ is dependent on the pilot-symbol period $L$ and the length of the filter $K_o$. This section outlines the rule of thumb for choosing the $(L, K_o)$ values, and further illustrates the impact that $L$ and $K_o$ have on $\rho$ through numerical results.

The choice of the values for $L$ and $K_o$ can be determined as follow.

1) The pilot symbols should be transmitted at a rate of $\geq 2 \times f_d$. This is inline

with the sampling theorem. Therefore [24],

$$L \leq \frac{1}{2f_d T_s}, \tag{4.53}$$

which is largely valid when the pilot symbols are not corrupted by noise.
2) For a noncausal detection, Meyr *et al.* [55, ch14, sec 14.2.2] suggested that the quasioptimal performance will be achieved if

$$K_o L >> \frac{1}{2f_D T_s}. \tag{4.54}$$

The correlation coefficient of the channel predictor, $\rho$, based on expression (4.52) is used for numerical computation. Note that the elements of $\mathbf{r}_j$ and $\mathbf{R}$ are obtained from the familiar Jakes' model [57]. That is, the correlation function $R(\tau)$ can be expressed as

$$R(\tau) = J_0\left(2\pi f_d \tau\right), \tag{4.55}$$

where $J_0(.)$ denotes the zero-order Bessel function of the first kind.

Figures 4.3 and 4.4 show the results of $\rho$ as a function of the normalized delay time $f_d T_s j$ for various $L$ and $K_o$ values. The normalized Doppler spread $f_d T_s$ is set to 0.001, and an arbitrary average SNR value, $\Gamma = 20$ dB, is chosen. Based on (4.53), $L \leq 200$. In Figure 4.3 the results for $L = 10, 15, 20$ are illustrated as these are typical values of pilot-symbol period that have been adopted in the current mobile systems. (See for example the WCDMA system [13]). For a fixed value of $L = 10$, $K_o$ will be $>> 50$ based on equation (4.54). Therefore $\rho$ in Figure 4.4 is computed for $K_o = 100, 500, 1000$. The two figures suggest that the choice of $K_o$ has a greater impact on $\rho$ variations if $K_o$ is set too near to the lower limit of 50.

Since $\rho$ is also a function of the average SNR, $\Gamma$, it will be of interest to show the variation of $\rho$ as a function of $\Gamma$. Figure 4.5 shows that the rate of change in $\rho$ value increases as SNR becomes lower. This implies a decrease in

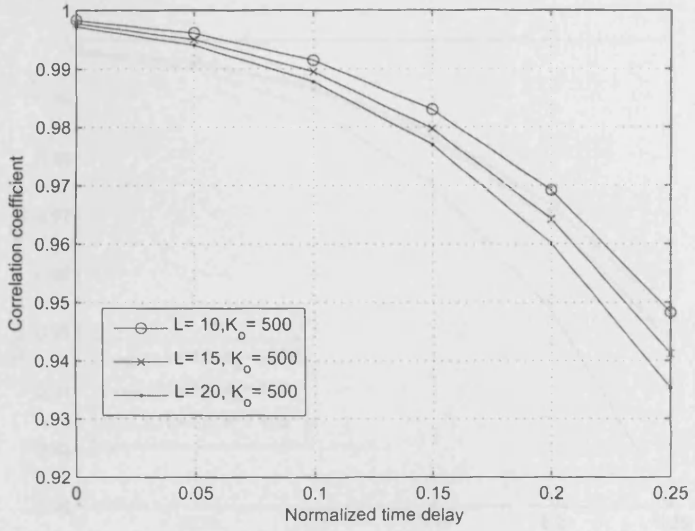


Figure 4.3: Correlation coefficient $\rho$ as a function of normalized time delay $f_d T_s j$. For $\Gamma = 20$ dB, $L = 10, 15, 20$ and $K_o = 500$.

the correlation between a true channel gain and its predicted channel gain as the channel condition degrades.

The numerical results in Figures 4.3-4.5 illustrate that correlation coefficient $\rho$ is dependent on both the channel conditions (parameters such as SNR and Doppler spread) and the channel predictor parameters ($L$ and $K_o$). The case when $\rho < 1$ relates to an imperfect CSI scenario since inaccurate channel state information is known at the receiver and/or transmitter. Subsequently, the performance of the LA system in terms of spectral efficiency and BER parameters will be affected.

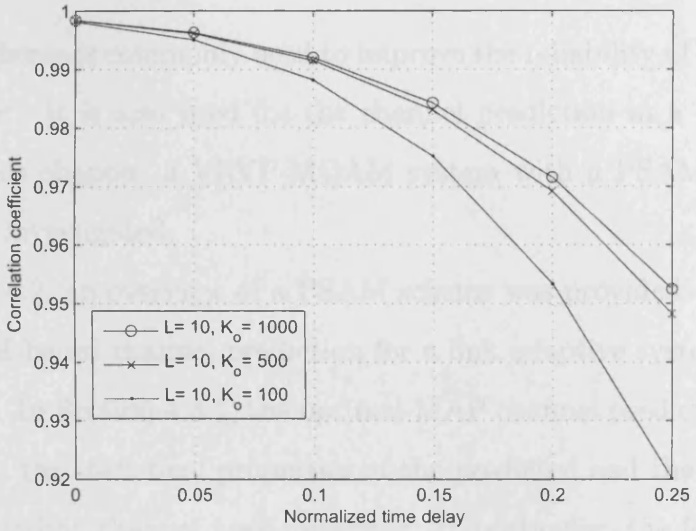


Figure 4.4: Correlation coefficient $\rho$ as a function of normalized time delay $f_d T_s j$. For $\Gamma = 20$ dB, $L = 10$ and $K_o = 100, 500, 1000$.

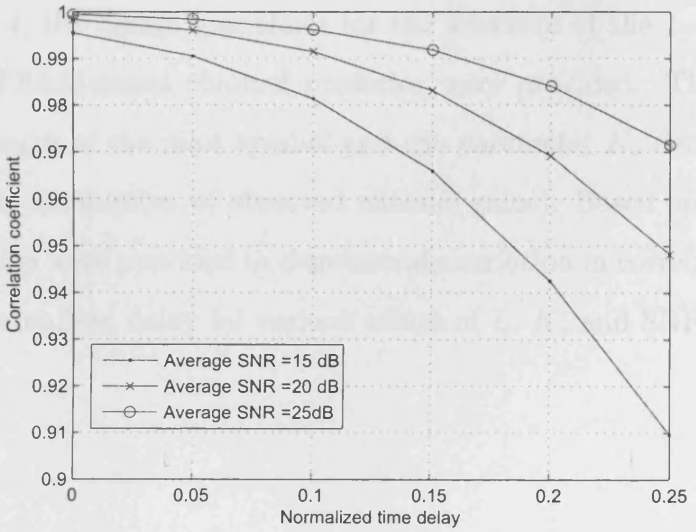


Figure 4.5: Correlation coefficient $\rho$ as a function of normalized time delay $f_d T_s j$. For $\Gamma = 15, 20, 15$ dB, $L = 10$ and $K_o = 500$.

## 4.5 Summary

The PSAM scheme is commonly used to improve the reliability of signal detection at the receiver. It is also used for the channel prediction in a link adaptation scheme. In this chapter, a VRVP-MQAM system with a PSAM-based channel predictor was investigated.

In Section 4.2, an overview of a PSAM scheme was provided. Then, a framework of PSAM-based channel prediction for a link adaptive system was detailed in Section 4.3. In Section 4.3.1, the optimal-MAP channel predictor was derived. In Section 4.4, the statistical properties of the predicted and the true amplitude of a Rayleigh fading channel were presented. In particular, the focus was on the derivations of the parameters $\rho$ and $r$. The parameter $\rho$ denotes the correlation coefficient of the predicted channel gain, $\breve{\alpha}$, and the true value, $\alpha$. The parameter $r$ denotes the ratio of the expectation of $\alpha$ to the expectation of $\breve{\alpha}$. Subsequently, it was shown that the correlation coefficient $\rho$ and the ratio $r$ are equal. Finally, in Section 4.4.4, the design guidelines for the selection of the $L$ and $K_o$ parameters for the PSAM-based channel predictor were provided. The parameter $L$ denotes the length of the pilot symbol and the parameter $K_o$ denotes the length of the filter (or the number of observed channel gains). Based on the guidelines, numerical results were provided to demonstrate variation in correlation coefficient in terms of normalised delay for various values of $L$, $K_o$ and SNR.

# Chapter 5

# VRVP-MQAM System under Imperfect CSI Knowledge

*This chapter provides one of the author's novel contributions. The work has been accepted for publication in IEEE Transactions on Communications* [58].

## 5.1 Introduction

The impact of inaccurate channel state information at the transmitter for a variable rate variable power multilevel quadrature amplitude modulation (VRVP-MQAM) system over a Rayleigh flat-fading channel is investigated. A system model is proposed with rate and power adaptation based on the estimates of instantaneous SNR and BER. A PSAM [50] scheme is used for SNR estimation. The BER estimator is derived using a MAP approach and a simplified closed-form solution is obtained as a function of only the second order statistical characterization of the channel state imperfection. Based on the proposed system model, rate and power adaptation is derived for the optimization of spectral efficiency

subject to an average power constraint and an instantaneous BER requirement. The performance of the VRVP-MQAM system under imperfect CSI is evaluated.

This chapter is organized as follows. In Section 5.2, the proposed system model is introduced. Next, the analytical approach in determining the BER estimate is provided in Section 5.3. The derivation for the analytical expressions for optimum rate and power adaptation that maximize spectral efficiency is presented in Section 5.4. In Section 5.5, the performance of the proposed VRVP-MQAM system based on two scenarios is provided. The first scenario is based on ideal CSI, i.e. perfect channel estimate at the receiver and feedback with negligible delay; and the second scenario is based on partial CSI, i.e. an inaccurate channel estimate at the receiver but with negligible feedback delay. Next the performance of the proposed VRVP-MQAM system is compared with two other MQAM systems: 1) a VRVP-MQAM system that employs adaptations based on an ideal CSI assumption, and 2) a nonadaptive transmission MQAM system. Finally, a summary is provided in Section 5.6, and proofs for all derivations are provided in Appendix A.

## 5.2 System Model

The block diagram of the proposed VRVP-MQAM system for a single user flat-fading channel is shown in Figure 5.1. Both the transmitter and the receiver employ a single antenna for transmission and reception. The channel is modelled in discrete-time, denoted by index $i$, with statistically stationary and ergodic time-varying gain $\alpha(i) = |c(i)|$, and zero mean AWGN $n(i)$. A PSAM [50] method is used for the estimation of the channel gain $\alpha(i)$ and it is represented by a channel estimator block in Figure 5.1. At time $i$, based on the channel gain and its respective SNR, the channel estimator will know the values of the

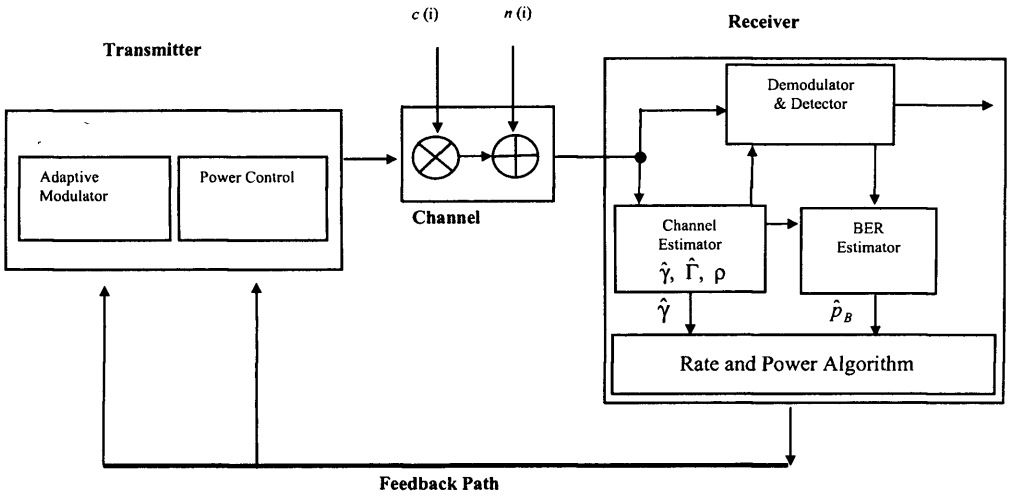


Figure 5.1: Block diagram of the proposed variable rate variable power MQAM system based on BER and SNR estimates. CSI parameters include: instantaneous SNR estimate $\hat{\gamma}$, average SNR estimate $\hat{\Gamma}$, correlation coefficient $\rho$ and BER estimate $\hat{p}_B$.

instantaneous received SNR estimate, the average SNR estimate and the correlation coefficient between the true channel SNR and its estimate. For a constant average transmit power $\bar{S}$, the instantaneous received SNR $\gamma(i)$ is defined as

$$\gamma(i) = \frac{\bar{S}[\alpha(i)]^2}{N_o B}, \tag{5.1}$$

and its estimate is defined as

$$\hat{\gamma}(i) = \frac{\bar{S}[\hat{\alpha}(i)]^2}{N_o B}, \tag{5.2}$$

where $\hat{\alpha}(i)$ is the estimate of $\alpha(i)$, $B$ denotes the received signal bandwidth and $N_o$ denotes the noise power spectral density. The average received SNR is $\Gamma = E[\gamma]$ and its estimate is $\hat{\Gamma} = E[\hat{\gamma}]$, where $E[.]$ denotes the statistical expectation operator. At time $i$, the transmitter adapts to channel variations by adjusting its transmitted power $S(\hat{\gamma}(i))$ based on $\hat{\gamma}(i)$ which is fed back from the receiver.

With power adaptation, the estimate of the SNR at the receiver can be written as

$$\sigma\left(\hat{\gamma}\left(i\right)\right) = \hat{\gamma}\left(i\right) S\left(\hat{\gamma}\left(i\right)\right)/\bar{S}. \tag{5.3}$$

An instantaneous BER estimate $\hat{p}_B\left(i\right)$ is obtained from the proposed BER estimator (full derivation will be shown in Section 5.3) using the Bayesian estimation approach [59]. For simplicity, the discrete time reference $i$ will be omitted in the remaining sections.

The transmitter adapts its rate by adjusting the constellation size $M$ of the MQAM scheme based on $\hat{\gamma}$ and a required BER target BERT. With data sent at $k\left(\hat{\gamma}\right) = \log_2\left(M\left(\hat{\gamma}\right)\right)$ bits/symbol, the instantaneous data rate is $k\left(\hat{\gamma}\right)/T_s$ bits/sec (bps), where $T_s$ denotes the symbol time duration, and $M\left(\hat{\gamma}\right)$ denotes the number of constellation points as a function of $\hat{\gamma}$. The spectral efficiency of an MQAM scheme can be expressed as its average data rate per unit bandwidth $R/B$. Assuming Nyquist data pulses of duration $T_s = 1/B$, the spectral efficiency (in bps/Hz) for continuous rate is

$$\frac{R}{B} = \int_{\hat{\gamma}} k\left(\hat{\gamma}\right) f_{\hat{\gamma}}(\hat{\gamma})\, d\hat{\gamma}, \tag{5.4}$$

where $f_{\hat{\gamma}}\left(\hat{\gamma}\right)$ denotes the PDF of $\hat{\gamma}$. The aim is to obtain optimal rate and power to maximise spectral efficiency (5.4) subject to an average power constraint

$$E\left[S\left(\hat{\gamma}\right)\right] = \int_{\hat{\gamma}} S(\hat{\gamma}) f_{\hat{\gamma}}(\hat{\gamma})\, d\hat{\gamma} = \bar{S}, \tag{5.5}$$

and an instantaneous BER requirement.

## 5.3 BER Estimate

The MAP approach is adopted to find the estimate of BER. The objective is to obtain an expression for the BER estimate $\hat{p}_B$ in terms of the observation

of $\hat{\gamma}$. The next section summarises this approach, and is followed by detailed derivations. The numerical results will be presented in the subsequent sections.

### 5.3.1 Derivations and Results

The instantaneous BER $p_B$ will be estimated by adopting the MAP-optimal approach. Hence, the $p_B$ that maximizes the conditional PDF $f_{p_B|\hat{\gamma}}(p_B|\hat{\gamma})$ will be derived using Bayes' theorem [37]

$$f_{p_B|\hat{\gamma}}(p_B|\hat{\gamma}) = \frac{f_{\hat{\gamma}|p_B}(\hat{\gamma}|p_B)\, f_{p_B}(p_B)}{f_{\hat{\gamma}}(\hat{\gamma})}, \tag{5.6}$$

where $f_{p_B}(p_B)$ denotes the PDF of $p_B$, and $f_{\hat{\gamma}|p_B}(\hat{\gamma}|p_B)$ is the conditional PDF of $\hat{\gamma}$ given $p_B$. Since $f_{\hat{\gamma}}(\hat{\gamma})$ is a normalization factor, (5.6) is simplified to a final form of the MAP equation

$$I_{MAP}(p_B) = f_{p_B,\hat{\gamma}}(p_B, \hat{\gamma}), \tag{5.7}$$

where $f_{p_B,\hat{\gamma}}(p_B, \hat{\gamma})$ is the joint PDF of $p_B$ and $\hat{\gamma}$. Therefore, finding the value of $p_B$ that maximizes $f_{p_B|\hat{\gamma}}(p_B|\hat{\gamma})$ is equivalent to finding the maximum of (5.7). The estimation of $\hat{p}_B$ can thus be obtained from the solution of

$$\frac{\partial I_{MAP}}{\partial p_B} = 0. \tag{5.8}$$

The closed-form expressions for $f_{p_B,\hat{\gamma}}(p_B, \hat{\gamma})$ and $\hat{p}_B$ is presented as follows.

In a VRVP-MQAM system with perfect CSI assumption, rate adaptation can be adjusted according to [4]

$$M(\gamma) = 1 + \frac{c_2\gamma}{-\ln(\mathrm{BERT}/c_1)}\frac{S(\gamma)}{\bar{S}}, \tag{5.9}$$

also defined in (3.30). However, in a practical system, the receiver will only have the knowledge of the SNR estimate $\hat{\gamma}$ through a particular channel gain estimator. If the estimated channel at the receiver is inaccurate, and if the

estimate is fed back to the transmitter with negligible delay, the adaptive rate and power algorithm will adjust the MQAM constellation size and transmitter power level as $M(\hat{\gamma})$ and $S(\hat{\gamma})$ instead of $M(\gamma)$ and $S(\gamma)$. Therefore, with the knowledge of only the channel estimate, $M(\hat{\gamma})$ is adjusted based on $\hat{\gamma}$ and BERT according to

$$M(\hat{\gamma}) = 1 + \frac{c_2\hat{\gamma}}{-\ln(\mathrm{BERT}/c_1)}\frac{S(\hat{\gamma})}{\overline{S}} \tag{5.10}$$

$$= 1 + \frac{c_2\sigma(\hat{\gamma})}{-\ln(\mathrm{BERT}/c_1)}. \tag{5.11}$$

Using the generic approximation of the BER expression for an MQAM scheme, the instantaneous BER at the receiver can be expressed as [4, eqn (42)]

$$p_B(\gamma,\hat{\gamma}) = c_1 \exp\left(-\frac{c_2\gamma}{M(\hat{\gamma})-1}\frac{S(\hat{\gamma})}{\overline{S}}\right), \tag{5.12}$$

where $c_1$ and $c_2$ are positive real numbers [4,5]. Alternatively, the BER expression in (5.12) can be expressed as

$$p_B(\gamma,\hat{\gamma}) = c_1 \exp\left(-\frac{c_2\sigma(\hat{\gamma})}{M(\hat{\gamma})-1}\frac{\gamma}{\hat{\gamma}}\right), \tag{5.13}$$

where $\sigma(\hat{\gamma})$ is defined in (5.3). Let $\sigma$ be a particular value of $\sigma(\hat{\gamma})$ at the receiver, and $M$ be the corresponding value of $M(\hat{\gamma})$ determined at the transmitter. The corresponding instantaneous BER at the receiver will be

$$p_B = c_1 \exp\left(-\frac{c_2\sigma}{M-1}\frac{\gamma}{\hat{\gamma}}\right). \tag{5.14}$$

For a Rayleigh flat-fading channel using the PSAM method for channel estimation [51], the amplitude $\alpha$ and its estimate $\hat{\alpha}$ for the channel gain have been shown to have a bivariate Rayleigh distribution [51]. Thus, the equivalent joint PDF of random variables $\gamma$ and $\hat{\gamma}$, denoted as $f_{\gamma,\hat{\gamma}}(\gamma,\hat{\gamma})$, can be written as (Refer to Appendix A.4 for the proof.)

$$f_{\gamma,\hat{\gamma}}(\gamma,\hat{\gamma}) = \frac{1}{(1-\rho)\Gamma\hat{\Gamma}} I_0\left(\frac{2\sqrt{\rho}}{1-\rho}\sqrt{\frac{\gamma\hat{\gamma}}{\Gamma\hat{\Gamma}}}\right)\exp\left(-\frac{1}{(1-\rho)}\left(\frac{\gamma}{\Gamma}+\frac{\hat{\gamma}}{\hat{\Gamma}}\right)\right)u(\gamma)\,u(\hat{\gamma}), \tag{5.15}$$

where $I_0(.)$ is the zero order modified Bessel function and $u(.)$ is the unit step function. The parameter $\rho$ defines the correlation coefficient between $\gamma$ and $\hat{\gamma}$. In practical situations, the information about $\rho$ at the transmitter could be assumed to be available through its estimate at the receiver. For a system employing PSAM with MAP-optimal prediction of SNR at pilot symbol instants under Rayleigh fading having Jakes spectrum, $\rho$ has been analytically derived in [24] (and provided in Section 4.4) as a function of normalized Doppler spread, namely the Doppler frequency $f_d$ times symbol duration $T_s$.

By exploiting (5.14) and (5.15), and through a transformation of random variables, a closed-form expression can be obtained for $f_{p_B,\hat{\gamma}}(p_B,\hat{\gamma})$, (Refer to Appendix A.1 for the proof.)

$$f_{p_B,\hat{\gamma}}(p_B,\hat{\gamma}) = c(p_B)\, I_0(b(p_B)\,\hat{\gamma}) \exp(-a(p_B)\,\hat{\gamma}), \tag{5.16}$$

where

$$a(p_B) = \frac{1}{1-\rho}\left(\frac{-(M-1)}{\sigma c_2}\ln\left(\frac{p_B}{c_1}\right)\frac{1}{\Gamma} + \frac{1}{\hat{\Gamma}}\right), \tag{5.17}$$

$$b(p_B) = \frac{2\sqrt{\rho}}{1-\rho}\sqrt{\frac{-(M-1)}{\sigma c_2}\ln\left(\frac{p_B}{c_1}\right)\frac{1}{\Gamma\hat{\Gamma}}}, \tag{5.18}$$

$$c(p_B) = \frac{(M-1)\,\hat{\gamma}}{p_B c_2 \sigma (1-\rho)\,\Gamma\hat{\Gamma}}. \tag{5.19}$$

Based on (5.7), and removing terms that are not functions of $p_B$, the final form for the MAP equation can be expressed as

$$I_{MAP} = \frac{1}{p_B} I_0(b(p_B)\,\hat{\gamma}) \exp(-a(p_B)\,\hat{\gamma}). \tag{5.20}$$

To perform the operation $\frac{\partial I_{MAP}}{\partial p_B}$, (5.20) is approximated using an approximation on $I_0(.)$ [45], (Refer to Appendix A.2 for the proof.)

$$I_{MAP_{eq}} = \frac{1}{p_B}\frac{\exp(b(p_B)\,\hat{\gamma})}{\sqrt{2\pi b(p_B)\,\hat{\gamma}}} \exp(-a(p_B)\,\hat{\gamma}), \tag{5.21}$$

where $I_{MAP_{eq}}$ denotes the approximate form of the MAP equation based on high SNR estimate $\hat{\gamma}$. Finally, an approximate closed-form expression for $\hat{p}_B$ is obtained as

$$\hat{p}_B \approx c_1 \exp\left(\frac{\rho \frac{-\sigma c_2}{M-1}\frac{\Gamma}{\hat{\Gamma}}}{\left((1-\rho)\frac{\sigma c_2}{M-1}\frac{\Gamma}{\hat{\gamma}}-1\right)^2}\right), \qquad \hat{\gamma} > \hat{\gamma}_{th}, \tag{5.22}$$

where $\hat{\gamma}_{th}$ is obtained as $\hat{\gamma}_{th} \triangleq (1-\rho)\left(-\ln\left(\frac{\text{BERT}}{c_1}\right)\right)\Gamma$. Exploiting numerical analysis to obtain the maximum value of $I_{MAP}$ and the corresponding BER estimate using the exact expression (5.20) leads to the result that realistic $\hat{p}_B$ values greater than zero exist only for the range of $\hat{\gamma} > \hat{\gamma}_{th}$. Otherwise, the optimum value for $\hat{p}_B$ will be zero. Therefore transmission will be stopped for $\hat{\gamma} \leq \hat{\gamma}_{th}$, as there is no practical and reliable BER estimate (and hence no reliable channel) available in that case. The proof of the $\hat{p}_B$ and $\hat{\gamma}_{th}$ expressions, and the numerical analysis are provided in Appendix A.3.

From (5.10), it is noted that for a given BERT and $\hat{\gamma}$, we could write $\frac{-\sigma c_2}{M-1} = \ln(\text{BERT}/c_1)$. Therefore using (5.10) and (5.22), the estimate of BER can be simplified as

$$\hat{p}_{B,\,\text{BERT}}(\hat{\gamma}) = c_1 \exp\left(\frac{\ln(\text{BERT}/c_1)\frac{\Gamma}{\hat{\Gamma}}\rho}{\left(-\ln(\text{BERT}/c_1)\frac{\Gamma}{\hat{\gamma}}(1-\rho)-1\right)^2}\right). \tag{5.23}$$

Note that the obtained BER estimate equation (5.23) is a useful expression as it relates to the channel state imperfection: i) the ratio $\Gamma/\hat{\Gamma}$ and ii) the correlation coefficient $\rho$. Subsequently, it will be shown in the next section that rate and power adaptation techniques derived based on the BER estimate will embed the statistical information of the channel state imperfection.

## 5.4 Optimal Rate and Power Adaptation

With the BER estimator known, the proposed rate and power adaptation that is based on the SNR estimate $\hat{\gamma}$ and the BER estimate $\hat{p}_B$ is now outlined. Consider that $\hat{\gamma}$ and the BER estimate $\hat{p}_B(\hat{\gamma})$ are known at the receiver. The corresponding MQAM constellation size $M_{\hat{p}_B}(\hat{\gamma})$ becomes

$$M_{\hat{p}_B}(\hat{\gamma}) = 1 + \frac{c_2\hat{\gamma}}{-\ln(\hat{p}_B(\hat{\gamma})/c_1)}\frac{S_{\hat{p}_B}(\hat{\gamma})}{\bar{S}} \tag{5.24}$$

$$= 1 + \frac{K\hat{\Gamma}}{\rho\Gamma}\left\{\frac{c_2\Gamma}{K\hat{\gamma}}(1-\rho) - 1\right\}^2 \frac{S_{\hat{p}_B}(\hat{\gamma})}{\bar{S}}\hat{\gamma}, \tag{5.25}$$

where $K = \frac{c_2}{-\ln\left(\frac{\text{BERT}}{c_1}\right)}$ and $S_{\hat{p}_B(\hat{\gamma})}$ is the power allocated at the transmitter. The corresponding transmission rate is

$$k_{\hat{p}_B}(\hat{\gamma}) = \log_2\left(M_{\hat{p}_B}(\hat{\gamma})\right). \tag{5.26}$$

Maximising spectral efficiency subject to the average power constraint $\bar{S}$, the optimal power control $S_{\hat{p}_B}(\hat{\gamma})$ is obtained from the following Lagrangian equation

$$F(S_{\hat{p}_B}(\hat{\gamma})) = \int_{\hat{\gamma}} k_{\hat{p}_B}(\hat{\gamma}) f(\hat{\gamma})\, d\hat{\gamma} + \mu\left[\int_{\hat{\gamma}} S_{\hat{p}_B}(\hat{\gamma}) f(\hat{\gamma})\, d\hat{\gamma} - \bar{S}\right], \tag{5.27}$$

where $\mu$ denotes the Lagrange multiplier. Optimal power $S_{\hat{p}_B}(\hat{\gamma})$ is obtained from the solution of $\partial F/\partial S_{\hat{p}_B}(.) = 0$ as

$$\frac{S_{\hat{p}_B}(\hat{\gamma})}{\bar{S}} = \begin{cases} U - \frac{\frac{\Gamma}{\hat{\Gamma}}\rho}{K\hat{\gamma}\left\{\frac{c_2}{K}\frac{\Gamma}{\hat{\gamma}}(1-\rho)-1\right\}^2}, & S_{\hat{p}_B}(\hat{\gamma}) \geq 0,\ k_{\hat{p}_B}(\hat{\gamma}) \geq 1, \\ 0, & \text{otherwise}, \end{cases} \tag{5.28}$$

where $U = \frac{1}{-\lambda\bar{S}\ln(2)}$ is a constant value found through numerical search such that the average power constraint (5.5) is satisfied. Subsequently, by invoking the optimal power adaptation expression (5.28) in (5.25), the optimal rate adaptation is obtained as

$$k_{\hat{p}_B}(\hat{\gamma}) = \begin{cases} \log_2\left[\frac{K\hat{\Gamma}}{\rho\Gamma}\left\{\frac{c_2}{K}\frac{\Gamma}{\hat{\gamma}}(1-\rho) - 1\right\}^2\hat{\gamma}U\right], & k_{\hat{p}_B}(\hat{\gamma}) \geq 1, \\ 0, & \text{otherwise}. \end{cases} \tag{5.29}$$

Note that $k_{\hat{p}_B}(\hat{\gamma}) \geq 1$ corresponds to a realistic MQAM constellation size $M \geq 2$. For $S_{\hat{p}_B}(\hat{\gamma}) \geq 0$ and $k_{\hat{p}_B}(\hat{\gamma}) \geq 1$, the SNR cutoff threshold can be determined as

$$\hat{\gamma}_0 = \hat{\gamma}_{th} + \chi, \tag{5.30}$$

where $\chi \triangleq \frac{\Gamma}{2KU\hat{\Gamma}} \left[2\rho + 2\sqrt{\rho\left(2Uc_2\hat{\Gamma} - 2Uc_2\hat{\Gamma}\rho + \rho\right)}\right]$ is greater than or equal to 0. (The proof of (5.30) is provided in Appendix A.5.) Hence, $S_{\hat{p}_B}(\hat{\gamma}) \geq 0$ and $k_{\hat{p}_B}(\hat{\gamma}) \geq 1$ imply that $\hat{\gamma} \geq \hat{\gamma}_0$ and transmission is allowed. These conditions also verify the appropriateness of using the derived BER estimator (5.22) since $\hat{\gamma}_0$ is always greater than $\hat{\gamma}_{th}$.

## 5.5 Results and Discussion

This section presents the performance of the VRVP-MQAM scheme through numerical results. The channel variations are modelled according to a Rayleigh distribution with $f_{\hat{\gamma}}(\hat{\gamma}) = \frac{1}{\hat{\Gamma}} \exp\left(-\frac{\hat{\gamma}}{\hat{\Gamma}}\right)$ and $\hat{\Gamma}$ is set to $\rho\Gamma$ [24]. No restriction on the constellation size of the MQAM system is assumed, that is, $M$ can be a non-integer value. The BER target is $10^{-3}$ and $c_1 = 0.2, c_2 = 1.5$ [4].

Based on the analytical expressions derived in the previous section, the performance of the proposed VRVP-MQAM system that employs adaptations based on CSI imperfection and MAP-optimal BER estimate will be evaluated. This system is denoted as 'VRVP-MQAM-CSI'. Next, the performance of the VRVP-MQAM-CSI system will be compared with two other MQAM systems. 1) The VRVP-MQAM system that employs adaptations based on an ideal CSI assumption, denoted as a 'VRVP-MQAM' system. 2) A nonadaptive transmission system that employs a constant-rate constant-power MQAM [4], is denoted as a 'CRCP-MQAM' system.

### 5.5.1 Instantaneous Rate and Power in the VRVP-MQAM-CSI System

Consider a system with partial CSI knowledge, that is, an imperfect estimate of the average SNR $\hat{\Gamma}$ is available at the receiver, and is denoted by $\rho\Gamma$. Consider that the feedback of such CSI to the transmitter has negligible delay. For an average SNR value, the solution sets $k_{\hat{p}_B}(\hat{\gamma})$ and $\frac{S_{\hat{p}_B}(\hat{\gamma})}{\bar{S}}$ for various $\rho$ values are obtained using the expressions derived in Section 5.4. Through numerical search, a set of $U$ values corresponding to the particular set of $\rho$ values is obtained. $U$ is also dictated by the instantaneous data rate $k(.) \geq 1$ and positive power requirements. The computed results for $\Gamma = 25$ dB over three settings of $\rho$ values: 0.8, 0.9 and 1 are provided in Figure 5.2 and Figure 5.3. At $\rho = 1$, the transmit power variation $\frac{S_{\hat{p}_B}(\hat{\gamma})}{\bar{S}}$ follows a smooth water-filling profile for $\hat{\gamma}$ beyond a cutoff value $\hat{\gamma}_0$, and the rate $k_{\hat{p}_B}(\hat{\gamma})$ increases linearly as $\hat{\gamma}$ increases beyond $\hat{\gamma}_0$. No data transmission is allowed for $\hat{\gamma}$ below $\hat{\gamma}_0$. Indeed, when $\rho = 1$, the adaptations are exactly the rate and power adaptations observed in [4] and [5] with adaptation based on the assumption of ideal CSI. For $\rho < 1$, higher cutoff SNR values are observed in the rate and power adaptation plots.

As depicted in Figure 5.2 and Figure 5.3, the power and rate adaptations scheme adapts to the CSI-imperfection by transmitting at a higher power level and a higher transmission rate for $\rho < 1$ and for larger SNR values. It is noted that the total average transmitted power is still maintained at $\bar{S}$, and this will be verified in Section 5.5.4.

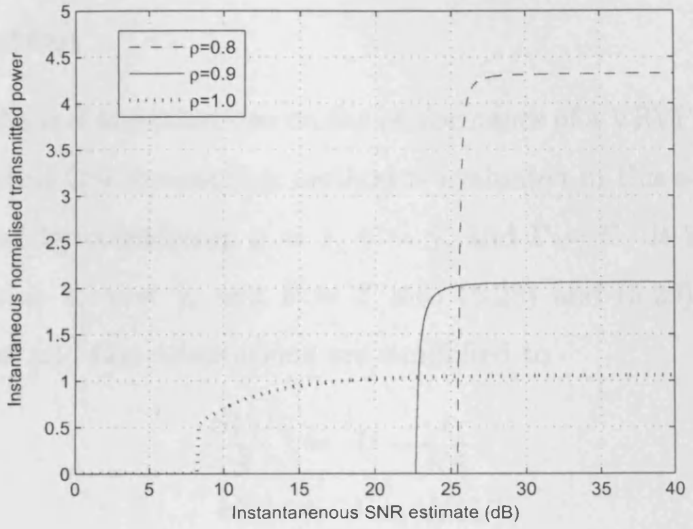


Figure 5.2: VRVP-MQAM-CSI system: instantaneous power $\frac{S_{\hat{p}_B}(\hat{\gamma})}{S}$ as a function of instantaneous SNR estimate $\hat{\gamma}$.

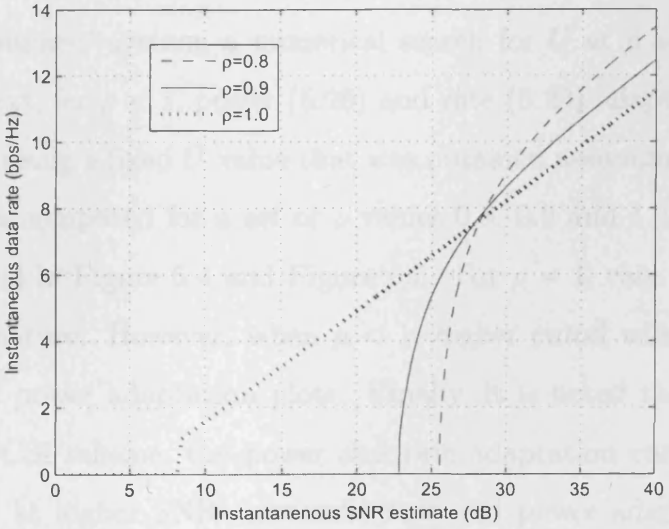


Figure 5.3: VRVP-MQAM-CSI system: instantaneous rate $k_{\hat{p}_B}(\hat{\gamma})$ as a function of instantaneous SNR estimate $\hat{\gamma}$.

### 5.5.2 Instantaneous Rate and Power in the VRVP-MQAM System

The effect of channel imperfections on the performance of a VRVP-MQAM system based on an ideal CSI assumption method is evaluated in this section. An ideal CSI is assumed by considering $\rho = 1$, $\gamma = \hat{\gamma}$, and $\hat{\Gamma} = \Gamma$. It is noted that by substituting $\rho = 1$, $\gamma = \hat{\gamma}$, and $\hat{\Gamma} = \Gamma$ into (5.28) and (5.29), the respective transmit power and rate adaptations are simplified to

$$\frac{S(\hat{\gamma})}{\bar{S}} = U - \frac{1}{K\hat{\gamma}}, \tag{5.31}$$

$$k(\hat{\gamma}) = \log_2 [K\hat{\gamma}U], \tag{5.32}$$

where $S(\hat{\gamma}) \geq 0$ and $k(\hat{\gamma}) \geq 1$. In fact, the optimal solutions (5.31) - (5.32) are those of [4], corresponding to a VRVP-MQAM scheme based on actual SNR ($\gamma$, $\Gamma$) knowledge.

To investigate the impact of CSI imperfection (i.e. $\rho < 1, \hat{\Gamma} = \rho\Gamma, \hat{\gamma} \neq \gamma$) on the 'ideal-assumed' system, a numerical search for $U$ at $\rho = 1$ is performed numerically. Next, for $\rho < 1$, power (5.28) and rate (5.29) adaptations for $\rho < 1$ are determined using a fixed $U$ value that was obtained assuming $\rho = 1$. Numerical results were computed for a set of $\rho$ values 0.8, 0.9 and 1.0, and at $\hat{\Gamma} = 25$ dB, and depicted in Figure 5.4 and Figure 5.5. For $\rho = 1$, rate and power have a water-filling nature. However, when $\rho < 1$, higher cutoff values are observed in the rate and power adaptation plots. Finally, it is noted that unlike in the VRVP-MQAM-CSI scheme, the power and rate adaptation curves converge to the same value at higher SNRs since the rate and power adaptations are not adapting to CSI imperfection. It is therefore clear that the resulting average transmitted power will vary across channel imperfections, which will be verified in Section 5.5.4.

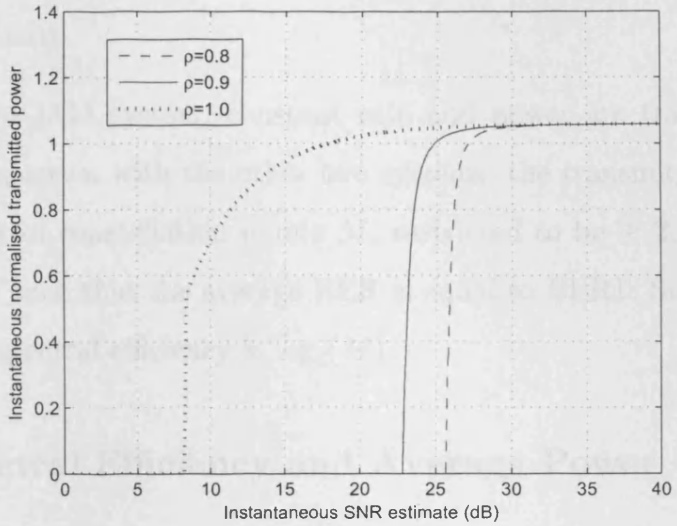


Figure 5.4: VRVP-MQAM system: instantaneous power $\frac{S_{\hat{p}_B}(\hat{\gamma})}{S}$ as a function of instantaneous SNR estimate $\hat{\gamma}$.

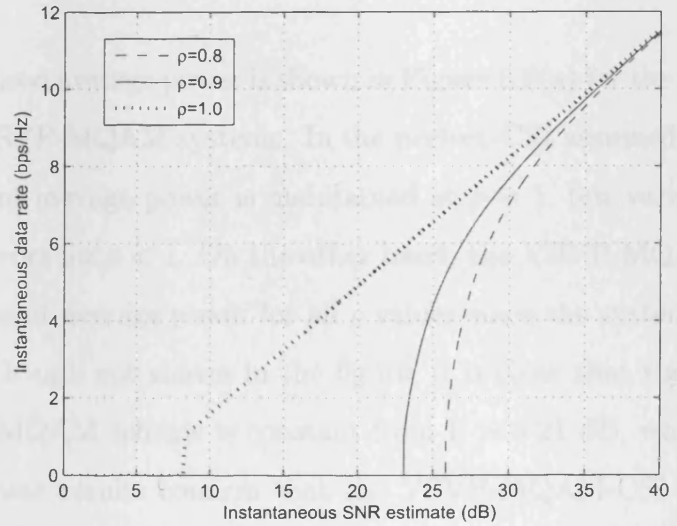


Figure 5.5: VRVP-MQAM system: instantaneous rate $k_{\hat{p}_B}(\hat{\gamma})$ as a function of instantaneous SNR estimate $\hat{\gamma}$.

### 5.5.3 Instantaneous Rate and Power in the CRCP-MQAM System

In the CRCP-MQAM system, constant rate and power are transmitted at all times. For comparison with the other two systems, the transmit power is set to $\bar{S}$. The number of constellation points $M$, restricted to be $\geq 2$, is obtained for a given $\Gamma$ value such that the average BER is equal to BERT. Subsequently, the corresponding spectral efficiency is $\log_2(M)$.

### 5.5.4 Spectral Efficiency and Average Power

The spectral efficiency and the average power can be obtained respectively from:

$$\frac{R}{B} = \int_{\hat{\gamma}_0}^{\infty} k_{\hat{p}_B}(\hat{\gamma})\, f(\hat{\gamma})\, d\hat{\gamma}, \tag{5.33}$$

$$E[S_{\text{norm}}] = \int_{\hat{\gamma}_0}^{\infty} \frac{S_{\hat{p}_B}(\hat{\gamma})}{\bar{S}} f(\hat{\gamma})\, d\hat{\gamma}. \tag{5.34}$$

The normalised average power is shown in Figure 5.6(a) for the VRVP-MQAM-CSI and the VRVP-MQAM systems. In the perfect-CSI assumed VRVP-MQAM system, constant average power is maintained at $\rho = 1$, but variation in the average power occurs for $\rho < 1$. On the other hand, the VRVP-MQAM-CSI system maintains constant average power for all $\rho$ values since the system is adapting to $\rho$ variations. Though not shown in the figure, it is clear that the average power for the CRCP-MQAM scheme is constant from $\Gamma >\approx 21$ dB, which corresponds to $M \geq 2$. These results confirm that the VRVP-MQAM-CSI system has appropriately exploited the power resource variation in the imperfect CSI scenario, and results in a higher spectral efficiency performance over a wide range of SNRs and for practical ranges of $\rho$, as verified in Figure 5.6(b).

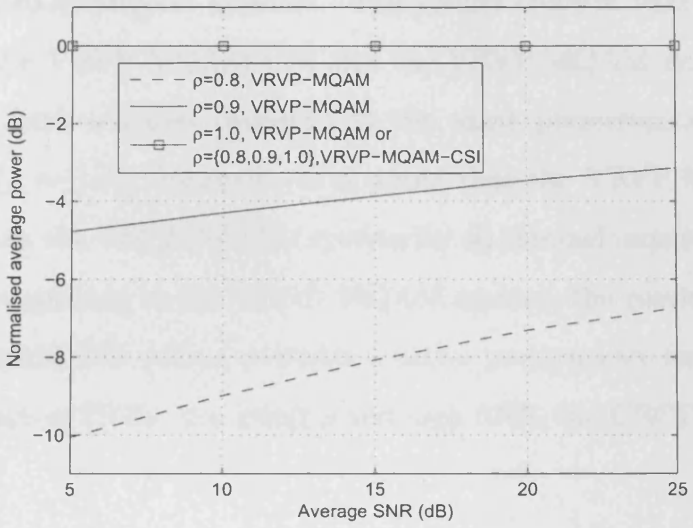


(a) Average normalised power.

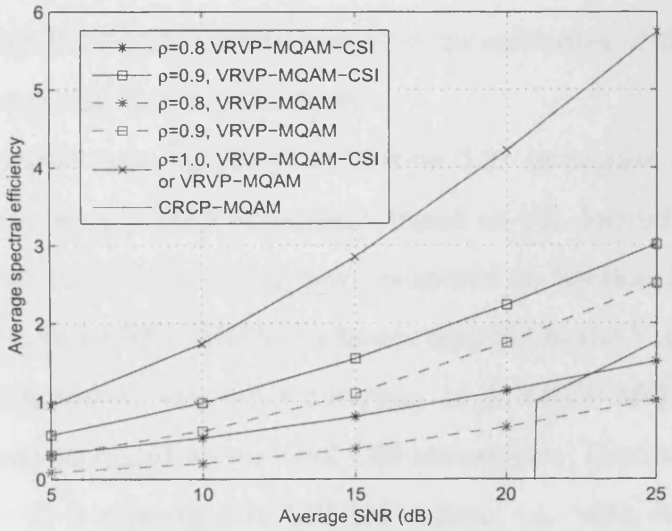


(b) Average spectral efficiency.

Figure 5.6: Average normalised power and spectral efficiency based on correlation coefficient $\rho$. Comparison of VRVP-MQAM-CSI, VRVP-MQAM and CRCP-MQAM systems across average SNR $\Gamma$.

Figure 5.6(b) shows the spectral efficiency for VRVP-MQAM-CSI, VRVP-MQAM and CRCP-MQAM systems. The results confirm that the spectral efficiencies for the VRVP-MQAM-CSI and the VRVP-MQAM systems decline as $\rho$ decreases. Both schemes converge to the same performance in the perfect CSI scenario ($\rho = 1.0$). However, it is noted that the VRVP-MQAM-CSI system outperforms the VRVP-MQAM system for all channel imperfection scenarios ($\rho < 1$). In comparison to the CRCP-MQAM system, the results illustrate that the VRVP-MQAM-CSI system provides a better performance for large value of $\rho$ and a wide range of SNRs. For small $\rho$ and high SNR, the CRCP-MQAM system could be used.

## 5.6 Summary

The proposed VRVP-MQAM system based on the estimates of the instantaneous SNR and BER was outlined in this chapter.

The system model was explained in Section 5.2. In section 5.3, a BER estimator was derived using a MAP approach. Based on the derived BER estimator, adaptive rate and power algorithms were proposed in Section 5.4. The performance of the proposed VRVP-MQAM scheme, denoted as the VRVP-MQAM-CSI system, were compared to two other systems. 1) A VRVP-MQAM system that employed adaptations based on an ideal CSI assumption, denoted as the VRVP-MQAM system. 2) A nonadaptive MQAM system, i.e. with constant rate and constant power, and was denoted as the CRCP-MQAM system. Simulations results were presented and discussed in Section 5.5 for perfect CSI ($\rho = 1$) and imperfect CSI ($\rho < 1$) scenarios. In the perfect CSI scenario, the VRVP-MQAM-CSI system and the VRVP-MQAM system have identical performance in terms of spectral efficiency. In an imperfect CSI scenario, i.e. $\rho < 1$, a degradation in

the spectral efficiency for both systems were observed. However the results also showed that the proposed VRVP-MQAM-CSI system achieves a higher spectral efficiency than the VRVP-MQAM system. In comparison to the CRCP-MQAM system, the results showed that the VRVP-MQAM-CSI system achieves a higher spectral efficiency for a wide range of $\rho$ and SNRs.

# Chapter 6

# VRVP-MQAM System with PSAM-Based Channel Prediction

## 6.1 Performance of the VRVP-MQAM System with Channel Prediction

In this chapter, the algorithms of the Bayesian estimation based VRVP-MQAM system proposed in Chapter 5 are generalized to incorporate a maximum a posteriori (MAP) channel predictor [24] and an MQAM scheme with practical constellation sizes. The proposed rate and power algorithms derived are based on the second order statistical characterization of the CSI. Based on a PSAM scheme, the performance of the VRVP-MQAM system will be evaluated over a Rayleigh flat-fading channel. Simulation results will be used to demonstrate the performance in terms of spectral efficiency and average BER. The results will also be compared to a rate and power adaptation algorithm that is derived with an ideal CSI assumption.

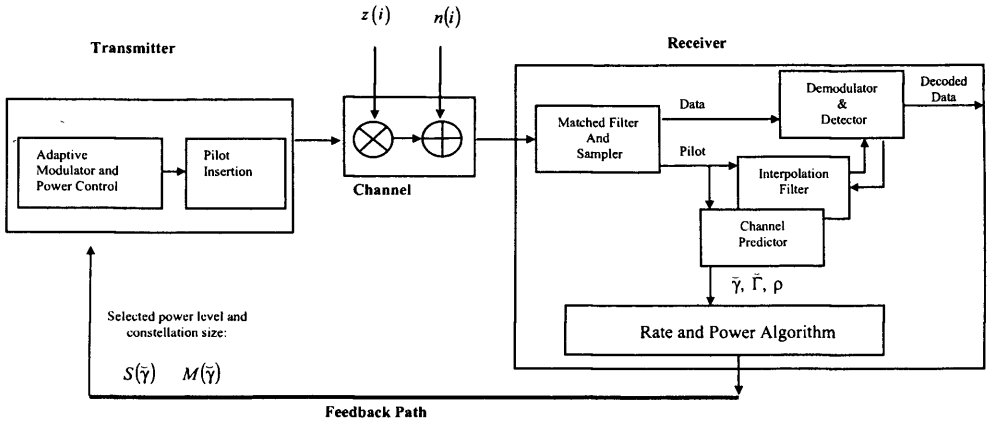


Figure 6.1: Block diagram of the proposed variable rate variable power MQAM system.

## 6.2 System Model

The block diagram of the proposed system is depicted in Figure 6.1. A PSAM scheme with the frame structure shown in Figure 6.2 is used. The pilot symbol is inserted at the first symbol location of each data slot and it is repeated periodically at $L$ symbols interval. For a complex baseband signal $x(i)$, where $i$ denotes the time index, the pilot symbol can be denoted as $x(i - kL)$, where $k \in \{0, 1, 2, ...K_o\}$ and $K_o$ denotes the number of fading observations used in the channel predictor. For simplicity, the power of the pilot signal is set to the average data signal power. At the receiver, after matched filtering and sampling with perfect symbol timing at a rate of $1/T_s$, where $T_s$ is the symbol duration,

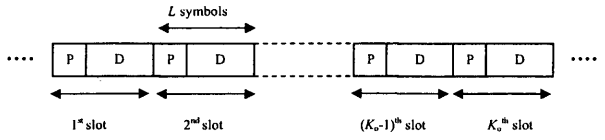


Figure 6.2: Frame structure: 'P' denotes pilot symbol and 'D' denotes data symbols.

the received complex-valued signal over a flat-fading channel can be written as

$$y(i) = z(i)\,x(i) + n(i), \tag{6.1}$$

where $z(i)$ denotes the complex fading and $n(i)$ is circularly symmetric complex AWGN. The noise variance is defined as $\sigma_n^2 = N_o B$, where $N_o$ denotes the noise power spectral density and $B$ denotes the received signal bandwidth. A perfect signal detection based on pilot symbols is assumed at the receiver. The instantaneous received SNR based on the predicted fading $\check{z}(i)$, is defined as $\check{\gamma}(i) = \bar{S}|\check{z}(i)|^2/(N_o B)$, where $\bar{S}$ denotes the average transmit signal power. Note that the actual instantaneous SNR based on the fading channel $z(i)$ is $\gamma(i) = \bar{S}|z(i)|^2/(N_o B)$. The average received SNR is $\Gamma = E[\gamma(i)]$ and its predicted value is $\check{\Gamma} = E[\check{\gamma}(i)]$, where $E[.]$ denotes the statistical expectation operator. Based on $\check{\gamma}(i)$, the transmitter updates its rate and power by adjusting respectively its constellation size $M(\check{\gamma}(i))$ and power $S(\check{\gamma}(i))$. Consider that $M(\check{\gamma}(i))$ and $S(\check{\gamma}(i))$ are computed based on $\check{\gamma}(i)$, which is predicted at the receiver and fed back (as CSI) to the transmitter. Consequently, by periodically updating its modulation and power level based on the feedback information, the transmitter will be able to adapt to varying channel conditions. The performance of such link prediction using CSI feedback varies with the channel Doppler spread. In a channel prediction context, the performance can be parameterized by the error variance of the channel predictor at the receiver, feedback delay in CSI, and the update rate at the transmitter (i.e. how frequently the transmitter updates its power and modulation level). This chapter intends to demonstrate the impact of delayed CSI on a VRVP-MQAM system, and has therefore considered an optimal predictor in the minimum error variance sense. That is, a Rayleigh fading envelope predictor that is based on an MAP-optimal solution [24] is adopted. For a particular Doppler spread, the length of the predictor, $K_o$, and the PSAM

period, $L$, are chosen such that the transmitter update rate is higher than the Doppler rate of the channel. More details on the channel prediction can be found in Chapter 4.

## 6.3 Adaptive Rate and Power Algorithm

The transmitter will update its rate and power based on an instantaneous predicted SNR $\breve{\gamma}(i)$. With the context clear, and for clarity of notation, the time index shall be omitted. The performance of the proposed adaptive rate and power algorithm in terms of the second order statistical characterization of the channel state imperfection will be investigated. This scheme is denoted as the 'VRVP-CSI' scheme. The performance of the VRVP-CSI scheme will be compared with an alternate scheme where rate and power algorithms are derived based on an ideal CSI assumption [4]. The second scheme is denoted as 'VRVP-IDEAL'. In the subsequent section, for clarity, superscripts '$C$' and '$I$' will be used to differentiate the algorithms for VRVP-CSI and VRVP-IDEAL schemes respectively. The superscripts shall be omitted if the expression is applicable to both schemes.

The spectral efficiency of an MQAM scheme is defined as its average data rate per unit bandwidth. With data sent at $k(\breve{\gamma}) = \log_2(M(\breve{\gamma}))$ bits/symbol, the instantaneous data rate is $k(\breve{\gamma})/T_s$ bits/sec, where $T_s$ is the symbol time. Assuming Nyquist data pulses of duration $T_s = 1/B$, the spectral efficiency for continuous rate can be expressed as

$$E[k(\breve{\gamma})] = \int_{\breve{\gamma}} k(\breve{\gamma}) f_{\breve{\gamma}}(\breve{\gamma}) d\breve{\gamma} \quad \text{bps/Hz}, \tag{6.2}$$

where $f_{\breve{\gamma}}(\breve{\gamma})$ denotes the PDF of $\breve{\gamma}$. Rate and power algorithms for both schemes were derived for maximum spectral efficiency subject to an average power con-

straint

$$E\left[S\left(\check{\gamma}\right)\right] = \int_{\check{\gamma}} S(\check{\gamma}) f_{\check{\gamma}}(\check{\gamma})\, d\check{\gamma} = \bar{S} \tag{6.3}$$

and an instantaneous BER target (BERT) requirement. To solve the constrained optimization problem, the following Lagrangian equation is used.

$$F(S(\check{\gamma})) = \int_{\check{\gamma}} k(\check{\gamma}) f_{\check{\gamma}}(\check{\gamma})\, d\check{\gamma} + \mu \left[ \int_{\check{\gamma}} S(\check{\gamma}) f_{\check{\gamma}}(\check{\gamma})\, d\check{\gamma} - \bar{S} \right], \tag{6.4}$$

where $\mu$ denotes the Lagrange multiplier. The optimal solution for power adaptation $S\left(\check{\gamma}\right)$ can be obtained from the solution of $\frac{\partial F}{\partial S(.)} = 0$.

### 6.3.1 VRVP-CSI Scheme

The algorithms presented in Chapter 5 are generalized to incorporate the MAP-optimal linear predictor [24]. The second order statistical characterization of the channel state imperfection is represented through: i) $\Gamma$, the true average SNR, ii) $\check{\Gamma}$, the estimate of the average SNR based on prediction method, and iii) $\rho$, the correlation coefficient between the predicted instantaneous SNR $\check{\gamma}$ and its true value $\gamma$.

Based on the observations of $\check{\gamma}$, a Bayesian BER estimator was first derived using a MAP approach. Using Bayes' theorem [37], the conditional PDF $f_{p_B|\check{\gamma}}\left(\check{\gamma}\right)$ is given by

$$f_{p_B|\check{\gamma}}\left(p_B|\check{\gamma}\right) = \frac{f_{\check{\gamma}|p_B}\left(\check{\gamma}|p_B\right) f_{p_B}\left(p_B\right)}{f_{\check{\gamma}}\left(\check{\gamma}\right)}, \tag{6.5}$$

where $p_B$ denotes the instantaneous BER, $f_{p_B}\left(p_B\right)$ denotes the PDF of $p_B$, and $f_{\check{\gamma}|p_B}\left(\check{\gamma}|p_B\right)$ is the conditional PDF of $\check{\gamma}$ given $p_B$. Since $f_{\check{\gamma}}\left(\hat{\gamma}\right)$ is a normalization factor, (6.5) is simplified to a final form of the MAP equation,

$$I_{MAP}\left(p_B\right) = f_{p_B,\check{\gamma}}\left(p_B, \check{\gamma}\right), \tag{6.6}$$

where $f_{p_B,\check{\gamma}}\left(p_B, \check{\gamma}\right)$ is the joint PDF of $p_B$ and $\check{\gamma}$. The approaches in deriving $f_{p_B,\check{\gamma}}\left(p_B, \check{\gamma}\right)$ and the solution to the BER estimate, which are obtained from the

solution of $\partial I_{MAP}/\partial p_B$=0, can be found in Chapter 5 (Note that the notation $\breve{\gamma}$ is also the notation $\hat{\gamma}$ presented in Chapter 5). Therefore the details shall not be repeated here. The derived BER estimate (5.23), written as a function of $\breve{\gamma}$ is

$$\hat{p}_B(\breve{\gamma}) = c_1 \exp\left(\frac{\ln(\mathrm{BERT}/c_1)\,\rho\Gamma/\breve{\Gamma}}{\left(-\ln(\mathrm{BERT}/c_1)\,\Gamma/\breve{\gamma}(1-\rho)-1\right)^2}\right), \qquad \breve{\gamma} > \breve{\gamma}_{th}, \tag{6.7}$$

where $\breve{\gamma}_{th} \triangleq (1-\rho)\left(-\ln\left(\frac{\mathrm{BERT}}{c_1}\right)\right)\Gamma$ (see (A.44) in Appendix A.3 for more details).

Through the generic approximate BER expression [4], the rate can be adjusted through the constellation size $M(\breve{\gamma})$ as

$$M^C(\breve{\gamma}) = 1 + \frac{c_2}{-\ln(\hat{p}_B(\breve{\gamma})/c_1)}\frac{S(\breve{\gamma})^C}{S}\breve{\gamma}. \tag{6.8}$$

Subsequently, substituting (6.7) into (6.8), the final form for $M^C(\breve{\gamma})$ is obtained as

$$M^C(\breve{\gamma}) = 1 + \frac{K\breve{\Gamma}}{\rho\Gamma}\left\{\frac{c_2\Gamma}{K\breve{\gamma}}(1-\rho)-1\right\}^2\frac{S(\breve{\gamma})^C}{S}\breve{\gamma}, \tag{6.9}$$

where $K = \frac{c_2}{-\ln\left(\frac{\mathrm{BERT}}{c_1}\right)}$. $\frac{S(\breve{\gamma})^C}{S}$ is the solution to the optimal power adaptation, expressed as (Chapter 5, eqn 5.28)

$$\frac{S(\breve{\gamma})^C}{\bar{S}} = \begin{cases} U^C - \frac{\frac{\Gamma}{\breve{\gamma}}\rho}{K\breve{\gamma}\left\{\frac{c_2}{K}\frac{\Gamma}{\breve{\gamma}}(1-\rho)-1\right\}^2}, & S(\breve{\gamma})^C \geq 0, \\ 0, & \text{otherwise}, \end{cases} \tag{6.10}$$

where $U^C$ is a constant value found through numerical search such that average power constraint (6.3) is satisfied. When $S(\breve{\gamma})^C < 0$, no data are transmitted.

Subsequently, by invoking the optimal power adaptation expression (6.10) in (6.8), the optimal rate adaptation is obtained as

$$k_{\hat{p}_B}(\breve{\gamma})^C = \begin{cases} \log_2\left[\frac{K\breve{\Gamma}}{\rho\Gamma}\left\{\frac{c_2}{K}\frac{\Gamma}{\breve{\gamma}}(1-\rho)-1\right\}^2\hat{\gamma}U^C\right], & k_{\hat{p}_B}(\breve{\gamma})^C \geq 1, \\ 0, & \text{otherwise}. \end{cases} \tag{6.11}$$

Note that $k_{\hat{p}_B}(\breve{\gamma})^C \geq 1$ corresponds to a realistic MQAM constellation size $M \geq 2$. For $S_{\hat{p}_B}(\breve{\gamma})^C \geq 0$ and $k_{\hat{p}_B}(\breve{\gamma})^C \geq 1$, the SNR cutoff threshold can be determined as

$$\breve{\gamma}_0 = \breve{\gamma}_{th} + \chi, \tag{6.12}$$

where $\chi \triangleq \frac{\Gamma}{2KU^C\breve{\Gamma}} \left[2\rho + 2\sqrt{\rho\left(2U^C c_2 \breve{\Gamma} - 2U^C c_2 \breve{\Gamma}\rho + \rho\right)}\right]$ is $\geq 0$. Hence, $S_{\hat{p}_B}(\breve{\gamma})^C \geq 0$ and $k_{\hat{p}_B}(\breve{\gamma})^C \geq 1$ imply $\breve{\gamma} \geq \breve{\gamma}_0$ and transmission is allowed. These conditions also verify the appropriateness of using the derived BER estimator since $\breve{\gamma}_0$ is always greater than $\breve{\gamma}_{th}$.

### 6.3.2 VRVP-IDEAL Scheme

The same channel predictor and discrete level MQAM scheme are used in the VRVP-IDEAL scheme. Adaptive rate is adjusted according to the constellation size $M(\breve{\gamma})$ using [4, eqn. (20)]

$$M^I(\breve{\gamma}) = 1 + K\frac{S(\breve{\gamma})^I}{S}\breve{\gamma}, \tag{6.13}$$

where $\frac{S(\breve{\gamma})^I}{S}$ is the power adaptation [4, eqn. (23)] written as

$$\frac{S(\breve{\gamma})^I}{\bar{S}} = \begin{cases} U^I - \frac{1}{\breve{\gamma}}, & S(\breve{\gamma})^I \geq 0, \\ 0, & \text{otherwise.} \end{cases} \tag{6.14}$$

$U^I$ is a constant value found through numerical search such that average power constraint (6.3) is satisfied. When $S(\breve{\gamma})^I < 0$ and $M(\breve{\gamma})^I < 2$, data are not transmitted. Since the VRVP-IDEAL scheme is based on an ideal CSI assumption, it is noted that unlike (6.9) and (6.10), the algorithms in (6.13) and (6.14) do not have parameters that relate to the channel state imperfections.

### 6.3.3 Spectral Efficiency and Average BER

For a practical MQAM scheme, the constellation size $M$ is restricted to a positive integer value and is a factor of two. Moreover, since the transceiver design complexity grows as the constellation size increases, a limitation on the maximum constellation size is imposed. Let $G$ denote the number of modulation levels considered for the system. The adaptive modulation level will be chosen from the set $\{M_d\}_{d=0}^{G-1}$, where element $M_d$ can be from the set $\{0, 2, 4, 8...\}$. Note that $M_d$=0 is assigned to the situation where no data transmission is allowed. Since the computed value of $M(\check{\gamma})$ is a real number, the largest possible discrete $M_d$ value that is smaller than or equal to $M(\check{\gamma})$ is chosen to ensure a BER lower than the BERT requirement.

The data transmission rate associated with each $M_d$ is $k_d/T_s$ bits/sec, where $k_d = \log_2(M_d)$ bits/symbol. The spectral efficiency for the discrete-rate approach can be expressed as

$$\frac{R}{B} = \sum_{d=1}^{G-1} k_d \left(\frac{L-1}{L}\right) P_d \quad \text{bps/Hz}, \tag{6.15}$$

where $P_d$ is the probability that the modulation level $M_d$ will be used. The term $(L-1)/L$ corresponds to an efficiency factor of the PSAM scheme since overhead is introduced in the data transmission.

The average BER can be expressed as

$$\overline{BER} = \frac{\sum_{d=1}^{G-1} k_d \, \overline{BER}_d}{R/B}, \tag{6.16}$$

where $\overline{BER}_d$ is the average BER experienced in each discrete rate $k_d$. It is noted the discrete $M_d$ level selection will result in a lower $\overline{BER}_d$ performance than the required BERT. This is due to the fact that $M_d$ is chosen to be less than or equal to $M(\check{\gamma})$.

## 6.4 Channel Prediction

At the receiver, based on the knowledge of the pilot symbols, the estimated channel fading at the pilot symbol instants can be written as

$$\hat{z}(v-kL) = \frac{y(v-kL)}{x(v-kL)} \tag{6.17}$$

$$= z(v-kL) + \frac{n(v-kL)}{x(v-kL)}, \tag{6.18}$$

where $(v-kL)$ denotes the time instant of the pilot symbol, $v = pL, p \in \mathbb{Z}$ and $k = 0, 1, ..., K-1$. Consider that the last observed fading gain occurs at $v$ symbol-instant, and that the predictor predicts the fading gain for $j$ symbol instants later, where $j = qL$ and $q \in \{1, 2, ...\}$. Assume that the total time for the processing at the receiver and the feedback delay is within the $j$ symbol period. Thus the transmitter will update its rate and power at the $(v+j)^{th}$ symbol-instant, where $j$ can be associated to the time delay parameter. Let denote the predicted channel gain at the $(v+j)^{th}$ symbol-instant as $\check{z}(v+j)$. For a linear predictor of order $K_o$, the predicted fading channel using $K_o$ fading estimates $\hat{z}(v-kL)$ can be expressed as (provided in Chapter 4, equation (4.4))

$$\check{z}(v+j) = \sum_{k=0}^{K_o-1} f_j^*(k)\,\hat{z}(v-kL) \tag{6.19}$$

$$= \mathbf{f}_j^{\mathrm{H}}\hat{\mathbf{z}}, \tag{6.20}$$

where $\mathbf{f}_j^{\mathrm{H}} = [f_j^*(0), f_j^*(1), ..., f_j^*(K_o-1)]$ is the predictor filter coefficient vector. The superscripts '*' and 'H' denote complex conjugate and Hermitian transpose respectively. $\hat{\mathbf{z}} = [\hat{z}(v), \hat{z}(v-L), ..., \hat{z}(v-(K_o-1)L)]^{\mathrm{T}}$ is the vector of the estimates of the complex fading amplitude in the last $K_o$ pilot-symbol instants. The superscript 'T' denotes transpose. A MAP-optimal envelope prediction which has been proposed in [24] (also provided in Chapter 4) as one of the best linear predictors (in the mean-square error sense) for Rayleigh fading channels is used.

It is shown in [24] that the MAP-optimal prediction filter coefficient vector is expressed as (provided in Chapter 4, equation (4.24))

$$\mathbf{f}_{j,\mathrm{MAP}}^{\mathrm{T}} = \mathbf{r}_j^{\mathrm{T}} \left( \mathbf{R} + \frac{1}{\Gamma} \mathbf{I}_{K_o} \right)^{-1}, \tag{6.21}$$

where $\mathbf{r}_j^{\mathrm{T}}$ is a vector whose elements $r_{j,k}$ are the correlations between the fading at the pilot-symbol time instants $v - kL$ and the fading at the prediction time instant $v + j$. $\mathbf{R}$ is a $K_o \times K_o$ covariance matrix whose elements $R_{k,l}$ are the correlations of the fading between two pilot-symbol instants of time difference $(|k - l|)LT_s$. Elements of $\mathbf{r}_j^{\mathrm{T}}$ and $\mathbf{R}$ can be expressed in terms of the normalized correlation function $R(.)$:

$$\begin{aligned} r_{j,k} &= \frac{1}{\Omega} E[z(v - kL)\, z^*(v + j)] && (6.22) \\ &= R((j + kL)\, T_s), && (6.23) \\ R_{k,l} &= R((|k - l|)\, LT_s), && (6.24) \end{aligned}$$

where $\Omega = E[|z|^2]$. When the standard Jakes' model is used, $R(.)$ can be expressed as [57],

$$R(\tau) = J_o(2\pi f_d \tau), \tag{6.25}$$

where $J_o(.)$ is the zeroth-order Bessel function of the first kind and $\tau$ denotes the time lag. The parameter $f_d$ is the maximum Doppler spread defined by $fv_t/c$, where $f$ is the carrier frequency (Hz), $v_t$ is the terminal speed (m/s) and $c = 3 \times 10^8$m/s is the speed of light.

Finally, with the MAP-optimal predictor, the correlation coefficient $\rho$ is equal to (provided in Chapter 4, equation (4.52)),

$$\rho = \mathbf{r}_j^{\mathrm{T}} \left( \mathbf{R} + \frac{1}{\Gamma} \mathbf{I} \right)^{-1} \mathbf{r}_j. \tag{6.26}$$

## 6.5 Simulation Results

The modified Jakes' model in [60] is adopted for the system simulation. The model produces uncorrelated fading waveforms that match the theoretical Jakes' model function in (6.25). An uncorrelated fading waveform with real and imaginary parts having equal power is represented as [60]

$$T(t) = \sqrt{\frac{2}{N_{osc}} \sum_{n=1}^{N_{osc}} [\cos(\beta_n) + I \sin(\beta_n)] \cos(\omega_n t + \theta_n)}, \tag{6.27}$$

where $t$ denotes the time index, $I$ denotes $\sqrt{-1}$ and $N_{osc}$ denotes the number of oscillators associated with the reflected rays arriving at the receiver. The parameters $\beta_n$ are the phases of the oscillators expressed as $\pi n/N_{osc}$ and $\theta_n$ are the initial phases of the oscillators. Each ray experiences a Doppler spread defined by $\omega_n = \omega_M \cos(\alpha_n)$, where $\omega_M = 2\pi f v_t/c$. The arrival angle $\alpha_n$ of ray $n$ is defined as $2\pi(n - 0.5)/N_{osc}$.

The complex fading waveform is generated using $N_{osc} = 16$ and a normalized Doppler spread of $f_d T_s = 0.001$. This setting simulates a practical communication transmission system that is in motion. For example, assume a practical carrier frequency $f = 2$ GHz, and transmission bandwidth $B = 200$kHz with Nyquist sampling and thus symbol duration $T_s = 1/B$ secs, the terminal velocity will be $v = 30$ m/sec. For a Doppler spread factor $f_d T_s = 0.001$, it has been shown in Section 4.4.4 that the optimal MAP predictor parameters can be set to $L = 10$ and $K_o = 500$. Finally, a practical constellation set for the MQAM scheme $M_D$ is set to $(0, 2, 4, 16, 64)$.

Simulation results for spectral efficiency and average BER performance over a set of normalized time delay parameter $f_d T_s j$ (Table 6.1) at $\Gamma = 15$ dB and 20 dB are computed. Table 6.1 illustrates the value of $f_d T_s j$ with its equivalent delay in symbol instants, and the associated $\rho$ values. Figure 6.3 shows that the

Table 6.1: Normalized time delay $f_dT_sj$ and its corresponding correlation coefficient $\rho$, at $f_dT_s$=0.001, $\Gamma$ = 15 dB, 20 dB, where $qL$ denotes delay in symbol units.

| *fdTsj* | *qL* (symbols) | $\Gamma$=20 dB | $\Gamma$=15 dB |
|---|---|---|---|
| | | $\rho$ | $\rho$ |
| 0.01 | 10 | 0.9981 | 0.9948 |
| 0.05 | 50 | 0.9961 | 0.9906 |
| 0.1 | 100 | 0.9915 | 0.9831 |
| 0.15 | 150 | 0.9831 | 0.966 |
| 0.2 | 200 | 0.9692 | 0.9426 |

VRVP-CSI system achieves improved spectral efficiency over the VRVP-IDEAL system. Figure 6.3 also shows that the VRVP-CSI system provides a higher spectral efficiency gain across the normalized time delay at a high average SNR (gain of $\approx 0.15$ bps/Hz at $\Gamma$=20 dB compared to gain of $\approx 0.05$ bps/Hz at $\Gamma$=15 dB). In terms of average BER performance, the simulation results in Figure 6.4 depict several interesting points. Firstly, both systems perform better than the BERT threshold at a low feedback delay. This is because the adaptive modulator uses the largest possible discrete $M_d$ which is below or equal to the actual optimal $M$. Secondly, the proposed VRVP-CSI algorithm tolerates a longer feedback delay before BER exceeds the BERT threshold. For instance, at $\Gamma$ = 15 dB, the VRVP-CSI scheme can tolerate up to 180 symbols delay before the average BER increases beyond the BERT ($10^{-3}$) requirement, whereas the VRVP-IDEAL scheme allows for only 150 symbols delay.

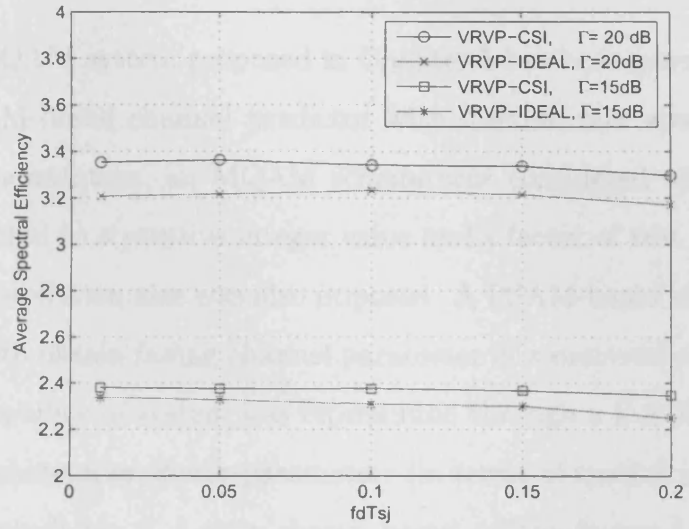


Figure 6.3: Average spectral efficiency versus normalized time delay $f_d T_s j$. At $\Gamma$=15 dB, 20 dB and BERT= $10^{-3}$.

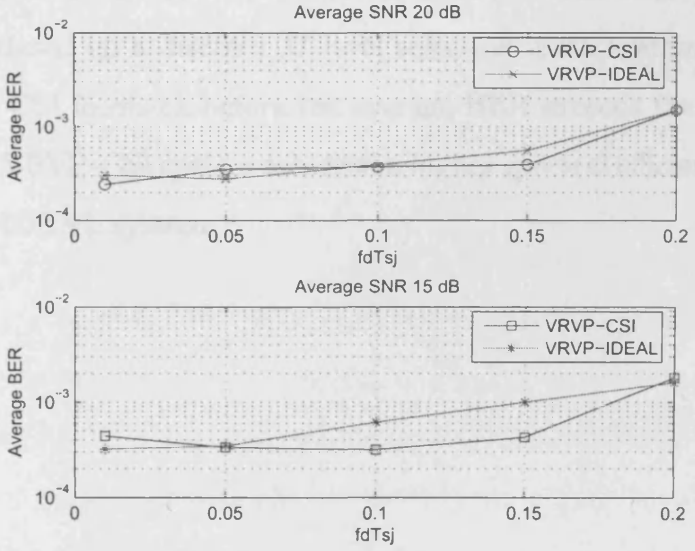


Figure 6.4: Average BER versus normalized time delay $f_d T_s j$. At $\Gamma$=15 dB, 20 dB and BERT= $10^{-3}$.

## 6.6 Summary

The VRVP-MQAM system proposed in Chapter 5 has been generalized to incorporate a PSAM-based channel predictor with discrete rate adaptation. In the discrete rate adaptation, an MQAM scheme was considered with constellation sizes $M$ restricted to a positive integer value and a factor of two. A limitation on maximum constellation size was also imposed. A PSAM-based channel predictor was employed to obtain fading channel parameter in a practical mobile communication. The mobility of system was represented through a Doppler spread factor $f_dT_s$, and the channel predictor parameters (in terms of symbol period $L$ and the length of the predictor $K_o$) were chosen based on the factor $f_dT_s$. A modified Jakes' model was employed to simulate the time-varying channel.

The performance of the proposed system, denoted as the VRVP-CSI system, was compared to a rate and power algorithms derived based on a perfect CSI assumption (denoted as the VRVP-IDEAL system). The following results were observed. 1) Based on a discrete $M$ level selection, both systems can tolerate a small delay in CSI feedback before the average BER exceeds the BER target. 2) The proposed VRVP-CSI system achieved a higher spectral efficiency as compared to the VRVP-IDEAL system.

# Chapter 7

# VRVP-MQAM System with Adaptive SNR Target

*This chapter discusses one of the author's contributions. The work has been published and presented in the IEEE ISWCS conference [15].*

## 7.1 Introduction

In CDMA-based systems, a sub-optimal power allocation strategy based on total channel inversion or truncated channel inversion is generally used. These strategies attempt to compensate for the effect of fading and maintain a constant SNR target at the receiver. This is accomplished in third generation WCDMA-based systems by using an inner-loop power control mechanism [13]. The capacity of a single-user channel with this kind of power control has been examined in [2] and [4]. Assuming perfect CSI at the transmitter, the channel capacity for this scheme is equal to the capacity of an AWGN channel with received SNR equal

to the desired SNR target. That is, the capacity with channel inversion is ( [2] or see (3.15))

$$\begin{aligned} C_{\mathrm{CI}} &= B\log_2(1+\sigma_{\mathrm{CI}}) \\ &= B\log_2(1+1/E[1/\gamma]), \end{aligned} \tag{7.1}$$

where subscript 'CI' denotes channel inversion, $\sigma_{\mathrm{CI}}$ denotes the fixed SNR target, and $E[1/\gamma] \triangleq \int_0^\infty \frac{1}{\gamma} f_\gamma(\gamma) d\gamma$ where $f_\gamma(\gamma)$ denotes the PDF of $\gamma$. The capacity with truncated channel inversion is ( [2] or see (3.19))

$$\begin{aligned} C_{\mathrm{TCI}} &= B\log_2(1+\sigma_{\mathrm{TCI}})\, p(\gamma \geq \gamma_0) \\ &= B\log_2(1+1/E_{\gamma_0}[1/\gamma])\, p(\gamma \geq \gamma_0), \end{aligned} \tag{7.2}$$

where subscript 'TCI' denotes truncated channel inversion, $\sigma_{\mathrm{TCI}}$ denotes the fixed SNR target and $p(\gamma \geq \gamma_0)$ denotes the probability of transmission. Recall that $E_{\gamma_0}[1/\gamma] \triangleq \int_{\gamma_0}^\infty \frac{1}{\gamma} f_\gamma(\gamma) d\gamma$ and $\gamma_0$ is the cutoff fade depth.

However, various mobility conditions often result in imperfect channel estimation, which degrades the BER performance. An outer-loop power control mechanism, which aims at setting the SNR target, to achieve a desired BER performance, would therefore compensate for imperfect estimation and poor tracking of the inner-loop. In [14,61] joint optimisation of the dynamic rate and SNR target adaptation based only on the perfect knowledge of the actual SNR ($\gamma$) and BER has been considered.

In this chapter, optimum SNR target and rate adaptation is derived based on an estimate of SNR and BER over a Rayleigh flat-fading channel. Using this scheme, higher spectral efficiency can be achieved for an adaptive MQAM system as compared to a similar system but with fixed SNR target as in [4].

The remainder of this chapter is organized as follows. In Section 7.2, the system model is described. The analytical approach to determining the BER

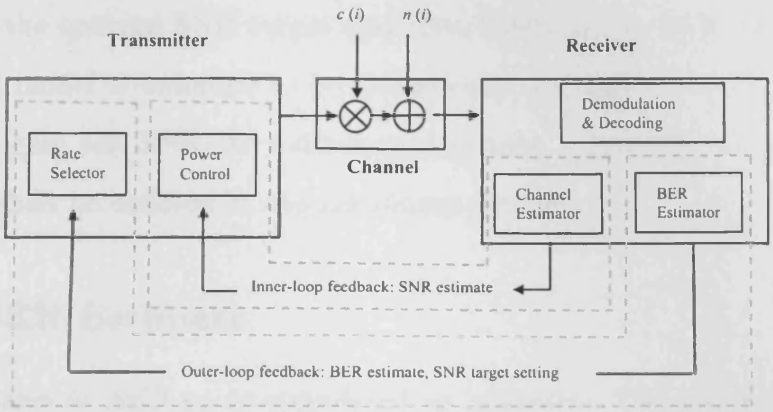


Figure 7.1: Block diagram of adaptive SNR target VRVP-MQAM system.

estimate and its statistics are also presented. Closed-form expressions for continuous SNR target and rate adaptation are also derived. In Section 7.3, numerical results to confirm the performance of the proposed system are presented. Finally, a summary of the chapter is provided in Section 7.4.

## 7.2 System Model and Analysis

Figure 7.1 shows the system model. The channel model is represented in discrete-time with statistically stationary and ergodic time-varying gain $\alpha(i) = |c(i)|$ and additive white Gaussian noise $n(i)$ with spectral density $N_o/2$. At the receiver, the channel gain estimate $\hat{\alpha}(i)$ is determined based on a PSAM scheme [50]. The instantaneous received SNR $\gamma(i)$ is $\gamma(i) \triangleq \bar{S}[\alpha(i)]^2/(N_o B)$ and its estimate is $\hat{\gamma}(i) \triangleq \bar{S}[\hat{\alpha}(i)]^2/(N_o B)$, where $B$ denotes the received signal bandwidth and $\bar{S}$ is the average transmit power. The truncated channel inversion scheme is considered for the inner-loop power control. At time $i$, the inner-loop mechanism attempts to maintain a desired SNR target at the receiver by adapting the transmitted power based on the estimate $\hat{\gamma}(i)$ of the received SNR $\gamma(i)$. In contrast, the outer-loop

aims to set the optimal SNR target and rate, based on the BER estimate. Since the channel model is assumed to be statistically stationary, the distributions of the channel gain and SNR are independent of time. Therefore, the discrete time reference $i$ shall be omitted in the remaining sections.

### 7.2.1 BER Estimate

The instantaneous BER $p_B$ is considered as unknown. The aim is to determine its estimate $\hat{p}_B$ in terms of the observation $\hat{\gamma}$. Using the maximum likelihood (ML) estimation approach [37, 56, 59], $\hat{p}_B$ can be obtained based on the most likely occurrence of $\hat{\gamma}$. That is, the likelihood function can be expressed as

$$l\left(p_B\right) = f_{\hat{\gamma}|p_B}\left(\hat{\gamma}|p_B\right), \tag{7.3}$$

where $f_{\hat{\gamma}|p_B}\left(\hat{\gamma}|p_B\right)$ is the conditional PDF of $\hat{\gamma}$ given $p_B$. The expression for $\hat{p}_B$ can be obtained from the solution of $\frac{\partial l(p_B)}{\partial p_B} = 0$. The derivation is as follows.

Using the approximate BER expression [4, 5], the instantaneous BER of a truncated channel inversion MQAM system in terms of $\gamma$ and $\hat{\gamma}$ can be expressed as [4, eqn.(42)]

$$p_B(\gamma, \hat{\gamma}) \;=\; c_1 \exp\left(-\frac{c_2\gamma}{M-1}\frac{S(\hat{\gamma})}{\bar{S}}\right), \tag{7.4}$$

where $S(\hat{\gamma})$ denotes transmit power based on $\hat{\gamma}$, $M$ denotes the constellation size, and $c_1$ and $c_2$ are positive real numbers. Consider that only the knowledge of channel estimate is available. For a channel inversion policy, the transmitted power is

$$\frac{S\left(\hat{\gamma}\right)}{\bar{S}} \triangleq \frac{\sigma}{\hat{\gamma}}, \tag{7.5}$$

where $\sigma$ denotes the received SNR target. For a given BERT and SNR target,

the signal constellation point $M$ is adjusted according to

$$M = 1 + \frac{c_2 \sigma}{-\ln\left(\frac{\text{BERT}}{c_1}\right)}. \tag{7.6}$$

Using (7.5), the instantaneous BER in (7.4) can be expressed as

$$p_B = c_1 \exp\left(-\frac{c_2 \sigma}{M-1}\frac{\gamma}{\hat{\gamma}}\right). \tag{7.7}$$

For a Rayleigh flat-fading channel using the PSAM technique for channel estimation [51], the amplitudes $\alpha$ and $\hat{\alpha}$ have a bivariate Rayleigh distribution. Consequently, the equivalent joint PDF of $\gamma$, and its estimate $\hat{\gamma}$, is [1]

$$f_{\gamma,\hat{\gamma}}(\gamma,\hat{\gamma}) = \frac{1}{(1-\rho)\,\Gamma\hat{\Gamma}} I_0\left(\frac{2\sqrt{\rho}}{1-\rho}\sqrt{\frac{\gamma\hat{\gamma}}{\Gamma\hat{\Gamma}}}\right) \exp\left(-\frac{1}{1-\rho}\left(\frac{\gamma}{\Gamma}+\frac{\hat{\gamma}}{\hat{\Gamma}}\right)\right) u(\gamma)\, u(\hat{\gamma}) \tag{7.8}$$

where $\Gamma = E[\gamma]$, $\hat{\Gamma} = E[\hat{\gamma}]$ and $\rho$ is the correlation coefficient between $\gamma$ and $\hat{\gamma}$. $E[.]$ denotes the statistical expectation operator. $I_0(.)$ is the zeroth order modified Bessel function and $u(.)$ is the unit step function. Exploiting (7.7) and (7.8), and through a transformation of random variables, the joint PDF of $\hat{\gamma}$ and $p_B$ is obtained as [2]

$$f_{p_B,\hat{\gamma}}(p_B,\hat{\gamma}) = c(p_B)\, I_0(b(p_B)\,\hat{\gamma}) \exp(-a(p_B)\,\hat{\gamma}), \tag{7.9}$$

where

$$a(p_B) = \frac{1}{1-\rho}\left(\frac{-(M-1)}{\sigma c_2}\ln\left(\frac{p_B}{c_1}\right)\frac{1}{\Gamma}+\frac{1}{\hat{\Gamma}}\right), \tag{7.10}$$

$$b(p_B) = \frac{2\sqrt{\rho}}{1-\rho}\sqrt{\frac{-(M-1)}{\sigma c_2}\ln\left(\frac{p_B}{c_1}\right)\frac{1}{\Gamma\hat{\Gamma}}}, \tag{7.11}$$

$$c(p_B) = \frac{(M-1)\,\hat{\gamma}}{p_B c_2 \sigma\,(1-\rho)\,\Gamma\hat{\Gamma}}. \tag{7.12}$$

[1] The derivation of $f_{\gamma,\hat{\gamma}}(\gamma,\hat{\gamma})$ is provided in Appendix A.4.

[2] The derivation of $f_{p_B,\hat{\gamma}}(p_B,\hat{\gamma})$ is provided in Appendix A.1.

From the property of the conditional density function [37],

$$f_{\hat{\gamma}|p_B}(\hat{\gamma}|p_B) = \frac{f_{p_B,\hat{\gamma}}(p_B,\hat{\gamma})}{f_{p_B}(p_B)}, \tag{7.13}$$

where $f_{p_B}(p_B)$ is the PDF of $p_B$, which is obtained from the marginalization operation of $\int_0^\infty f_{p_B,\hat{\gamma}}(p_B,\hat{\gamma})\,d\hat{\gamma}$. [3] From (7.13) and neglecting the constant term, the final form of the likelihood function is obtained as [4]

$$l(p_B) = I_0(b(p_B)\hat{\gamma}) \exp(-a(p_B)\hat{\gamma}) \frac{[a(p_B)^2 - b(p_B)^2]^{3/2}}{a(p_B)}. \tag{7.14}$$

As shown in Appendix A.2, function $I_0(b(p_B)\hat{\gamma}) \approx \frac{\exp(b(p_B)\hat{\gamma})}{\sqrt{2\pi b(p_B)\hat{\gamma}}}$ for a high SNR estimate $\hat{\gamma}$. Thus the equivalent expression for (7.14) when based on a high SNR estimate $\hat{\gamma}$ is written as

$$l_{eq}(p_B) = \frac{\exp(b(p_B)\hat{\gamma})}{\sqrt{2\pi b(p_B)\hat{\gamma}}} \exp(-a(p_B)\hat{\gamma}) \frac{[a(p_B)^2 - b(p_B)^2]^{3/2}}{a(p_B)}. \tag{7.15}$$

Equation (7.15) is a highly non-linear expression where a closed-form solution for $\frac{\partial l_{eq}}{\partial p_B} = 0$ is difficult to find. However, a simple closed-form expression is obtained when based on high $\hat{\gamma}$ as [5]

$$\hat{p_B} = c_1 \exp\left(\frac{-c_2\sigma}{M-1}\frac{\rho\Gamma}{\hat{\Gamma}}\right). \tag{7.16}$$

In an MQAM system which exploits a truncated channel inversion policy over a Rayleigh fading channel, the SNR cutoff value $\gamma_0$ to achieve maximum spectral efficiency is known to be relatively high [4]. Note that no transmission is allowed when SNR is below the cutoff value. Therefore the BER estimate expression in (7.16), that is derived based on a high SNR estimate, is considered applicable for such a truncated channel inversion system. Equation (7.16) is a useful expression as it relates to the statistics of the channel estimation: i) $\Gamma$, the true average

[3] Refer to Appendix B.1 for the proof.

[4] Refer to Appendix B.2 for the proof.

[5] Refer to Appendix B.3 for the proof.

SNR, ii) $\hat{\Gamma}$, the estimate of the average SNR, and iii) $\rho$, the correlation coefficient between the estimated instantaneous SNR $\hat{\gamma}$ and its true value $\gamma$.

From earlier research works, for example [56], it is known that the analytical expression for the PDF of the ML estimation is usually impossible to derive. Hence the asymptotic properties of ML estimation that displays a Gaussian distribution is usually assumed. Therefore the PDF of $\hat{p}_B$ having a Gaussian distribution can be written as

$$f_{\hat{p}_B}(\hat{p}_B) = \frac{1}{\sigma_{\hat{p}_B}\sqrt{2\pi}} \exp\left(\frac{-\left(\hat{p}_B - \bar{\hat{p}}_B\right)^2}{2{\sigma_{\hat{p}_B}}^2}\right)\left[\frac{1}{F_{c_1} - F_{p_{B\min}}}\right], \tag{7.17}$$

where $\bar{\hat{p}}_B$ is the mean BER value and $\sigma_{\hat{p}_B}$ denotes the standard deviation of $\hat{p}_B$. The normalisation factor $\frac{1}{F_{c_1} - F_{p_{B\min}}}$ can be obtained from the cumulative distribution function of $\hat{p}_B$, written as

$$F_{c_1} - F_{p_{B\min}} = \int_{p_{B\min}}^{c_1} \frac{1}{\sigma_{\hat{p}_B}\sqrt{2\pi}} \exp\left(\frac{-\left(\hat{p}_B - \bar{\hat{p}}_B\right)^2}{2{\sigma_{\hat{p}_B}}^2}\right) d\hat{p}_B \tag{7.18}$$

$$= 0.5 \operatorname{erf}\left(\frac{\sqrt{2}}{2\sigma_{\hat{p}_B}}(\hat{p}_B - \bar{\hat{p}}_B)\right)\Bigg|_{p_{B\min}}^{c_1} \tag{7.19}$$

for the respective BER limits, $c_1$ and $p_{B\min}$. The erf function is [43]

$$\operatorname{erf}(x) = \frac{2}{\sqrt{\pi}} \int_x^{\infty} \exp(-t^2) dt. \tag{7.20}$$

Note that when the BER estimates have large deviations, the BER estimator will approach that of a uniform distribution. The impact of the standard deviation of the BER estimate on the spectral efficiency of the proposed scheme will be verified in the numerical section.

### 7.2.2 Rate and SNR Target Adaptation

The proposed adaptive SNR target adaptation is intended to vary in accordance with the BER variations for the outer-loop adaptive system. At the receiver,

with the BER estimate ($\hat{p}_B$) known, the SNR target can therefore be adjusted in accordance with $\hat{p}_B$. Let $\sigma(\hat{p}_B)$ denote the adaptive SNR target based on $\hat{p}_B$. Subsequently, by rearranging (7.16), $M$ at the transmitter can be adjusted as

$$M\left(\hat{p}_B\right) = 1 + \frac{c_2\sigma(\hat{p}_B)}{-\ln(\hat{p}_B/c_1)}\frac{\rho\Gamma}{\hat{\Gamma}}. \tag{7.21}$$

The spectral efficiency of an MQAM scheme can be expressed as its average data rate per unit bandwidth $R/B$. With data sent at $k\left(\hat{p}_B\right) = \log_2\left(M\left(\hat{p}_B\right)\right)$ bits/symbol, the instantaneous data rate is $k\left(\hat{p}_B\right)/T_s$, where $T_s$ is the symbol time. Assuming Nyquist data pulses of duration $T_s = 1/B$, the spectral efficiency of the proposed joint inner-loop and outer-loop adaptation system can be written as

$$\frac{R}{B} = P_T \int_{\hat{p}_B} k\left(\hat{p}_B\right) f_{\hat{p}_B}\left(\hat{p}_B\right) d\hat{p}_B. \tag{7.22}$$

where the integration is for $\hat{p}_B \in [0, c_1]$. The parameter $P_T$ denotes the probability of transmission resulting from the channel truncation of the inner-loop power control scheme, and is given by

$$P_T = \int_{\hat{\gamma}_0}^{\infty} f_{\hat{\gamma}}(\hat{\gamma})\, d\hat{\gamma}. \tag{7.23}$$

Maximum spectral efficiency is obtained by maximising (7.22) subject to the average power constraint

$$E[S] = \int_{\hat{p}_B}\int_{\hat{\gamma}} S\left(\hat{\gamma}, \hat{p}_B\right) f_{\gamma,\hat{p}_B}\left(\hat{\gamma}, \hat{p}_B\right) d\hat{\gamma}\, d\hat{p}_B = \bar{S}, \tag{7.24}$$

where $f_{\gamma,\hat{p}_B}\left(\hat{\gamma}, \hat{p}_B\right)$ denotes the joint PDF of $\hat{\gamma}$ and $\hat{p}_B$. $S\left(.,.\right)$ is the instantaneous transmit power and it is expressed as a function of $\hat{\gamma}$ and $\hat{p}_B$,

$$S\left(\hat{\gamma}, \hat{p}_B\right) = \frac{\sigma\left(\hat{p}_B\right)}{\hat{\gamma}}\bar{S}. \tag{7.25}$$

The constrained optimisation problem can be solved using the Lagrangian equa-

tion, written as

$$F(\sigma(\hat{p}_B)) = P_T \int_{\hat{p}_B} k(\hat{p}_B) f_{\hat{p}_B}(\hat{p}_B)\, d\hat{p}_B + \mu \left[ \int_{\hat{p}_B} \int_{\hat{\gamma}} \frac{\sigma(\hat{p}_B)}{\hat{\gamma}} \bar{S} f_{\hat{p}_B,\hat{\gamma}}(\hat{p}_B, \hat{\gamma})\, d\hat{\gamma}\, d\hat{p}_B - \bar{S} \right], \tag{7.26}$$

where $\mu$ denotes the Lagrange multiplier. The adaptive SNR target $\sigma(.)$ is obtained from the solution of

$$\frac{\partial F}{\partial \sigma(\hat{p}_B)} = 0. \tag{7.27}$$

The case of higher SNR estimate ($\hat{\gamma} \geq \hat{\gamma}_0$), which is the basis of deriving (7.16), is considered. It is appropriate to assume that the statistics of $\hat{\gamma}$ and $\hat{p}_B$ are independent. That is, $f_{\hat{p}_B,\hat{\gamma}}(\hat{p}_B, \hat{\gamma}) = f_{\hat{p}_B}(\hat{p}_B) f_{\hat{\gamma}}(\hat{\gamma})$, where $f_{\hat{p}_B}(\hat{p}_B)$ is derived as in (7.17) and $f_{\hat{\gamma}}(\hat{\gamma})$ is the PDF of $\hat{\gamma}$. For a Rayleigh fading channel, $f_{\hat{\gamma}}(\hat{\gamma}) = \frac{1}{\hat{\Gamma}} \exp\left(-\frac{\hat{\gamma}}{\hat{\Gamma}}\right)$. With these statistics, the solution to (7.27) is obtained as

$$\sigma_{op}(\hat{p}_B) = \begin{cases} \frac{\hat{\Gamma} \ln(\hat{p}_B/c_1)}{\Gamma \rho c_2} - \frac{1}{U_0}, & \sigma_{op}(\hat{p}_B) \geq 0, \\ 0, & \text{otherwise}, \end{cases} \tag{7.28}$$

where $U_o \triangleq 1/P_T \mu \ln(2) \bar{S} E_{\hat{\gamma}_0}[1/\hat{\gamma}]$ and $E_{\hat{\gamma}_0}[1/\hat{\gamma}] \triangleq \int_{\hat{\gamma}_0}^{\infty} 1/\hat{\gamma}\, f_{\hat{\gamma}}(\hat{\gamma})\, d\hat{\gamma}$. The value $U_o$ can be found through numerical search such that the power constraint (7.24) is satisfied. By substituting (7.28) into (7.21), the rate adaptation is obtained as

$$k_{op}(\hat{p}_B) = \begin{cases} \log_2\left(\frac{\Gamma \rho c_2}{U_o \ln(\hat{p}_B/c_1)\hat{\Gamma}}\right), & k_{op}(\hat{p}_B) \geq 0, \\ 0, & \text{otherwise}. \end{cases} \tag{7.29}$$

Finally, substituting (7.29) into (7.22), the maximum spectral efficiency can be written as

$$\frac{R}{B} = P_T \int_{\hat{p}_B} \log_2\left(\frac{c_2 \rho \Gamma}{U_0 \ln(\hat{p}_B/c_1)\hat{\Gamma}}\right) f_{\hat{p}_B}(\hat{p}_B)\, d\hat{p}_B. \tag{7.30}$$

## 7.3 Numerical Results

The VRVP-MQAM system with truncated channel inversion at the inner-loop and adaptive SNR target at the outer-loop , is denoted as the 'adaptive SNR target' (AST) system. For comparison, an alternate system using the VRVP-MQAM scheme with truncated channel inversion at the inner loop and a fixed SNR target at the outer-loop power control, denoted as the 'fixed SNR target' (FST) system, is considered. The FST system corresponds to a truncated channel inversion scheme of the VRVP-MQAM system in [4], which assumes availability of perfect CSI at the transmitter and the receiver. Both systems assume that $M(.)$ can be a non-integer value and use $c_1 = 0.2$ and $c_2 = 1.5$ [4]. The cutoff value $\hat{\gamma}_0$ is determined to maximize the spectral efficiency of the FST system [4]. For comparison to the FST system, the same cutoff value $\gamma_0$ is used in the AST system. The proposed BER estimator is assumed to be unbiased with $\bar{\hat{p}}_B$ set to the desired BER target BERT $= 10^{-3}$, and the standard deviation (std) values are set to $\sigma_{p_B} = \{20, 100, 1000\}$ times the value of BERT. The low std value, $\sigma_{p_B} = 20 \times 10^{-3}$, is used to denote the scenario where the AST system can obtain accurate estimates of the channel variations. Thus the BER of the system is nearly always achieving the BER target value. The high std value, $\sigma_{p_B} = 1000 \times 10^{-3}$, is used to denote the scenario where the AST system is unable to estimate accurately the channel variations, probably due to relatively fast channel variations or a less accurate estimation technique. As a result, the BER value of the adaptive system varies away from the BER target value. The mid std value, $\sigma_{p_B} = 100 \times 10^{-3}$, denotes a situation which is between the two scenarios mentioned above.

The PDFs of the BER distribution for the respective cases are shown in Figure 7.2. The PDF is also reproduced in Figure 7.3 with the x-axis represented in logarithmic scale. The logarithmic scale could be a more suitable representation,

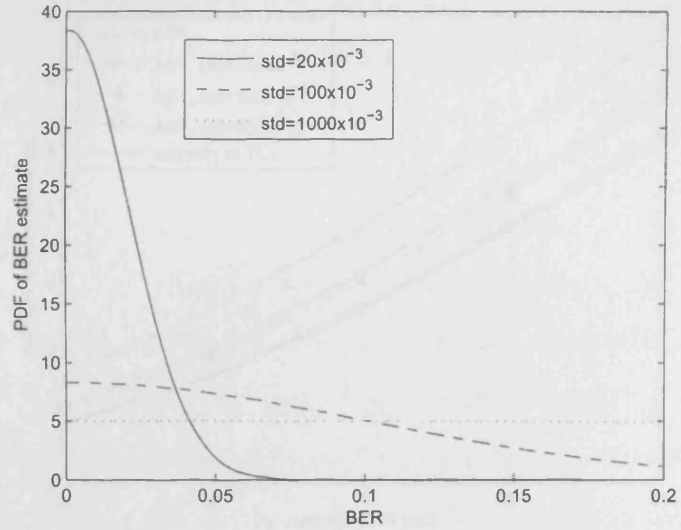


Figure 7.2: PDF of BER estimate with BERT = $10^{-3}$.

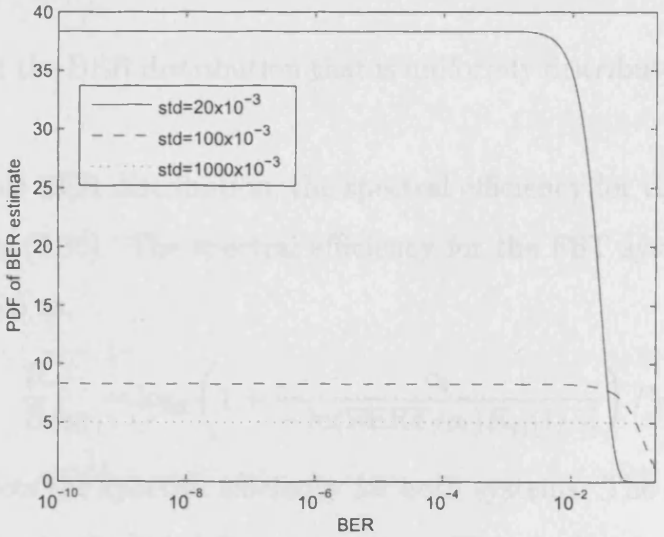


Figure 7.3: PDF of BER estimate with BERT = $10^{-3}$.

since it corresponds to practical BER values. It is also noted that regardless of wide difference in the std values used, the PDF of BER for the logarithm scale shows a uniform distribution for BER $< 0.01$. Clearly, the case $\sigma_{p_B} = 1000 \times 10^{-3}$

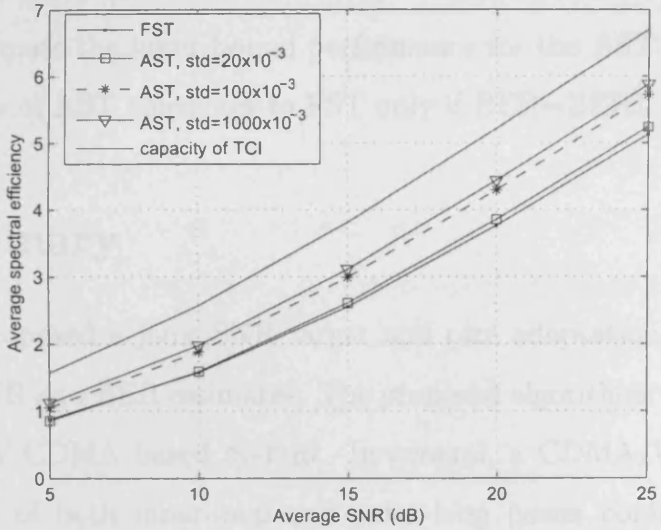


Figure 7.4: Comparisons of average spectral efficiency.

would represent the BER distribution that is uniformly distributed between 0 and $c_1$.

Based on this BER distribution, the spectral efficiency for the AST system is computed using (7.30). The spectral efficiency for the FST system is computed using [4], written as,

$$\frac{R}{B}_{\text{FST}} = \log_2\left(1 + \frac{c_2}{-\ln(\text{BERT}/c_1)E_{\gamma_0}[1/\hat{\gamma}]}\right) P_T \tag{7.31}$$

Figure 7.4 depicts the spectral efficiency for both systems. The channel capacity for TCI (7.2) is also included for comparison. The results show that the AST system provides higher spectral efficiency compared to the FST system. The spectral efficiency of the FST system increases as the standard deviation of the BER increases. This implies that the proposed AST scheme maximises the spectral efficiency through an adaptive SNR target that exploits BER variations. Note that the case $\sigma_{p_B} = 1000 \times 10^{-3}$ (BER is uniformly-distributed) is used to represent



CARDIFF UNIVERSITY * PRIFYSGOL CAERDYDD *

the upper bound performance for the AST system and the case $\sigma_{p_B} = 20 \times 10^{-3}$ is used to approximate the lower bound performance for the AST system. Clearly, the performance of AST converges to FST only if BER=BERT at all times.

## 7.4 Summary

This chapter proposed a joint SNR target and rate adaptation MQAM system based on the SNR and BER estimates. The proposed algorithms were generalized for a CDMA/W-CDMA based system. In general, a CDMA/W-CDMA based system consists of both inner-loop and outer-loop power control mechanisms. The inner-loop power control follows the channel-inversion type power control algorithm. That is, based on a fixed SNR target, the inner-loop power mechanism adjusts the transmitter power inversely proportional to the channel fading. On the other hand, the outer-loop mechanism sets the SNR target according to a QoS requirement. The parameters SNR and BER are common indicators used for QoS. However, in a practical scenario, only the estimates of SNR and BER are available. Therefore, the proposed algorithms were derived based on the estimates of SNR and BER.

To verify the performance of the proposed system, namely 'Adaptive SNR Target' (AST) system, numerical evaluation was considered for the following scenarios. In a time-varying channel, the adaptive system would experience variation in the received BER. The variation is dependent on the accuracy of the CSI estimation, and the update rate of the link adaptation technique. Subsequently, the BER estimator model was simulated for three cases: 1) A relatively fast channel variation where the system was unable to estimate the channel accurately and/or unable to track the variations. The instantaneous BER varies away from the BER target value and the resulting PDF of the BER estimates approaches a uniform

distribution. 2) A relatively slow channel variation where the system was able to track and estimate accurately the channel variations most of the times. The BER of the system was nearly always equal to BERT and the resulting PDF of the BER estimator corresponds to a Gaussian function with an arbitrary low variance. 3) A scenario that falls between case (1) and case (2). Numerical results showed that the AST achieved higher spectral efficiency by exploiting the BER variations, with the highest spectral efficiency in case (1) and lowest spectral efficiency in case (3). The spectral efficiency of case (3) approaches that of a VRVP-MQAM system with fixed SNR target at the outer-loop power control, denoted as the 'Fixed SNR Target' (FST) system. Therefore, by exploiting the BER variations, the AST system outperformed the FST system in terms of spectral efficiency.

# Chapter 8

# MIMO Based VRVP-MQAM System

*The content of the work in Section 8.6 provides another one of the author's novel contributions. The work has been submitted for possible publication in IEEE Transactions on Communications [62], and was presented in part at the IEEE ICCS conference [33].*

## 8.1 Introduction

In the recent years, increasing demand for capacity has resulted in huge interest in multiple-antenna systems. As a result, numerous works on the capacity of MIMO systems over time-varying channels have been performed. The link adaptation of such systems along temporal and spatial dimensions has been considered in [19, 20]. The capacity of a single-input multiple-output (SIMO) and a multiple-input single-output (MISO) system over a Rayleigh flat-fading with side information on CSI at both the transmitter and receiver has been studied in [22].

High data rate services generally impose very stringent demand on bandwidth and require efficient adaptive rate and power control algorithm to optimise capacity. These services may have more tolerance to delay. However, voice services may be flexible on the bandwidth requirement but impose a stringent real-time and continuous transmission requirement. Therefore, the quality of service for voice and data are in general different. Solutions for optimal performance of integrated voice and data services have been worked on, from the work for wireline [63], to the work on wireless communication systems [64, 65]. However, these works mainly focussed on the upper layer aspects, such as the media access control (MAC) technique and protocols. An exception is the work in [66], which proposed solutions based on the link/physical layer adaptation. In particular, [66] proposed fixed rate binary phase shift keying (BPSK) and variable power allocation for voice on a quadrature channel; and a variable rate M-ary amplitude modulation (M-AM) with water-filling power adaptation for data in the inphase channel. The aim was to provide high average spectral efficiency for data services while maintaining satisfactory quality of services for voice.

In this chapter, a general framework for integrated voice and data transmission over a MIMO system is analyzed. The aim is to enhance spectral efficiency while maintaining the required quality of service for voice and data. Moreover, for higher spectral efficiency, an MQAM scheme is adopted.

The remainder of this chapter is organized as follows. In the respective sections 8.2-8.4, an overview of the MIMO channel model is first presented, this is then followed by the discussion of the statistical properties and the capacity of the MIMO channel. A MIMO based VRVP-MQAM system is introduced in Section 8.5. Finally, having clarified all definitions, rate and power allocation schemes are proposed for an integrated voice and data MIMO based system in Section 8.6.

## 8.2 MIMO Channel Model

Consider a MIMO system with $n_T$ transmit and $n_R$ receive antennas for a single-user flat-fading communication channel. The MIMO channel can be written as

$$\mathbf{y} = \mathbf{H}\mathbf{x} + \mathbf{n}, \tag{8.1}$$

where $\mathbf{y}$ is the complex $n_R \times 1$ column vector of the received signal, $\mathbf{x}$ is the complex $n_T \times 1$ column vector for the transmitted signal and $\mathbf{n}$ is the complex $n_R \times 1$ column vector for the receiver noise. The elements of $\mathbf{n}$ are drawn from zero mean, circularly symmetric, complex independent and identically distributed Gaussian noise. The $n_R \times n_T$ matrix $\mathbf{H}$ represents independent complex fading coefficients. Using the singular value decomposition (SVD), any matrix $\mathbf{H}$ can be written as

$$\mathbf{H} = \mathbf{U}\mathbf{\Lambda}\mathbf{V}^{\mathrm{H}}, \tag{8.2}$$

where $\mathbf{U}$ and $\mathbf{V}$ are unitary matrices of dimension $n_R \times n_R$ and $n_T \times n_T$ respectively. The $n_R \times n_T$ matrix $\mathbf{\Lambda}$ is diagonal whose elements are the nonnegative square roots of the eigenvalues of $\mathbf{H}\mathbf{H}^{\mathrm{H}}$ (if $n_R \leq n_T$) or $\mathbf{H}^{\mathrm{H}}\mathbf{H}$ (if $n_R > n_T$). By substituting (8.2) into (8.1), the MIMO channel can be written as

$$\mathbf{y} = \mathbf{U}\mathbf{\Lambda}\mathbf{V}^{\mathrm{H}}\mathbf{x} + \mathbf{n}. \tag{8.3}$$

The parallel MIMO channel model can be obtained through the following transformation,

$$\mathbf{U}^{\mathrm{H}}\mathbf{y} = \mathbf{U}^{\mathrm{H}}\mathbf{U}\mathbf{\Lambda}\mathbf{V}^{\mathrm{H}}\mathbf{x} + \mathbf{U}^{\mathrm{H}}\mathbf{n}, \tag{8.4}$$

$$\tilde{\mathbf{y}} = \mathbf{\Lambda}\tilde{\mathbf{x}} + \tilde{\mathbf{n}}, \tag{8.5}$$

where $\tilde{\mathbf{y}} = \mathbf{U}^{\mathrm{H}}\mathbf{y}$, $\tilde{\mathbf{x}} = \mathbf{V}^{\mathrm{H}}\mathbf{x}$ and $\tilde{\mathbf{n}} = \mathbf{U}^{\mathrm{H}}\mathbf{n}$. Note that multiplication by a unitary matrix does not change the distribution of noise, thus $\tilde{\mathbf{n}}$ has the same distribution

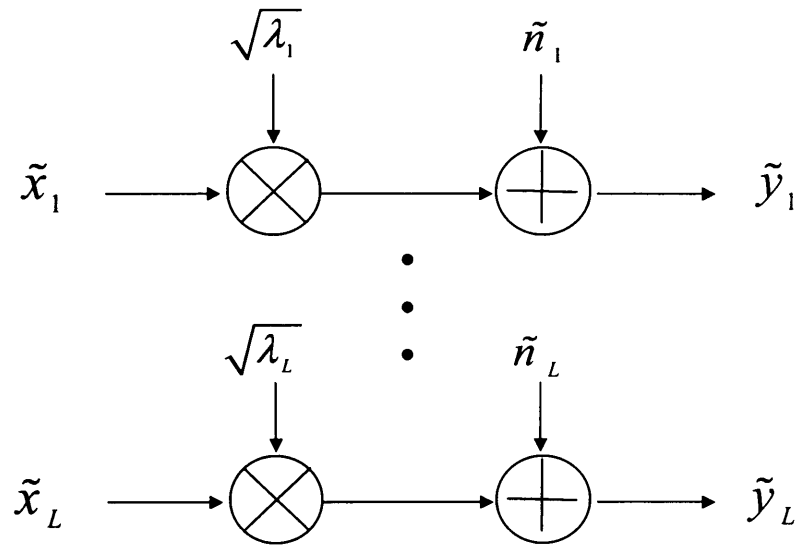


Figure 8.1: Parallel MIMO channel representation based on the SVD.

as $\mathbf{n}$. For $\mathbf{H}$ with a rank of at most $L = \min\{n_T, n_R\}$, the matrix $\mathbf{\Lambda}$ has at most $L = \min\{n_T, n_R\}$ nonzero diagonal elements $\{\sqrt{\lambda_i}\}_{i=1}^{L}$, where $\lambda_i$ denotes the $i^{th}$ eigenvalue. Thus the channel model can be decomposed into $L$ equivalent parallel eigen subchannels. Figure 8.1 shows the parallel MIMO channel model. The antenna configuration of the equivalent MIMO system shall be denoted by $(N, L)$, where $N = \max\{n_T, n_R\}$.

## 8.3 Statistical Properties of H

In a Rayleigh fading channel with a rich scattering environment, the signals from each transmitter could appear highly uncorrelated at each of the receive antennas. Thus $\mathbf{H}$ can be modelled as a random matrix with its elements forming independent zero-mean circularly symmetric complex Gaussian (ZMCSCG) random variables [17, ch.3] [20]. The matrix $\mathbf{W}$, defined as $\mathbf{W} = \mathbf{H}\mathbf{H}^{\mathrm{H}}$ or $\mathbf{W} = \mathbf{H}^{\mathrm{H}}\mathbf{H}$, is known as a Wishart matrix. $\mathbf{W}$ is an $n_R \times n_R$ random non-negative definite ma-

trix with real and non-negative eigenvalues. $\mathbf{W}$ follows the Wishart distribution and the joint density of its ordered eigenvalues has been shown in [20,67] to be

$$f_{\boldsymbol{\lambda}}(\boldsymbol{\lambda}) = (K_{L,N})^{-1} \mathrm{e}^{-\sum_i \lambda_i} \prod_i \lambda_i^{N-L} \prod_{i<j} (\lambda_i - \lambda_j)^2, \tag{8.6}$$

where $\boldsymbol{\lambda} = (\lambda_1, ..., \lambda_L)$ and $\lambda_1 \geq ... \geq \lambda_L \geq 0$. $K_{L,N}$ is a normalizing factor written as,

$$K_{L,N} = \prod_{i=1}^{L} (L-1)!\,(N-1)!. \tag{8.7}$$

The joint density of its unordered eigenvalues is [20,67]

$$f_{\boldsymbol{\lambda}}(\boldsymbol{\lambda}) = (L! K_{L,N})^{-1} \mathrm{e}^{-\sum_i \lambda_i} \prod_i \lambda_i^{N-L} \prod_{i<j} (\lambda_i - \lambda_j)^2. \tag{8.8}$$

The marginal PDF of any of the unordered eigenvalues can be computed in terms of its joint density functions [37]

$$f_{\lambda_1}(\lambda_1) = \int_{\lambda_2} \cdots \int_{\lambda_L} f_{\boldsymbol{\lambda}}(\boldsymbol{\lambda})\, d\lambda_2 \cdots d\lambda_L. \tag{8.9}$$

In [20], Telatar derived the integration operations and obtained the solution as

$$f_{\lambda_1}(\lambda_1) = \frac{1}{L} \sum_{i=0}^{L-1} \frac{i!}{(i+D)!} \left[L_i^{L-N}(\lambda_1)\right]^2 \lambda_1^{N-L} \exp(-\lambda_1). \tag{8.10}$$

where $D = (N-L)$ and $L_i^{L-N}(\lambda_1) \triangleq \frac{1}{i!} \exp(\lambda_1) \lambda_1^{L-N} \frac{d^i}{d\lambda_1^i} \left(\exp(-\lambda_1)\, \lambda_1^{L-N+i}\right)$ is the associated Laguerre polynomial of order $i$ [39]. From (8.10), Mischa [68] simplified the PDF to an alternate convenient form, written here as

$$f_{\lambda_1}(\lambda_1) = \frac{1}{L} \sum_{i=0}^{L-1} \frac{i!}{(i+D)!} \sum_{l_1=0}^{i} \sum_{l_2=0}^{i} (-1)^{l_1+l_2} A_{l_1}(i,D)\, A_{l_2}(i,D)\, \lambda^{l_1+l_2+D} e^{-\lambda}, \tag{8.11}$$

where

$$A_l(i,D) = \frac{(i+D)!}{(i-l)!\,(D+l)!\,l!}. \tag{8.12}$$

Based on (8.6) and (8.8), several mathematical functions for the probability density functions of maximum and minimum eigenvalues have been derived (see for example [22,69,70]). Assume that $f(x)$ denotes the PDF for a related eigenvalue, for later use (Section 8.6), closed-form solutions are to be obtained from the integral functions, $f(x)\,dx$ and $\int \frac{1}{x} f(x)\,dx$. For this aim, a suitable PDF for the maximum eigenvalue is [69]

$$f_{\lambda_{max}}(\lambda) = \sum_{i=1}^{L} \sum_{m=N-L}^{(N+L)i-2i^2} d_{i,m} \frac{i^{m+1} \lambda^m e^{-i\lambda}}{m!}, \tag{8.13}$$

where the coefficients $d_{i,m}$ can be obtained numerically [69]. A suitable PDF for minimum eigenvalue $f_{\lambda_{min}}(\lambda)$ is [22]

$$f_{\lambda_{min}}(\lambda) = Le^{-\lambda L}, \tag{8.14}$$

which is applicable only when $L = N$.

## 8.4 MIMO Channel Capacity

In general, a MIMO channel can be decomposed into $L$ parallel subchannels possibly with nonequal gains. A power allocation scheme is employed to distribute the total power available at the transmitter among the $L$ subchannels. The two power allocation schemes commonly considered are the water filling power allocation and equal power control policy. The water filling power allocation scheme is considered for maximizing channel capacity when CSI is perfectly known at the receiver and the transmitter, whereas the equal power allocation scheme is for maximizing channel capacity when CSI is known at the receiver but not available at the transmitter. This section provides an overview of the two schemes and more details can be found in [17,20].

### 8.4.1 Channel Capacity with Full Channel Knowledge

When the MIMO channel is known at the transmitter and the receiver, the individual subchannel may be accessed through adaptive techniques at the transmitter and the receiver with the aim of maximizing the system performance over channel variations. In a deterministic MIMO channel $\mathbf{H}$ with uncorrelated Rayleigh fading, Telatar [20] showed that the capacity is the sum of the individual subchannel capacities, written here as

$$C = \sum_{i=1}^{L} B \log_2 \left(1 + \frac{P_i}{\sigma_n^2}\lambda_i\right), \tag{8.15}$$

where $P_i$ denotes the transmit power at subchannel $i$. This is subject to the total transmit power constraint

$$\sum_{i=1}^{L} P_i = P. \tag{8.16}$$

The resulting optimal power adaptation is water-filling across the subchannels,

$$P_i = \left(U - \frac{\sigma_n^2}{\lambda_i}\right)^+, \tag{8.17}$$

where $(x)^+ \triangleq \max(x, 0)$ and $U$ is chosen to satisfy the power constraint (8.16). Finally, substituting (8.17) into (8.15), the maximum capacity is simplified to

$$C_{max} = \sum_{i=1}^{L} B \log_2 \left(U\frac{\lambda_i}{\sigma_n^2}\right). \tag{8.18}$$

The above derivations are for the case of a deterministic MIMO channel. For a random matrix $\mathbf{H}$, the channel capacity $\bar{C}$ is the ensemble average of the capacity achieved when the water-filling power adaptation is performed for each channel realization of $\mathbf{H}$. In [20], Telatar expresses $\bar{C}$ in terms of the distribution of the eigenvalues $\boldsymbol{\lambda}$

$$\bar{C} = E_{\boldsymbol{\lambda}}\left[\sum_{i=1}^{L} \log_2 \left(1 + \frac{P_i}{\sigma_n^2}\lambda_i\right)\right], \tag{8.19}$$

where $E_{\boldsymbol{\lambda}}$ denotes the statistical expectation with respect to $\boldsymbol{\lambda}$.

### 8.4.2 Channel Capacity with Partial Channel Knowledge

A possible scenario that could occur in a MIMO system is when the receiver knows the CSI but the transmitter does not. Let 'CSIR' refers to the CSI received at the receiver and 'CSIT' refers to the CSI at the transmiter. Without CSIT, the transmitter could not distribute power among the individual subchannel optimally. However, for $\mathbf{x}$ that is circularly symmetric complex Gaussian with zero-mean and convariance $\frac{P}{L}\mathbf{I}_t$, Telatar shows that for a deterministic channel in the absence of CSIT, the maximum capacity is given by [20],

$$C = \sum_{i=1}^{L} \log_2 \left(1 + \frac{P\lambda_i}{L\sigma_n^2}\right). \tag{8.20}$$

The average capacity in the absence of CSIT is therefore [20]

$$\bar{C} = E_{\boldsymbol{\lambda}}[\sum_{i=1}^{L} \log_2 \left(1 + \frac{P\lambda_i}{L\sigma_n^2}\right)]. \tag{8.21}$$

### 8.4.3 Numerical Results

Figure 8.2 compares the average capacities for the case when full channel knowledge (CSIR and CSIT) is available at the receiver and transmitter (8.19) with the case when only CSIR is available at the receiver (8.21). The results show a small gap in the capacity between the two cases at low SNR. This difference diminishes as SNR increases.

## 8.5 MIMO Based VRVP-MQAM System

### 8.5.1 System Model and Definition

This section describes the VRVP-MQAM scheme for a MIMO system. Figure 8.3 shows the system diagram. The equivalent SVD based MIMO system

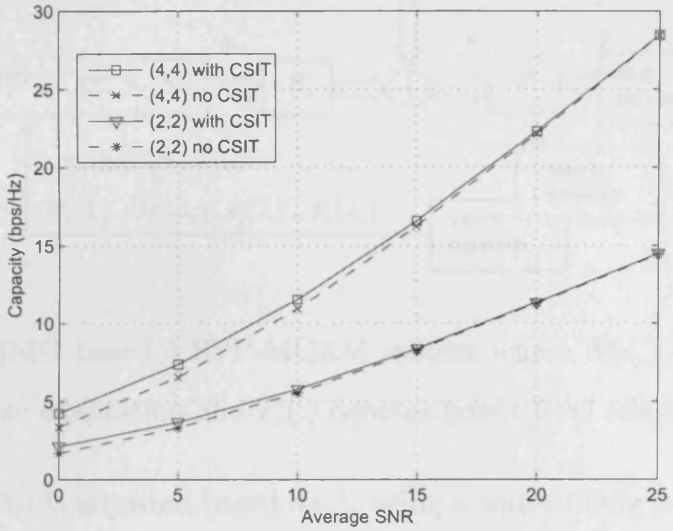


Figure 8.2: Capacity for MIMO system (2,2),(4,4). Comparison between full CSI and partial CSI.

model uses the antenna setting notation $(L, N)$, where $L = \min\{n_T, n_R\}$ and $N = \max\{n_T, n_R\}$. For a Rayleigh fading environment with independent fading between each transmit-receive antenna pair, the SVD of $\mathbf{H} = \mathbf{U}\mathbf{\Lambda}\mathbf{V}^{\mathrm{H}}$ discussed in Section 8.2 and the statistical properties of $\mathbf{H}$ in Section 8.3 shall apply. The spatial and temporal MIMO channel is modelled by a random channel matrix $\mathbf{H}$ with its entries having an i.i.d. Gaussian form with zero-mean independent real and imaginary parts, each with variance 1/2. Perfect channel information is assumed available at the receiver and it is fed back error free to the transmitter. For a given BER target BERT requirement, the VRVP module adapts rate and power in accordance with the spatial and temporal channel variations, i.e. rate and power are varied across the time and space dimension. Let the index $i$ denote the particular (spatial) subchannel. Rate adaptation $k_i$ is adjusted by varying the constellation size $M(\lambda_i)$ based on the instantaneous eigenvalue $\lambda_i$. The power

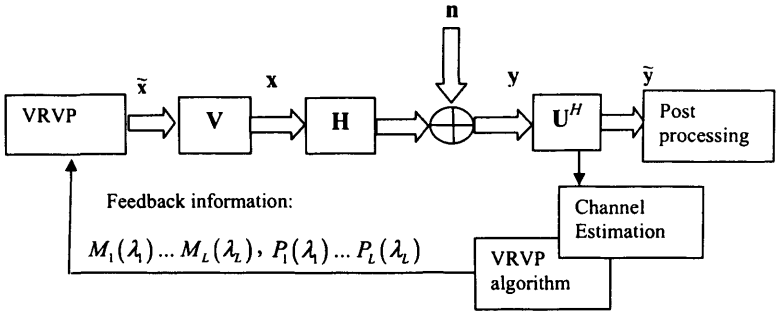


Figure 8.3: MIMO based VRVP-MQAM system where $M_i(.)$ denotes MQAM constellation size adaptation and $P_i(.)$ denotes power level adaptation.

adaptation $P_i(\lambda_i)$ is adjusted based on $\lambda_i$ using a water-filling policy.

In analogy to a SISO based MQAM scheme (Section 3.3), at each subchannel the instantaneous BER is expressed as a function of the instantaneous received SNR $\gamma_i$ as (c.f. 3.29),

$$\mathrm{BER}_i(\gamma_i) = c_1 \exp\left(-\frac{c_2\gamma_i}{2^{k_i(\gamma_i)}-1}\frac{P_i(\gamma_i)}{P}\right). \tag{8.22}$$

Therefore for a given BERT, the constellation size of each subchannel can be expressed as

$$M_i(\gamma_i) = 1 + \frac{-c_2\gamma_i}{\ln\left(\frac{\mathrm{BERT}}{c_1}\right)}\frac{P_i(\gamma_i)}{P}. \tag{8.23}$$

Alternatively, (8.23) can be expressed in terms of the eigenvalue $\lambda_i$ as

$$M_i(\lambda_i) = 1 + \frac{-c_2\lambda_i}{\ln(\mathrm{BERT}/c_1)}\frac{P_i(\lambda_i)}{\sigma_n^2}, \tag{8.24}$$

since $\gamma_i \triangleq \frac{P\lambda_i}{\sigma_n^2}$. Subsequently, the transmit rate $k_i$ for each subchannel can be expressed as

$$k_i(\lambda_i) = \log_2\left(1 + \frac{-c_2\lambda_i}{\ln(\mathrm{BERT}/c_1)}\frac{P_i(\lambda_i)}{\sigma_n^2}\right). \tag{8.25}$$

The average spectral efficiency of an MQAM MIMO based system can be deduced from the capacity analysis of a MIMO channel. For full CSI knowledge,

the average spectral efficiency can be written as [23]

$$ASE = E_{\boldsymbol{\lambda}}\left[\sum_{i}^{L}\log_2\left(1+\frac{-c_2\lambda_i}{\ln\left(\mathrm{BERT}/c_1\right)}\frac{P_i\left(\lambda_i\right)}{\sigma_n^2}\right)\right] \tag{8.26}$$

$$= E_{\boldsymbol{\lambda}}\left[\sum_{i}^{L}k_i\left(\boldsymbol{\lambda}\right)\right], \tag{8.27}$$

subject to a long term average power constraint,

$$\mathrm{P_{avg}} = E_{\boldsymbol{\lambda}}\left[\sum_{i}^{L}P_i\left(\boldsymbol{\lambda}\right)\right]. \tag{8.28}$$

Note that notations $k_i\left(\boldsymbol{\lambda}\right)$ and $P_i\left(\boldsymbol{\lambda}\right)$ explicitly indicate the dependency on $L$ subchannels.

### 8.5.2 Optimisation Problems

The aim is to maximise $ASE$ subject to an average transmit power and instantaneous BER constraint. The transmit power and rate at each subchannel are varied according to the statistics of the subchannel gains and the time variations. This can be a complex optimization problem to solve. For a constrained power $P_{\mathrm{avg}} = P$ and an instantaneous BER target BERT, the full optimisation problem is formulated as [23]

$$\underset{P_i,\,k_i}{\text{maximize}} \quad ASE = E_{\boldsymbol{\lambda}}[\textstyle\sum_i^L k_i\left(\boldsymbol{\lambda}_i\right)] \tag{8.29}$$

$$\text{subject to} \quad E_{\boldsymbol{\lambda}}\left[\textstyle\sum_i^L P_i\left(\boldsymbol{\lambda}\right)\right] \leq P, \tag{8.30}$$

$$\mathrm{BER}_i\left(\boldsymbol{\lambda}\right) \leq \mathrm{BERT}, \tag{8.31}$$

$$k_i\left(\boldsymbol{\lambda}\right) \geq 0, \quad P_i\left(\boldsymbol{\lambda}\right). \tag{8.32}$$

That is, in the full optimisation problem, solutions for optimal rate and power involve adaptation in both the spatial and time domains. This is a complicated

multi-dimension problem to solve. However, Zhou *et al.* proved in [23] that, when based on an unordered eigenvalue distribution, the full optimisation problem can be simplified to $L$ equivalent parallel SISO optimisation problem. The simplified optimisation problem is given by,

$$\underset{P_1, k_1}{\text{maximize}} \quad ASE = LE_{\lambda_1}[k_1(\lambda_1)], \tag{8.33}$$

$$\text{subject to} \quad E_{\lambda_1}\left[P_1(\lambda_1)\right] \leq P/L, \tag{8.34}$$

$$\text{BER}_1(\lambda_1) \leq \text{BERT}, \tag{8.35}$$

$$k_1(\lambda_1) \geq 0, \quad P_1(\lambda_1), \tag{8.36}$$

where $k_1(\lambda_1)$, $P_1(\lambda_1)$ and $\text{BER}_1(\lambda_1)$ denote respectively the rate, transmit power and BER of the first subchannel.

In summary, when based on an unordered eigenvalue subchannel model, the rate and power adaptation of the MIMO based VRVP-MQAM system is equivalent to $L$ SISO VRVP-MQAM systems. Therefore, the solutions for rate and power adaptation of the VRVP-MQAM multi-antenna system can be obtained from the works of the VRVP single antenna system. (Discussed in Section 3.3)

## 8.6 VRVP-MIMO for Integrated Voice and Data Services

Consider a MIMO system that assigns one subchannel for voice transmission and the remaining subchannels for data transmission. Given a MIMO system with constrained available power, voice service is allocated with appropriate transmission power to satisfy a BER requirement for the voice transmission. Subsequently, based on the remaining average power, optimal rate and power adaptations for maximum spectral efficiency under a BER requirement are considered for data transmission. Three integrated schemes are proposed. In the first scheme, voice and data are allocated on any of the unordered singular value channels. In the second and third schemes, voice is allocated on the subchannel associated with the largest and the smallest singular values, respectively, while data is allocated on the remaining subchannels. The full optimization problem is first formulated in terms of the spatial and temporal variations, and then the problem will be simplified to an equivalent optimization problem in terms of only the temporal variation. Based on the simplified optimization problem and the eigenvalue distribution of random Wishart matrices, solutions for the rate and power adaptations on voice and data transmissions will be derived. Finally, the performance of the system will be investigated using numerical simulations.

### 8.6.1 Problem Formulation

An $(L, N)$ MIMO channel is considered, where one subchannel is allocated for voice transmission and the remaining $(L-1)$ subchannels are allocated for data transmission. The first proposed scheme, where voice and data are transmitted through any of the unordered singular value channels, is denoted as the unordered

singular value for voice (USVV) scheme. The second scheme, where voice is transmitted through the largest singular value channel, shall be denoted as the largest singular value for voice (LSVV) scheme. Finally, the last scheme, where voice is transmitted through the smallest singular value channel, shall be denoted as the smallest singular value for voice (SSVV) scheme. Note that for all three schemes, data services are transmitted through the remaining $(L-1)$ unordered subchannels. For simplicity and without loss of generality, the voice transmission channel is denoted by subchannel index 1 and data transmission channels are denoted by the subchannel index $j$, where $j = \{2...L\}$.

For all three schemes, priority is given to voice transmission by allocating instantaneous voice signal power $P_v(\lambda_1)$ to satisfy a required bit error rate (BER) target, $\text{BERT}_v$. To refrain from excessive power allocation for voice transmission, a power constraint $P_{vo}$ is imposed on the maximum allowable instantaneous transmit power for voice. This power constraint will result in voice outage. Both BER and voice outage $Pout_v$ will be used as the performance indicators for the quality of service (QoS) for voice.

An adaptive rate and power scheme is considered for data transmission. That is, the system adapts its rate and power to both spatial and temporal variations. Based on an MQAM scheme, adaptive rate can be achieved by varying its constellation size in accordance with the spatial and temporal variations of the subchannels characterized by the singular values. Similar to the work in [23] that optimizes an $L$ unordered eigen subchannels VRVP-MQAM (data-only) MIMO system based on $L$ independent SISO optimization problems, the data transmission of the three schemes will be based on $L-1$ SISO optimization problems.

Therefore the average spectral efficiency for data services can be expressed as

$$ASE_d = \int_{\lambda_2} \cdots \int_{\lambda_L} \sum_{j=2}^{L} [k_j (\boldsymbol{\lambda}^{L-1})] f_{\boldsymbol{\lambda}}^{L-1} (\boldsymbol{\lambda}^{L-1}) \, d\lambda_2 \ldots d\lambda_L \quad (8.37)$$

$$= (L-1) \int_{\lambda_u} k(\lambda_u) \, f_{\lambda_u}^{L-1}(\lambda_u) \, d\lambda_u, \quad (8.38)$$

where $\boldsymbol{\lambda}^{L-1} = (\lambda_2 ... \lambda_L)$ is the remaining $L-1$ unordered eigenvalues and $f_{\boldsymbol{\lambda}}^{L-1} (\boldsymbol{\lambda}^{L-1})$ denotes the PDF of the $L-1$ unordered eigenvalues. In the full optimization problem statement in (8.37), $k_j (\boldsymbol{\lambda}^{L-1})$ denotes the data rate in bits/symbol for the $j^{\text{th}}$ subchannel and explicitly indicates its dependence on the other subchannels. In the simplified $L-1$ independent SISO optimization problem statement in (8.38), $f_{\lambda_u}^{L-1}(\lambda_u)$ denotes the marginal PDF of any of the $L-1$ unordered eigenvalues $\lambda_u$, and the data rate can be simplified by the notation $k(\lambda_u)$. Assuming an ergodic channel gain, $ASE_d$ can be approximated through the statistical average,

$$ASE_d \approx (L-1) \, E_{\lambda_u}[k(\lambda_u)], \quad (8.39)$$

where $E_{\lambda_u}[.]$ denotes the statistical expectation with respect to $\lambda_u$. Similarly, define the instantaneous power adaptation for the $j^{\text{th}}$ subchannel as $P_{d_j} (\boldsymbol{\lambda}^{L-1})$ in the full optimization statement in (8.40), and as $P_d(\lambda_u)$ in the simplified $L-1$ independent SISO optimization problem statement in (8.41). The average power for data services can be obtained from

$$ATP_d = \int_{\lambda_2} \cdots \int_{\lambda_L} \sum_{j=2}^{L} [P_{d,j} (\boldsymbol{\lambda}^{L-1})] f_{\boldsymbol{\lambda}^{L-1}} (\boldsymbol{\lambda}^{L-1}) \, d\lambda_2 \ldots d\lambda_L \quad (8.40)$$

$$= (L-1) \int_{\lambda_u} P_d(\lambda_u) \, f_{\lambda_u}^{L-1}(\lambda_u) \, d\lambda_u \quad (8.41)$$

$$\approx (L-1) \, E_{\lambda_u}[P_d(\lambda_u)]. \quad (8.42)$$

Finally, the complete optimization problem for the integrated voice and data

services is formulated as follows,

$$P_v(\lambda_1) \leq P_{vo}, \tag{8.43}$$

$$\mathrm{BER}_{\mathrm{voice}}(\lambda_1) \leq \mathrm{BERT}_v, \tag{8.44}$$

$$\underset{P_d(\lambda_u),\, k(\lambda_u)}{\text{maximize}} \quad ASE_d = (L-1)\, E_{\lambda_u}[k(\lambda_u)], \tag{8.45}$$

$$\text{subject to } ATP_d = \left(P - \overline{P}_v\right), \tag{8.46}$$

$$\mathrm{BER}_{\mathrm{data}}(\lambda_u) \leq \mathrm{BERT}_d. \tag{8.47}$$

In summary, solutions for the integrated optimization problem are derived in two parts. The first part is the power adaptation policy for voice transmission for a given power constraint $P_{vo}$ (8.43) and $\mathrm{BERT}_v$ (8.44). Based on this, the average power required for voice transmission can be computed from $\overline{P}_v \triangleq \int_{\lambda_1} P_v(\lambda_1)\, f_{\lambda_v}(\lambda_1)\, d\lambda_1$, where $f_{\lambda_v}(\lambda_1)$ denotes the PDF of the eigenvalue used for voice transmission. In the second part, rate $k(\lambda_u)$ and power $P_d(\lambda_u)$ adaptations are derived for maximum spectral efficiency subject to the remaining average power $(P - \overline{P}_v)$ (8.46) and an instantaneous BER target $\mathrm{BERT}_d$ (8.47). Note that $P$ denotes the total average transmission power available in the system.

### 8.6.2 Statistics of Related Eigenvalues

This section presents the derivation for the PDF and cumulative distribution function (CDF) of the remaining $L-1$ unordered eigenvalues.

Proposition 1: The marginal PDF of any of the remaining $L-1$ unordered eigenvalues is determined as

$$f_{\lambda_u}^{L-1}(\lambda) = \frac{1}{L-1}\left[L\, f_{\lambda_u}^{L}(\lambda) - f_{\lambda_v}(\lambda)\right], \tag{8.48}$$

where $f_{\lambda_u}^{L}(.)$ denotes the marginal PDF of any of the $L$ unordered eigenvalues and $f_{\lambda_v}(.)$ denotes the PDF of the eigenvalue dedicated for voice subchannel. In

the LSVV scheme, $f_{\lambda_v}(.)$ is the PDF of the largest eigenvalue $f_{\lambda_{max}}(.)$, while in the SSVV scheme, $f_{\lambda_v}(.)$ is the PDF of the smallest eigenvalue $f_{\lambda_{min}}(.)$. Note that in the USVV scheme, since both data and voice transmission are transmitted through any of the $L$ unordered singular value channels, the marginal PDF of the eigenvalue for the voice or data channels is clearly defined by $f^L_{\lambda_u}(.)$.

The proof is based on the theory of random variables (RVs) [37]. Let $f(x)$ denotes the PDF of a RV X. The area of $f(x)$ in an interval $(x_1, x_2)$ equals the probability that X is in this interval. If $x_1 = x$, $x_2 = x + \Delta x$ and $\Delta x$ is arbitrary small, the probability of the event $\{x \leq \mathrm{X} < x + \Delta x\}$ can be defined as

$$P\{x \leq \mathrm{X} \leq x + \Delta\} = \int_x^{x+\Delta x} f(x)\, dx \quad \simeq f(x)\, \Delta x. \tag{8.49}$$

The density $f(x)$ can be defined directly as a limit involving probability,

$$f(x) = \underset{\Delta x \to 0}{\text{limit}} \frac{P\{x \leq \mathrm{X} \leq x + \Delta\}}{\Delta x}. \tag{8.50}$$

For large $n$ and small $\Delta x$, with the event $\{x \leq \mathrm{X} < x + \Delta x\}$ occurring $n_k$ times in $n$, the density $f(x)$ can be approximated by

$$f(x) \simeq \frac{n_k}{n}. \tag{8.51}$$

In the context here, let $\{\lambda_1, ..., \lambda_L\}$ be considered as an event in an experiment and the experiment is repeated $n$ times. Let $\Omega_1$ denotes a set of all $L$ eigenvalues in $n$ experiments. Next, assume either the largest or the smallest eigenvalue is drawn out from each experiment set. Let $\Omega_2$ denotes a set of the largest (or smallest) eigenvalue in $n$ experiments. Correspondingly, in each experiment, $L-1$ eigenvalues will remain. Let $\Omega_3$ denotes a set of the remaining $L-1$ eigenvalues in the $n$ experiments. Based on (8.51), the density of the three respective events

can be approximated as

$$f_{\lambda_u}^{L}(\lambda) \simeq P_{\Omega_1}\{\lambda \leq \boldsymbol{\lambda_u^L} < \lambda + \Delta\lambda\} = \frac{n_1}{nL}, \tag{8.52}$$

$$f_{\lambda_v}(\lambda) \simeq P_{\Omega_2}\{\lambda \leq \boldsymbol{\lambda_v} < \lambda + \Delta\lambda\} = \frac{n_2}{n}, \tag{8.53}$$

$$f_{\lambda_u}^{L-1}(\lambda) \simeq P_{\Omega_3}\{\lambda \leq \boldsymbol{\lambda_u^{L-1}} < \lambda + \Delta\lambda\} = \frac{n_1 - n_2}{n(L-1)}, \tag{8.54}$$

where $n_k$ denotes the number of times the respective events occur. $\boldsymbol{\lambda_u^L}, \boldsymbol{\lambda_v}, \boldsymbol{\lambda_u^{L-1}}$ denote the RVs of the respective events. By simple algebraic manipulation, (8.54) can be re-arranged as

$$f_{\lambda_u}^{L-1}(\lambda) = \frac{n_1}{n(L-1)} - \frac{n_2}{n(L-1)} \tag{8.55}$$

$$= \frac{1}{L-1}\left[L f_{\lambda_u}^{L}(\lambda) - f_{\lambda_v}(\lambda)\right]. \qquad \square \tag{8.56}$$

For later use, closed-form expressions are required for the integral functions $\int f(x)\,dx$ and $\int \frac{1}{x} f(x)\,dx$, where $f(x)$ in the context here refers to the PDF of the related eigenvalues, $f_{\lambda_u}^{L}(.)$, $f_{\lambda_{max}}(.)$ and $f_{\lambda_{min}}(.)$. With this aim, the PDF for $f_{\lambda_u}^{L}(\lambda)$ is [23]

$$f_{\lambda_u}^{L}(\lambda) = \frac{1}{L}\sum_{i=0}^{L-1}\frac{i!}{(i+D)!}\sum_{l_1=0}^{i}\sum_{l_2=0}^{i}(-1)^{l_1+l_2} \cdot A_{l_1}(i,D)\, A_{l_2}(i,D)\, \lambda^{l_1+l_2+D} e^{-\lambda}, \tag{8.57}$$

where $A_l(i,D) = \frac{(i+D)!}{(i-l)!(D+l)!\,l!}$ and $D = (N-L)$. The PDF for $f_{\lambda_{max}}(\lambda)$ is [69]

$$f_{\lambda_{max}}(\lambda) = \sum_{i=1}^{L}\sum_{m=N-L}^{(N+L)i-2i^2} d_{i,m}\frac{i^{m+1}\lambda^m e^{-i\lambda}}{m!}, \tag{8.58}$$

where the coefficients $d_{i,m}$ can be obtained numerically [69]. Finally, the PDF for $f_{\lambda_{min}}(\lambda)$ is [22]

$$f_{\lambda_{min}}(\lambda) = Le^{-\lambda L}, \tag{8.59}$$

which is applicable only when $L = N$.

Subsequently, the CDF of the remaining $L-1$ unordered eigenvalues can be obtained from (8.48) as

$$F_{\lambda_u}^{L-1}(u) = \frac{1}{L-1}\left[L\,F_{\lambda_u}^{L}(u) - F_{\lambda_v}(u)\right], \tag{8.60}$$

where $F_{\lambda_u}^{L}(.)$ denotes the CDF of any of the $L$ unordered eigenvalues and $F_{\lambda_v}(.)$ denotes the CDF of the eigenvalue used for the voice channel. The closed-form CDF of the density functions are written as

$$\begin{aligned} F_{\lambda_u}^{L}(u) &= \int_0^u f_{\lambda_u}^{L}(\lambda)\,d\lambda \\ &= \frac{1}{L}\sum_{i=0}^{L-1}\frac{i!}{(i+D)!}\sum_{l_1=0}^{i}\sum_{l_2=0}^{i}(-1)^{l_1+l_2} \\ &\quad \cdot A_{l_1}(i,D)\,A_{l_2}(i,D)\,\Gamma_L(\xi+1,u), \end{aligned} \tag{8.61}$$

$$\begin{aligned} F_{\lambda_{max}}(u) &= \int_0^u f_{\lambda_{max}}(\lambda)\,d\lambda \\ &= \sum_{i=1}^{L}\sum_{m=N-L}^{(N+L)i-2i^2}\frac{i^{m+1}d_{i,m}}{m!}\,\frac{\Gamma_L(m+1,ui)}{i^{m+1}}, \end{aligned} \tag{8.62}$$

$$\begin{aligned} F_{\lambda_{min}}(u) &= \int_0^u f_{\lambda_{min}}(\lambda)\,d\lambda \\ &= 1-e^{-uL}. \end{aligned} \tag{8.63}$$

Note that $\xi \triangleq l_1 + l_2 + D$ and $\Gamma_L(a,u) \triangleq \int_0^u x^{(a-1)}e^{-x}\,dx$ is the lower incomplete Gamma function [45].

## Simulation results and verification

This section verifies the PDF of the related eigenvalues, $f_{\lambda_u}^{L}(\lambda)$, $f_{\lambda_{\max}}(\lambda)$ and $f_{\lambda_u}^{L-1}(\lambda)$ using the analytical expressions (8.57), (8.58) and (8.48) respectively. Figure 8.4 and Figure 8.5 show respectively the density plots for (2,2) and (4,4) configurations. The graphs clearly illustrate the absence of the maximum eigenvalues in the density plot $f_{\lambda_u}^{L-1}(\lambda)$.

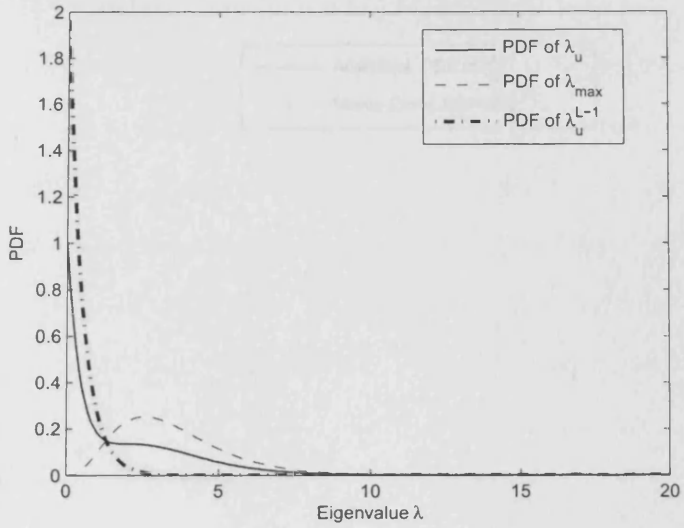


Figure 8.4: PDF of related eigenvalues for a (2,2) MIMO system.

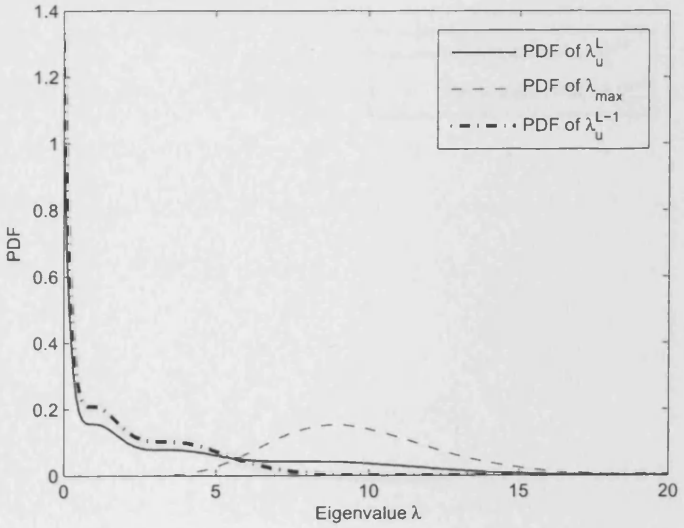


Figure 8.5: PDF of related eigenvalues for a (4,4) MIMO system.

To validate the derived analytical expression for PDF $f_{\lambda_u}^{L-1}(\lambda)$ (8.48), results based on the analytical expression and Monte Carlo simulation are compared. Figure 8.6 and Figure 8.7 illustrate that the Monte Carlo simulation results match

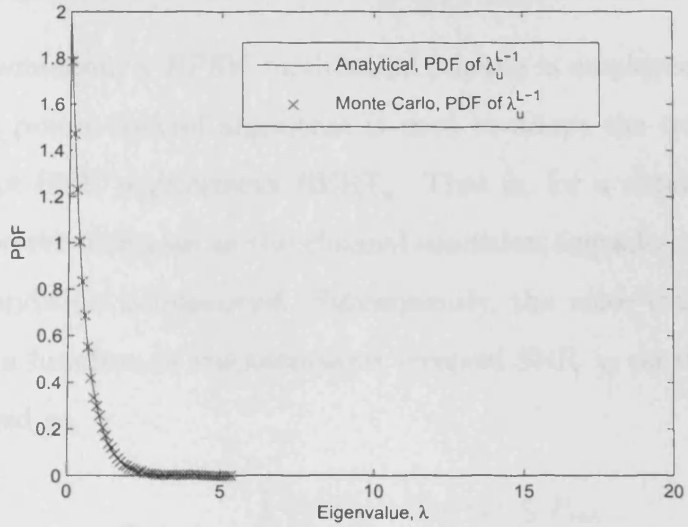


Figure 8.6: PDF of $L-1$ unordered eigenvalues for a (2,2) MIMO system.

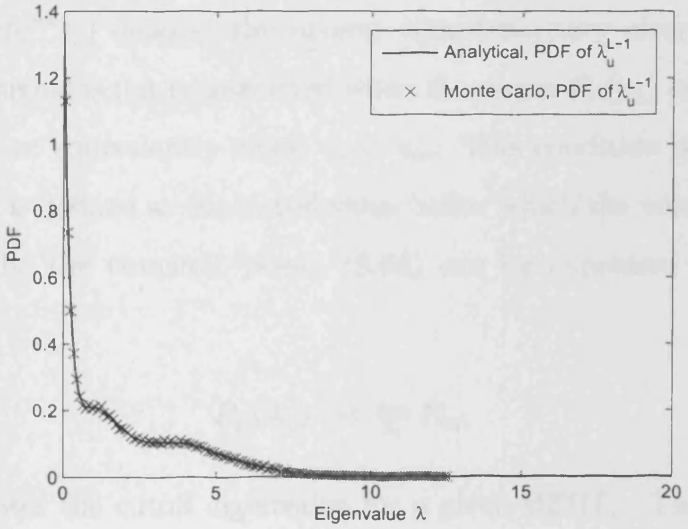


Figure 8.7: PDF of $L-1$ unordered eigenvalues for a (4,4) MIMO system.

perfectly with the analytical result.

### 8.6.3 Adaptive Power for Voice Transmission

For voice transmission, a BPSK modulation scheme is employed, and a channel inversion type power control algorithm is used to adapt the transmit power to meet the target BER requirement $\text{BERT}_v$. That is, for a required $\text{BERT}_v$, the transmission power increases as the channel condition degrades, and decreases as the channel condition is improved. Subsequently, the voice transmission power adaptation as a function of instantaneous received SNR $\gamma_1$ on the voice channel can be expressed as

$$P_v(\gamma_1) = \begin{cases} \frac{\gamma_{vo}}{\gamma_1} P_{vo}, & P_v(\gamma_1) \leq P_{vo}, \\ 0, & \text{otherwise}, \end{cases} \tag{8.64}$$

where $\gamma_{vo} \triangleq [\text{erfc}^{-1}(2\text{BERT}_v)]^2$ is the threshold SNR for a given BER value $\text{BERT}_v$ and $\text{erfc}^{-1}(.)$ denotes the inverse complementary error function. Note that the voice signal is not transmitted when the power $P_v(\gamma_1)$ exceeds the power constraint $P_{vo}$, or equivalently when $\gamma_1 < \gamma_{vo}$. This condition is known as voice outage and $\gamma_{vo}$ is defined as the cutoff value below which the voice outage occurs.

Alternatively, the transmit power (8.64) can be expressed in terms of the variable $\lambda_1$ as

$$P_v(\lambda_1) = \frac{\lambda_{vo}}{\lambda_1} P_{vo}, \tag{8.65}$$

where $\lambda_{vo}$ denotes the cutoff eigenvalue for a given $\text{BERT}_v$. The parameter $\lambda_{vo}$ can be obtained as

$$\lambda_{vo} = \gamma_{vo} \frac{\sigma_n^2}{P_{vo}} = \gamma_{vo} \frac{\sigma_n^2}{RP} = \gamma_{vo} \frac{1}{R\Gamma}, \tag{8.66}$$

where $\Gamma = P/\sigma_n^2$ is the average received SNR at the receiver, $\sigma_n^2$ denotes the noise variance and $R$ refers to the ratio $P_{vo}/P$. The normalized transmit power can be

expressed as

$$\frac{P_v(\lambda_1)}{P} = \frac{\lambda_{vo}}{\lambda_1}\frac{P_{vo}}{P} = \frac{\lambda_{vo}}{\lambda_1}R. \tag{8.67}$$

Subsequently, the average normalized power for USVV, LSVV and SSVV are obtained respectively as

$$\begin{aligned}
\frac{\overline{P}_v}{P}_{\text{USVV}} &= \lambda_{vo}R\int_{\lambda_{vo}}^{\infty}\frac{1}{\lambda_1}f_{\lambda_u}^{L}(\lambda_1)\,d\lambda_1 \\
&= \frac{1}{L}\sum_{i=0}^{L-1}\frac{i!}{(i+D)!}\sum_{l_1=0}^{i}\sum_{l_2=0}^{i}(-1)^{l_1+l_2}A_{l_1}(i,D)\,A_{l_2}(i,D)\,\Gamma_U(\xi,\lambda_{vo}), \qquad (8.68)\\
\frac{\overline{P}_v}{P}_{\text{LSVV}} &= \lambda_{vo}R\int_{\lambda_{vo}}^{\infty}\frac{1}{\lambda_1}f_{\lambda_{max}}(\lambda_1)\,d\lambda_1 \\
&= \lambda_{vo}R\sum_{i=1}^{L}\sum_{m=N-L}^{(N+L)i-2i^2}\frac{i^{m+1}d_{i,m}}{m!}\frac{\Gamma_U(m,\lambda_{vo}i)}{i^m}, \qquad (8.69)\\
\frac{\overline{P}_v}{P}_{\text{SSVV}} &= \lambda_{vo}R\int_{\lambda_{vo}}^{\infty}\frac{1}{\lambda_1}f_{\lambda_{min}}(\lambda_1)\,d\lambda_1 \\
&= \lambda_{vo}RL\,\mathrm{E}_1(\lambda_{vo}L). \qquad (8.70)
\end{aligned}$$

Note that $\Gamma_U(a,u) \triangleq \int_u^{\infty} x^{(a-1)}e^{-x}dx$ is the upper incomplete Gamma function [45] and the exponential integral function $\mathrm{E}_1(yu) \triangleq \int_u^{\infty} x^{-1}e^{-xy}dx$ [45].

Finally, the probability for voice outage $Pout_v$ for USVV is written as

$$Pout_v \triangleq \int_0^{\lambda_{vo}} f_{\lambda_u}^{L}(\lambda_1)\,d\lambda_1 = F_{\lambda_u}(\lambda_{vo}). \tag{8.71}$$

For the LSVV scheme, $Pout_v$ is written as

$$Pout_v \triangleq \int_0^{\lambda_{vo}} f_{\lambda_{max}}(\lambda_1)\,d\lambda_1 = F_{\lambda_{max}}(\lambda_{vo}). \tag{8.72}$$

For SSVV scheme, $Pout_v$ is written as

$$Pout_v \triangleq \int_0^{\lambda_{vo}} f_{\lambda_{min}}(\lambda_1)\,d\lambda_1 = F_{\lambda_{min}}(\lambda_{vo}). \tag{8.73}$$

### 8.6.4 Adaptive Rate and Power for Data Transmission

An adaptive uncoded MQAM scheme is considered for data transmission. Based on the approximate BER expression [4,5], the constellation size $M(\lambda_u)$ on the $j^{th}$ subchannel as a function of $\lambda_u$ and a given BER target $\text{BERT}_d$ can be expressed as

$$M(\lambda_u) = 1 + K\,\lambda_u \frac{P_d(\lambda_u)}{\sigma_n^2}, \tag{8.74}$$

where $K = \frac{-c_2}{\ln(\text{BERT}_d/c_1)}$, and $c_1$ and $c_2$ are positive real numbers. The data are sent at

$$k(\lambda_u) = \log_2\left(1 + K\,\lambda_u \frac{P_d(\lambda_u)}{\sigma_n^2}\right) \text{bits/symbol} \tag{8.75}$$

per subchannel. The instantaneous data rate is $k(\lambda_u)/T_s$ bps, where $T_s$ denotes the symbol time duration. Assuming Nyquist data pulses of duration $T_s = 1/B$, where $B$ denotes the received signal bandwidth, the spectral efficiency per subchannel is expressed as its average data rate per unit bandwidth

$$\frac{R}{B} = \int_{\lambda_u} k_u(\lambda_u) f_{\lambda_u}^{L-1}(\lambda_u)\, d\lambda_u. \tag{8.76}$$

To solve for optimal rate and power adaptation, the following Lagrangian equation is used,

$$\begin{aligned} F(P_d(\lambda_u)) &= (L-1)\int_{\lambda_u} k(\lambda_u) f_{\lambda_u}^{L-1}(\lambda_u)\, d\lambda_u \\ &\quad +\mu\left[(L-1)\int_{\lambda_u} P_d(\lambda_u) f_{\lambda_u}^{L-1}(\lambda_u)\, d\lambda_u - ATP_d\right], \end{aligned} \tag{8.77}$$

where $\mu$ denotes the Lagrange multiplier. Substituting (8.75) into (8.77) and solving $\frac{\partial F(.)}{\partial P_d(.)}$=0, the optimal power adaptation is obtained as

$$\frac{P_d(\lambda_u)}{P} = \begin{cases} \left(\frac{1}{\lambda_{do}} - \frac{1}{\lambda_u}\right)\frac{1}{K\Gamma}, & P_d(\lambda_u) \geq 0, \\ 0, & \text{otherwise}, \end{cases} \tag{8.78}$$

where $\lambda_{do}$ denotes the cutoff eigenvalue below which no data transmission is allowed. $\lambda_{do}$ is dictated by the average power constraint (8.46).

The average normalized power for USVV, LSVV and SSVV schemes can be obtained respectively as

$$\begin{aligned}
\frac{\overline{P}_d}{P}_{\text{USVV}} &= \frac{1}{K\Gamma}\int_{\lambda_{do}}^{\infty}\left(\frac{1}{\lambda_{do}}-\frac{1}{\lambda_u}\right) f_{\lambda_u}^{L}(\lambda_u)\,d\lambda_u \\
&= \frac{G_1(\lambda_{do})}{K\Gamma}, \qquad (8.79)\\
\frac{\overline{P}_{d,j}}{P}_{\text{LSVV}} &= \frac{1}{K\Gamma}\int_{\lambda_{do}}^{\infty}\left(\frac{1}{\lambda_{do}}-\frac{1}{\lambda_u}\right) f_{\lambda_u}^{L-1}(\lambda_u)\,d\lambda_u \\
&= \frac{1}{K\Gamma(L-1)}\left[LG_1(\lambda_{do})-G_2(\lambda_{do})\right], \qquad (8.80)\\
\frac{\overline{P}_d}{P}_{\text{SSVV}} &= \frac{1}{K\Gamma}\int_{\lambda_{do}}^{\infty}\left(\frac{1}{\lambda_{do}}-\frac{1}{\lambda_u}\right) f_{\lambda_u}^{L-1}(\lambda_u)\,d\lambda_u \\
&= \frac{1}{K\Gamma(L-1)}\left[LG_1(\lambda_{do})-G_3(\lambda_{do})\right], \qquad (8.81)
\end{aligned}$$

where

$$\begin{aligned}
G_1(\lambda_{do}) &= \int_{\lambda_{do}}^{\infty}\left(\frac{1}{\lambda_{do}}-\frac{1}{\lambda_u}\right) f_{\lambda_u}^{L}(\lambda_u)\,d\lambda_u \\
&= \frac{1}{L}\sum_{i=0}^{L-1}\frac{i!}{(i+d)!}\sum_{l_1=0}^{i}\sum_{l_2=0}^{i}(-1)^{l_1+l_2}A_{l_1}(i,d)\,A_{l_2}(i,d) \\
&\quad\cdot\left[\frac{1}{\lambda_{do}}\Gamma_U(\xi+1,\lambda_{do})-\Gamma_U(\xi,\lambda_{do})\right], \qquad (8.82)\\
G_2(\lambda_{do}) &= \int_{\lambda_{do}}^{\infty}\left(\frac{1}{\lambda_{do}}-\frac{1}{\lambda_u}\right) f_{\lambda_{max}}(\lambda_u)\,d\lambda_u \\
&= \sum_{i=1}^{L}\sum_{m=N-L}^{(N+L)i-2i^2}\frac{i^{m+1}d_{i,m}}{m!}\left[\frac{1}{\lambda_{do}}\frac{\Gamma_U(m+1,\lambda_{do}i)}{i^{m+1}}-\frac{\Gamma_U(m,\lambda_{do}i)}{i^m}\right], \\
G_3(\lambda_{do}) &= \int_{\lambda_{do}}^{\infty}\left(\frac{1}{\lambda_{do}}-\frac{1}{\lambda_u}\right) f_{\lambda_{min}}(\lambda_u)\,d\lambda_u \\
&= \left[\frac{1}{\lambda_{do}}e^{-\lambda_{do}L}-L\,\mathrm{E}_1(\lambda_{do}L)\right].
\end{aligned}$$

With closed-form expressions known for $\overline{P}_d/P$ (see expressions (8.79)-(8.81)) and $\overline{P}_v/P$ (see expressions (8.68)-(8.70)), $\lambda_{do}$ for any of the proposed schemes

can be determined numerically by solving the average power constraint (8.46), represented in terms of normalized power as

$$(L-1)\,\overline{P}_d/P + \overline{P}_v/P = 1. \tag{8.83}$$

Finally, substituting (8.78) into (8.75), the optimal rate adaptation is obtained as

$$k\left(\lambda_u\right) = \log_2\left(\frac{\lambda_u}{\lambda_{do}}\right). \tag{8.84}$$

The average spectral efficiency for data transmission on $(L-1)$ subchannels can be determined from

$$ASE_d = (L-1)\int_{\lambda_{do}}^{\infty} \log_2\left(\frac{\lambda_u}{\lambda_{do}}\right) f_{\lambda_u}^{L-1}(\lambda_u)\, d\lambda_u. \tag{8.85}$$

### 8.6.5 Evaluation Results

In this section, numerical results based on the expressions derived earlier are evaluated. All numerical results are based on $\mathrm{BERT}_v = 10^{-2}$ and $\mathrm{BERT}_d = 10^{-3}$. For simplicity, $P_{vo} = P$, and the constellation size of the MQAM scheme is assumed to be a non-integer value. The results are also verified with Monte-Carlo simulations. The simulation results are obtained by generating 100,000 channel realizations $\mathbf{H}$.

## USVV, LSVV and SSVV schemes

The performance of the USVV, LSVV and SSVV schemes are compared in terms of voice outage for voice transmission, and spectral efficiency for data transmission. In all results, a close match between the Monte-Carlo (MC) results and the analytical results are observed.

Figure 8.8(a) and Figure 8.8(b) show the voice outage performance of the proposed three schemes for antenna sets $(2,2)$ and $(4,4)$. The results demonstrate

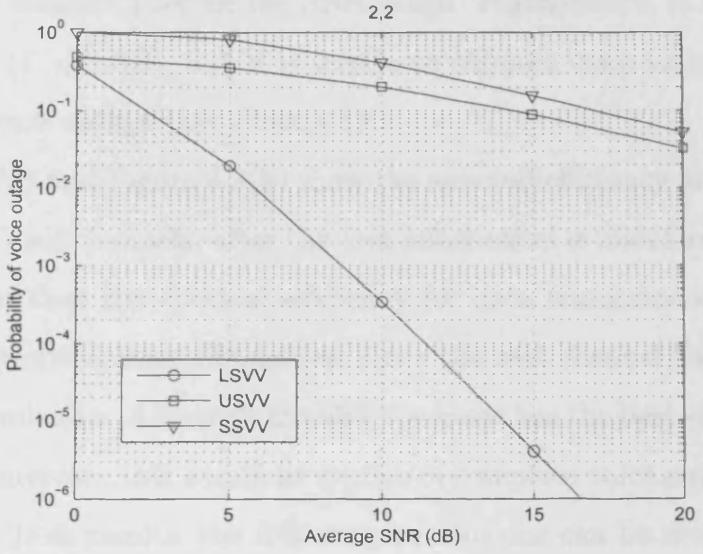


(a) (2,2)

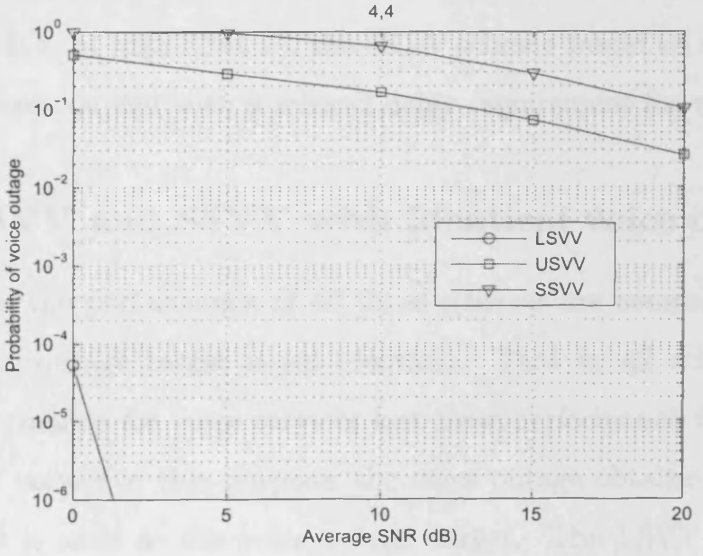


(b) (4,4)

Figure 8.8: Probability of voice outage for USVV, LSVV and SSVV schemes with antenna sets (2,2) and (4,4).

that the probability of voice outage for LSVV is significantly lower than that of the other two schemes over all the SNR range. Furthermore, it is observed that at lower SNR ($\Gamma < 5$ dB), SSVV is unable to support voice transmission as it is in complete voice outage (i.e. $Pout_v$=1).

Figure 8.9(a) and Figure 8.9(b) show the spectral efficiency for data transmission on $(L-1)$ subchannels, after the first subchannel is allocated for voice. The results confirm that the spectral efficiency for data transmission for the LSVV scheme is the worst among all schemes, since the best channel has been allocated for voice transmission. Although the SSVV scheme has the best spectral efficiency for data transmission, this comes at a price of complete voice outage at low SNR values. From these results, the following conclusions can be drawn. The LSVV scheme is suitable for real-time voice services with a stringent delay requirement, and a moderate capacity requirement for data services. When the channel condition is good (i.e. at high SNR $\Gamma$), the SSVV scheme would be suitable for data intensive services coupled with a relaxed delay requirement for voice services.

## USVV, LSVV and SSVV with identical voice outage

In this section, the performance of all three schemes are compared for the case when the voice outage target is set identical. That is, all schemes will have identical performance for voice services but their performance for data services is expected to vary. For this purpose, the voice outage obtained from the (4,4) USVV scheme is used as the voice outage target. The LSVV and the SSVV schemes operating at this voice outage target shall be denoted as $\text{LSVV}_{\text{out}}$ and $\text{SSVV}_{\text{out}}$ respectively. The new results are obtained as follow. For the respective schemes, expressions (8.71) - (8.73) are used to determine the cutoff eigenvalue $\lambda_{vo}$ such that the corresponding voice outage target is achieved for a particular

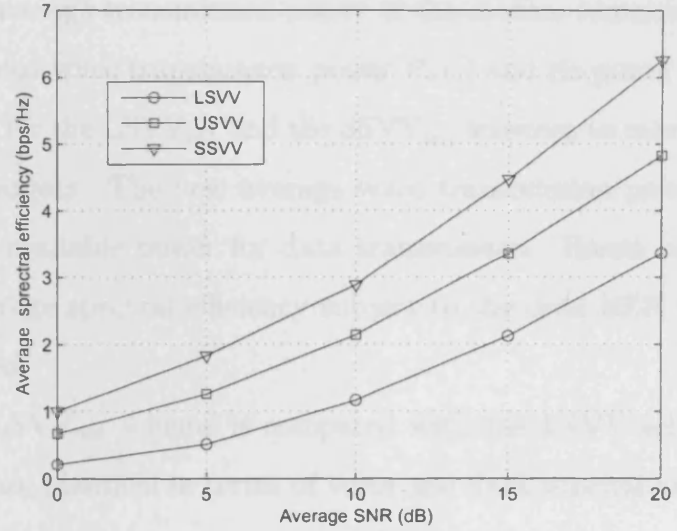


(a) (2,2)

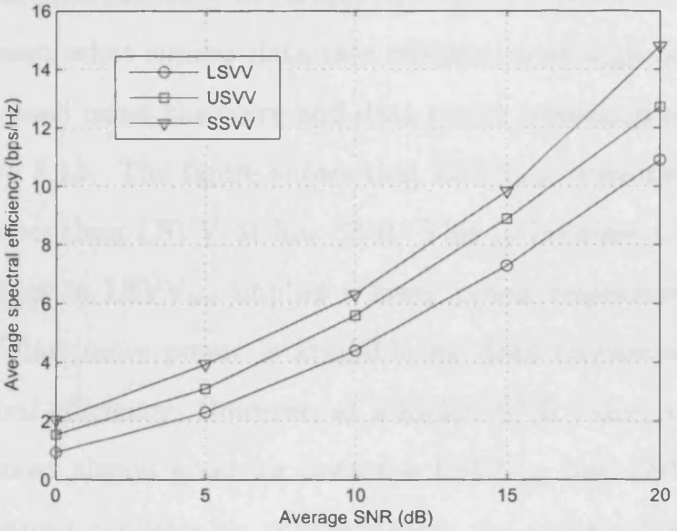


(b) (4,4)

Figure 8.9: Average spectral efficiency for data transmissions with antenna sets (2,2) and (4,4), and comparisons are performed between USVV, LSVV and SSVV schemes.

SNR $\Gamma$. For each $\Gamma$ value, the same voice BER target $\text{BERT}_v = 10^{-2}$ is used, and the total average transmission power of the system remains as $P$. However, the instantaneous voice transmission power $P_v(.)$ and its power constraint $P_{vo}$ is varied in order for the $\text{LSVV}_{\text{out}}$ and the $\text{SSVV}_{\text{out}}$ schemes to meet their respective voice outage targets. The new average voice transmission power $\overline{P}_v$ is used to determine the available power for data transmission. Based on this remaining power, the average spectral efficiency subject to the data BER target $\text{BERT}_d = 10^{-3}$ is obtained.

First, the $\text{LSVV}_{\text{out}}$ scheme is compared with the LSVV scheme. Note that both schemes are identical in terms of voice and data subchannel allocation, but the $\text{LSVV}_{\text{out}}$ scheme has a higher probability of voice outage as compared with the LSVV scheme. Figure 8.10 shows that at low SNR, $\text{LSVV}_{\text{out}}$ contributes to a small increase in data efficiency as compared to LSVV, however, both LSVV and $\text{LSVV}_{\text{out}}$ have somewhat similar data rate efficiencies at high SNR. This behavior can be explained using the voice and data power consumption characteristics shown in Figure 8.11. The figure shows that $\text{LSVV}_{\text{out}}$ consumes less power for voice transmission than LSVV at low SNR. This is because a higher probability of voice outage in $\text{LSVV}_{\text{out}}$ implies a lower power requirement for the voice transmission. Thus more power is available for data transmission resulting in increased spectral efficiency. However, at a higher SNR value, since the channel condition is almost always good for both the $\text{LSVV}_{\text{out}}$ and LSVV schemes, the power consumptions converge to approximately the same value. Therefore, no variation in the average spectral efficiency is observed at high SNR.

Next, the $\text{SSVV}_{\text{out}}$ scheme is compared with the SSVV scheme. Recall that both schemes are identical in terms of the voice and data subchannel allocation but $\text{SSVV}_{\text{out}}$ has a lower probability of voice outage. From the spectral efficiency plot in Figure 8.12, it is observed that $\text{SSVV}_{\text{out}}$ starts to decline in spectral

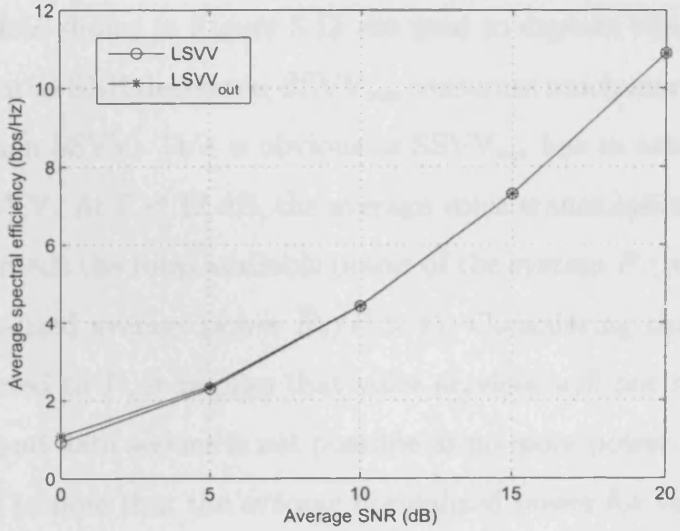


Figure 8.10: Average spectral efficiency for data transmissions with antenna set (4,4), comparisons are made between LSVV and $\text{LSVV}_{\text{out}}$ schemes.

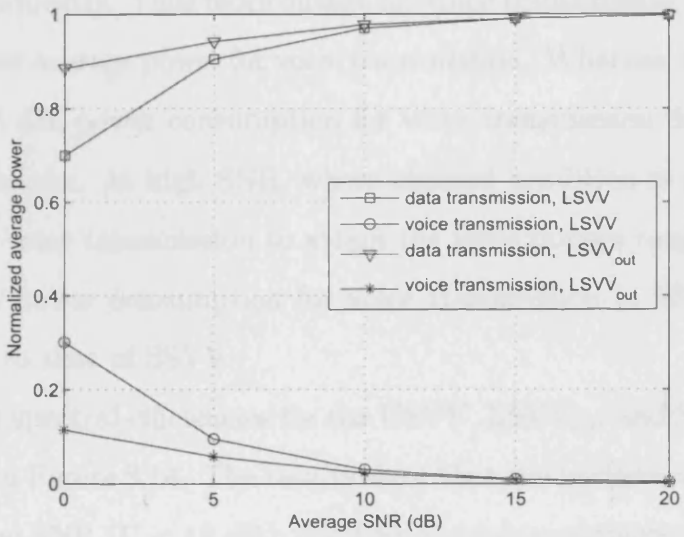


Figure 8.11: Average power consumption for voice and data transmissions with antenna set (4,4), comparisons are made between LSVV and $\text{LSVV}_{\text{out}}$ schemes.

efficiency as SNR $\Gamma$ decreases and reduces to zero when $\Gamma < 12$ dB. The power consumption plots shown in Figure 8.13 are used to explain this behaviour. The figure shows that as SNR decreases, $\text{SSVV}_{\text{out}}$ consumes much more power for voice transmission than SSVV. This is obvious as $\text{SSVV}_{\text{out}}$ has to attain a lower voice outage than SSVV. At $\Gamma < 12$ dB, the average voice transmission power required for $\text{SSVV}_{\text{out}}$ exceeds the total available power of the system $P$ (represented in the figure by normalized average power $\overline{P}_v/P > 1$). Considering that the maximum power is restricted to $P$, it implies that voice services will not achieve the voice outage target, and data service is not possible as no more power is available. It is also interesting to note that the average normalized power for voice transmission in the SSVV scheme starts to decline (at $\Gamma \approx 15$ dB) towards zero as SNR decreases towards zero. This can be explained as follows. In the SSVV scheme, the instantaneous voice transmission power $P_v(.)$ is constrained by $P_{vo}$, and $P_{vo}$ is fixed to $P$. At low SNR, the event that instantaneous power $P_v(.)$ exceeds $P_{vo}$ occurs more frequently. Thus more outage for voice transmission is declared. This results in a lower average power for voice transmission. Whereas, as SNR increases beyond $\Gamma \approx 15$ dB, power consumption for voice transmission decreases. This is explained as follows. At high SNR, where channel condition is good, less power is required for voice transmission to attain the voice outage target. Similarly, at high SNR, the power consumption for voice transmission in $\text{SSVV}_{\text{out}}$ decreases and converges to that of SSVV.

Finally, the spectral efficiencies for the USVV, $\text{LSVV}_{\text{out}}$ and $\text{SSVV}_{\text{out}}$ schemes are compared in Figure 8.14. The results show that the performance is dependent on SNR. At low SNR ($\Gamma < 18$ dB), the USVV scheme outperforms all the other schemes and $\text{SSVV}_{\text{out}}$ turns out to be the worst. At high SNR, the $\text{SSVV}_{\text{out}}$ scheme is the best while the USVV scheme remains better than $\text{LSVV}_{\text{out}}$.

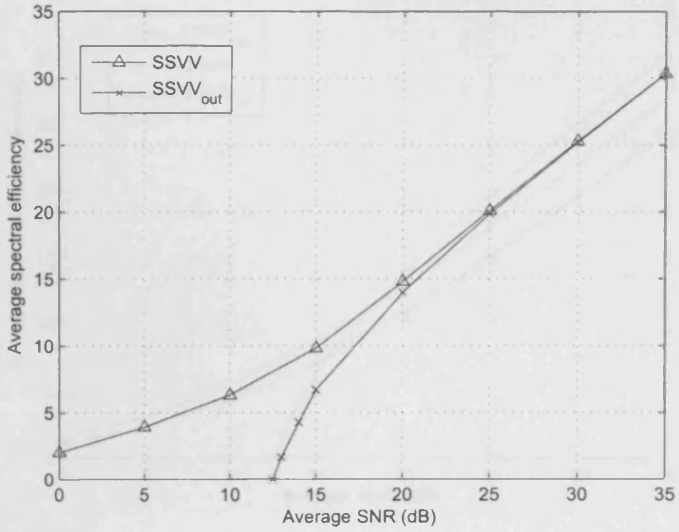


Figure 8.12: Average spectral efficiency for voice and data transmissions with antenna set (4,4), comparisons are made between SSVV and SSVV$_{out}$ schemes.

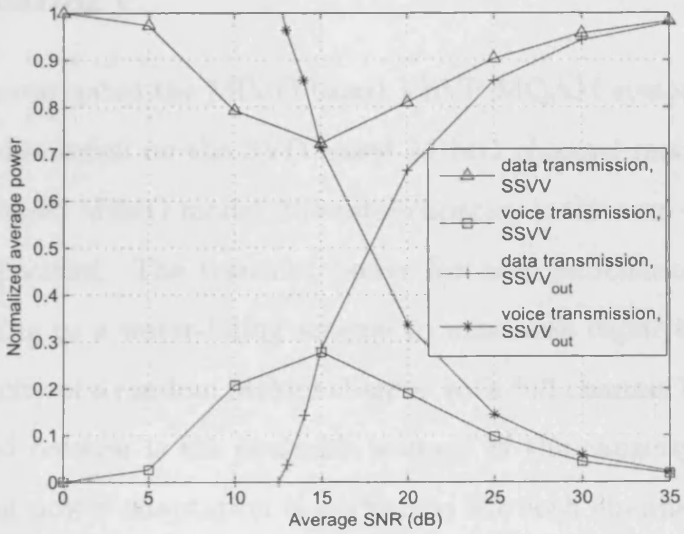


Figure 8.13: Average power consumption for voice and data transmissions with antenna set (4,4), comparisons are made between SSVV and SSVV$_{out}$ schemes.

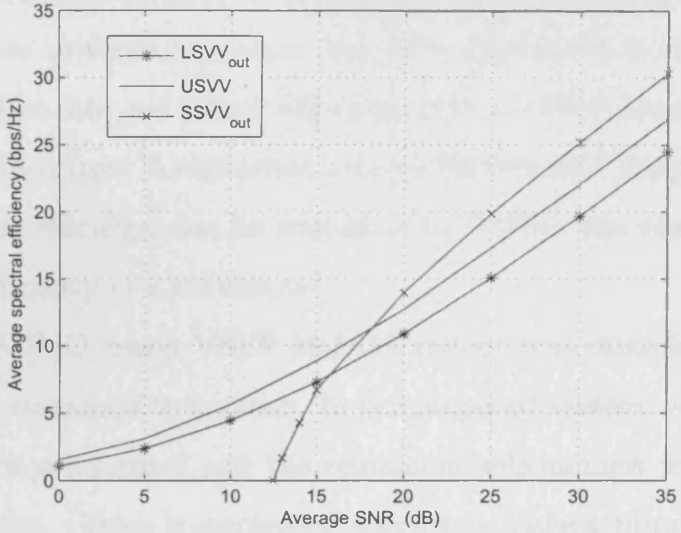


Figure 8.14: Average spectral efficiency for voice and data transmissions with antenna set (4,4), comparisons are made between $\text{LSVV}_{\text{out}}$, $\text{SSVV}_{\text{out}}$ and USVV schemes.

## 8.7 Summary

This chapter investigated the MIMO based VRVP MQAM systems. The chapter stared with a discussion on the SVD based MIMO channel model. For a deterministic SVD based MIMO model, the total capacity is the sum of the individual subchannel capacities. The transmit power for each subchannel should be allocated according to a water-filling scheme to maximise capacity. On the other hand, the capacity of a random MIMO channel with full channel knowledge at the transmitter and receiver is the ensemble average of the capacity achieved when the water-filling power adaptation is performed for each channel realization. In this case, a MIMO based VRVP MQAM system will have to adapt its transmit power and rate in accordance to both temporal and spatial variations. This is a complicated optimisation problem as it involves temporal and spatial dimensions.

However, if the MIMO channel is based on an unordered eigenvalue distribution, the optimization problem for power and rate adaptation is simplified. Therefore, the adaptive rate and power algorithms for a MIMO based VRVP-MQAM system is obtained from $L$ equivalent parallel SISO VRVP-MQAM system. The average spectral efficiency can be simplified to $L$ times the ensemble average of the spectral efficiency of a subchannel.

Next, the MIMO based VRVP-MQAM system was extended for integrated voice and data transmission services. In the proposed system, voice transmission was allocated a subchannel and the remaining subchannels were allocated for data transmission. Voice transmission was given highest priority by allocating voice signal power to satisfy a BER target. A fixed BPSK and channel inversion type power control was employed for voice transmission. Based on the remaining available system power, the water-filling type power control algorithm was employed for data transmission. The adaptive rate and power solutions for the $L-1$ subchannels data transmission were derived based on the simplified optimization problem explained in Section 8.5. To solve the new optimization problem, analytical expressions for the statistics of the $L-1$ subchannel eigenvalues were derived and presented in Section 8.6.2. Monte Carlo (MC) simulations were performed, and the simulation results were compared to the numerical results of the analytical expressions. The results showed a perfect match between the two cases, and validated the correctness of the derivations. Based on the derived statistical functions, closed-form solutions were obtained for the adaptive algorithms in voice and data transmission. Three schemes were considered. 1) The unordered singular value for voice (USVV) scheme, where voice and data were transmitted through any of the unordered singular value channels. 2) The largest singular value for voice (LSVV) scheme, where voice was transmitted through the largest singular channel and data were transmitted through the remaining $L-1$ sub-

channel. 3) The smallest singular value for voice (SVVV) scheme, where voice was transmitted through the smallest singular channel and data were transmitted through the remaining $L-1$ subchannel.

The performance of the three schemes were investigated using numerical evaluation. The following conclusions were made. The LSVV scheme provided the best performance in terms of voice outage, but provided the lowest spectral efficiency for data transmission. At high SNR, the SSVV scheme provided the best spectral efficiency for data transmission, but incurred higher outage for voice transmission. Lastly, the USVV scheme provided a good balance between the SSVV and LSVV schemes for voice and data transmission.

# Chapter 9

# Conclusions and Future Work

## 9.1 Conclusions

Due to the finite radio spectrum, techniques for sharing the radio spectrum in the most efficient way are required. Radio resource management (RRM) and allocation aim to maximize the system spectral efficiency under the constraint that the QoS is met. Examples of RRM schemes for the physical layer include power control, adaptive modulation and adaptive coding. In the MAC and higher layer, RRM schemes include scheduling and admission control. A comprehensive coverage of the field of RRM can be found in [71].

Among the several topics in RRM, this thesis focused on resource allocation techniques at the link/physical layer. In particular, this thesis investigated adaptive rate and power control for a time-varying channel. In a practical wireless communication system, only estimates of the channel state information are available, and the accuracy of these estimates is crucial to the system performance. This motivated the investigation of adaptive rate and power control based on SNR and BER estimates, and the novel algorithms which have been proposed (Chap-

ter 5). The SNR and BER estimates based algorithms were generalized for two practical systems: a VRVP-MQAM system which incorporated a PSAM-based channel predictor with discrete rate adaptation (Chapter 6), and an inner-loop and outer loop power control for a CDMA-based system (Chapter 7).

Although adaptive power, rate and coding techniques have been studied well in the literature, not much work has been performed for the link/physical layer, in particular for multi-service application such as voice and data convergence technology. The recent demand for enhanced QoS for voice and data convergence technology pushes the need to investigate optimal resource allocation schemes for diverse QoS requirements. This motivated the final thesis contributions on adaptive rate and power allocation schemes for integrated voice and data services in MIMO systems (Chapter 8).

The thesis contribution chapters are summarized as follows:

Chapter 5 investigated the impact of imperfect channel estimation on a VRVP-MQAM system over a Rayleigh flat-fading channel. A VRVP-MQAM system based on the estimates of the instantaneous SNR and BER was proposed. A BER estimator was derived using a maximum a posteriori approach. Based on the proposed model, optimal solutions for the rate and power algorithms were derived, and the solutions were compared with an ideal CSI assumption based VRVP-MQAM system and a nonadaptive MQAM system. Simulation results showed that i) the proposed system achieved a higher spectral efficiency as compared to the ideal CSI assumption based VRVP-MQAM system in all cases (i.e. for $\rho < 1$ and over all the SNR range), and ii) the proposed system performs better than a nonadaptive MQAM system when under reasonable channel imperfection scenarios.

In Chapter 6, the proposed VRVP-MQAM system derived in Chapter 5 was generalized to a practical system. That is, a PSAM-based channel predictor

and an MQAM scheme was adopted with practical constellation sizes considered. Simulation results were used to support the impact of feedback delay on channel prediction for an uncoded VRVP-MQAM system. The performance of the proposed system (denoted as the VRVP-CSI system) was compared to an alternate system with rate and power algorithms derived based on a perfect CSI assumption (denoted as the VRVP-IDEAL system). The simulation results showed that the VRVP-CSI system outperforms the VRVP-IDEAL system in terms of spectral efficiency. In terms of BER performance, both systems that used practical discrete $M$-level selection can tolerate a small delay in CSI feedback before the average BER exceeds the BER target requirement. Moreover, the results showed that the proposed VRVP-CSI scheme is less sensitive to feedback delay as compared with the VRVP-IDEAL scheme.

In Chapter 7, a BER estimator of a 'joint SNR target and rate adaptation' MQAM system over a Rayleigh flat-fading channel using maximum likelihood estimation approach was derived. The joint optimization of the proposed system was also derived for maximum spectral efficiency based on the resulting BER estimate and its density function. Through numerical evaluation, it was shown that the joint adaptation scheme, which exploits BER variations, achieved higher spectral efficiency when compared to an adaptive rate and power MQAM system with no outer-loop power control.

Chapter 8 provided another contribution work. Adaptive rate and power algorithms for integrated voice and data services in a MIMO system were proposed. The MIMO system assigns one subchannel for voice transmission and leaves the remaining subchannels for data transmission. Three schemes for voice and data subchannel allocations were investigated, namely, 'USVV', 'LSVV' and 'SSVV' schemes. In the USVV scheme, voice and data are transmitted through any of the unordered singular value subchannels. In the LSVV or SSVV schemes,

voice is transmitted through the largest and the smallest singular value channels, respectively, while the data are transmitted through the remaining unordered subchannels. Analytical and simulation results confirmed that the LSVV scheme outperforms the USVV and SSVV schemes in terms of voice outage performance, with the SSVV scheme being the worst. The SSVV scheme provided high spectral efficiency but incurs unacceptable voice outage at low SNR. However, the USVV scheme maintains a good balance between the quality of services for data and voice for a wide range of SNRs. Therefore all schemes are feasible but the choice would depend on the classes of services for voice and data. The LSVV scheme is recommended for real-time voice services with a stringent requirement on delay, but a relaxed requirement on the data rate. The USVV scheme is recommended for services with a relaxed delay requirement for voice and a moderate data rate requirement. Finally, if the channel condition is good, the SSVV scheme is recommended for data intensive services with a relaxed requirement on the quality of services for voice.

## 9.2 Future Work

The recommendations for future work are as follows:

i) As imperfect CSI knowledge and channel estimation have been common aspects that degrade the performance of an adaptive rate and power control system, the proposed SNR and BER estimates based algorithms can be extended to a MIMO channel as well as a frequency selective channel. The derived algorithms will be suitable for MIMO and OFDM systems.

ii) The concept of BER and SNR estimates based rate and power adaptation can be investigated from a cross-layer optimisation perspective. That is, beside the BER parameter, a higher layer QoS parameter such as packet error rate could be

incorporated.

iii) Adaptive rate and power techniques for integrated voice and data services for a MIMO system are definitely an important topic to pursue. In the proposed scheme in this thesis, voice has the highest priority and is always allocated a particular subchannel, and the remaining subchannels are allocated for data transmission. The extension would be for the voice to still remain with highest priority, but the allocation of voice transmission is not fixed to a particular subchannel. Instead, any one of the subchannels can be assigned for voice transmission, as long as the QoS for voice is guaranteed. Subsequently, the remaining subchannels will be allocated for data transmission. This approach will require a complete joint optimisation to allocate voice and data optimally through appropriate subchannels.

# Appendix A

# Appendix: Proofs for the Derivations in Chapter 5

## A.1 Proof of $f_{p_B,\hat{\gamma}}(p_B,\hat{\gamma})$ expression

The joint PDF $f_{p_B,\hat{\gamma}}(p_B,\hat{\gamma})$ is obtained based on the transformation of two functions of two random variables [37].

Form a system of two random variables

$$p_B = c_1 \exp\left(-\frac{c_2\sigma}{M-1}\frac{\gamma}{\hat{\gamma}}\right), \tag{A.1}$$

$$w = \hat{\gamma}. \tag{A.2}$$

The system has a single set of solutions:

$$\gamma_1 = -\frac{\ln(p_B/c_1)}{c_2}\frac{(M-1)}{\sigma}w, \tag{A.3}$$

$$\hat{\gamma}_1 = w. \tag{A.4}$$

The joint PDF can be obtained based on

$$f_{p_B,\hat{\gamma}}(p_B,\hat{\gamma}) = \frac{f_{\gamma,\hat{\gamma}}(\gamma_1,\hat{\gamma}_1)}{|J(\gamma_1,\hat{\gamma}_1)|}, \tag{A.5}$$

where

$$J(\gamma_1, \hat{\gamma}_1) = \begin{vmatrix} \frac{\partial p_B}{\partial \gamma} & \frac{\partial p_B}{\partial \hat{\gamma}} \\ \frac{\partial w}{\partial \gamma} & \frac{\partial w}{\partial \hat{\gamma}} \end{vmatrix} \tag{A.6}$$

$$= \begin{vmatrix} \left[c_1 \exp\left(-\frac{c_2\sigma}{M-1}\frac{\gamma}{\hat{\gamma}}\right)\right]\frac{-c_2\sigma}{M-1}\frac{1}{\hat{\gamma}} & \left[c_1 \exp\left(-\frac{c_2\sigma}{M-1}\frac{\gamma}{\hat{\gamma}}\right)\right]\frac{-c_2\sigma}{M-1}\frac{\gamma 1}{\hat{\gamma}^2} \\ 0 & 1 \end{vmatrix} \tag{A.7}$$

$$= -\frac{c_2\sigma}{M-1}\frac{p_B}{w} \tag{A.8}$$

is the Jacobian of the transformation of (A.1) and (A.2), and $f_{\gamma,\hat{\gamma}}(\gamma_1, \hat{\gamma}_1)$ is obtained by substituting $\gamma = \gamma_1$ and $\hat{\gamma} = \hat{\gamma}_1$ into the joint PDF $f_{\gamma,\hat{\gamma}}(\gamma, \hat{\gamma})$,

$$f_{\gamma,\hat{\gamma}}(\gamma, \hat{\gamma}) = \frac{1}{(1-\rho)\Gamma\hat{\Gamma}} I_0\left(\frac{2\sqrt{\rho}}{1-\rho}\sqrt{\frac{\gamma\hat{\gamma}}{\Gamma\hat{\Gamma}}}\right) \exp\left(-\frac{1}{(1-\rho)}\left(\frac{\gamma}{\Gamma} + \frac{\hat{\gamma}}{\hat{\Gamma}}\right)\right) u(\gamma)\, u(\hat{\gamma}). \tag{A.9}$$

Subsequently, after some algebraic operations, the final form of (A.5) is simplified as

$$f_{p_B,\hat{\gamma}}(p_B, \hat{\gamma}) = c(p_B)\, I_0(b(p_B)\hat{\gamma}) \exp(-a(p_B)\hat{\gamma}), \tag{A.10}$$

where the definitions for $a(p_B)$, $b(p_B)$ and $c(p_B)$ are shown in Section 5.3.1 and shall not be repeated here.

## A.2 Proof of the $I_{MAPeq}$ expression

The following Bessel function polynomial approximation [45, eqn (9.8.2)] is used.

$$\begin{aligned} \sqrt{x}\exp(-x)I_0(x) = {} & 0.3984228 + 0.01328592t^{-1} + 0.00225319t^{-2} \\ & - 0.00157565t^{-3} + 0.00916281t^{-4} - 0.02057706t^{-5} \\ & + 0.02635537t^{-6} - 0.01647633t^{-7} + 0.00392377t^{-8} + \epsilon, \end{aligned} \tag{A.11}$$

where $3.75 < x < \infty$, $t = x/3.75$ and $|\epsilon| < 1.9 * 10^{-7}$. In the context here, $b(p_B)\,\hat{\gamma} = x$. Subsequently, (A.11) is re-arrange in the following from

$$\exp\left(-b(p_B)\hat{\gamma}\right) I_0\left(b(p_B)\hat{\gamma}\right) = \frac{1}{\sqrt{2\pi b(p_B)\hat{\gamma}}}\left(1 + \Delta + \epsilon\sqrt{2\pi}\right), \tag{A.12}$$

where

$$\Delta = \frac{g_1}{b(p_B)\hat{\gamma}} + \frac{g_2}{\left(b(p_B)\hat{\gamma}\right)^2} + ... + \frac{g_8}{\left(b(p_B)\hat{\gamma}\right)^8} \tag{A.13}$$

and $g_1 = 0.1249$, $g_2 = 0.0794$, $g_3 = -0.2083$, $g_4 = 4.5420$, $g_5 = -38.2498$, $g_6 = 183.7159$, $g_7 = -430.6945$, $g_8 = 384.5912$. Without loss of generality, $I_{MAP}$ (5.20) can be written as

$$I_{MAP} = \frac{1}{p_B}\exp\left(b\left(p_B\right)\hat{\gamma}\right)\exp\left(-b\left(p_B\right)\hat{\gamma}\right) I_0\left(b\left(p_B\right)\hat{\gamma}\right)\exp\left(-a\left(p_B\right)\hat{\gamma}\right), \tag{A.14}$$

and can be simplified using (A.12) as

$$I_{MAP_{eq}} = \frac{1}{p_B}\exp\left(b\left(p_B\right)\hat{\gamma}\right)\frac{\left(1 + \Delta + \epsilon\sqrt{2\pi}\right)}{\sqrt{2\pi b\left(p_B\right)\hat{\gamma}}}\exp\left(-a\left(p_B\right)\hat{\gamma}\right). \tag{A.15}$$

Finally, when based on a higher $\hat{\gamma}$, the MAP function can be approximated as

$$I_{MAP_{eq}} = \frac{1}{p_B}\exp\left(b\left(p_B\right)\hat{\gamma}\right)\frac{1}{\sqrt{2\pi b\left(p_B\right)\hat{\gamma}}}\exp\left(-a\left(p_B\right)\hat{\gamma}\right), \tag{A.16}$$

as the term $\Delta$ is insignificant in the MAP function.

## A.3 Proof of the $\hat{p}_B$ expression

### Step I: First derivative of the MAP function

The expression of $\hat{p}_B$ is obtained by finding the root of $\frac{\partial I_{MAP_{eq}}}{\partial p_B} = 0$, where $I_{MAP_{eq}}$ is as shown in (A.16). For simplicity and without loss of generality, the differentiation is performed based on the natural logarithm of $I_{MAP_{eq}}$. The final form of

the expression, after removing the constant terms, is shown here as

$$\frac{\partial \ln\left(I_{MAP_{eq}}\right)}{\partial p_B} = -1 - \frac{1}{4\ln\left(\frac{p_B}{c_1}\right)} - \frac{b_1\hat{\gamma}}{2\sqrt{-\ln\left(\frac{p_B}{c_1}\right)}} - a_1\hat{\gamma}, \tag{A.17}$$

where

$$a_1 = \frac{1}{1-\rho}\left(\frac{-(M-1)}{\sigma c_2}\frac{1}{\Gamma}\right), \tag{A.18}$$

$$b_1 = \frac{2\sqrt{\rho}}{1-\rho}\left(\sqrt{\frac{M-1}{\sigma c_2}}\sqrt{\frac{1}{\Gamma\hat{\Gamma}}}\right). \tag{A.19}$$

Multiplying (A.17) by $\sqrt{-\ln\left(\frac{p_B}{c_1}\right)}$, the expression becomes

$$-\sqrt{-\ln\left(\frac{p_B}{c_1}\right)} + \frac{\sqrt{-\ln\left(\frac{p_B}{c_1}\right)}}{4\sqrt{-\ln\left(\frac{p_B}{c_1}\right)}\sqrt{-\ln\left(\frac{p_B}{c_1}\right)}} - \frac{b_1\hat{\gamma}\sqrt{-\ln\left(\frac{p_B}{c_1}\right)}}{2\sqrt{-\ln\left(\frac{p_B}{c_1}\right)}} - a_1\hat{\gamma}\sqrt{-\ln\left(\frac{p_B}{c_1}\right)} = 0,$$

$$-\sqrt{-\ln\left(\frac{p_B}{c_1}\right)} + \frac{1}{4\sqrt{-\ln\left(\frac{p_B}{c_1}\right)}} - \frac{b_1\hat{\gamma}}{2} - a_1\hat{\gamma}\sqrt{-\ln\left(\frac{p_B}{c_1}\right)} = 0,$$

$$(-1 - a_1\hat{\gamma})\sqrt{-\ln\left(\frac{p_B}{c_1}\right)} + \frac{1}{4\sqrt{-\ln\left(\frac{p_B}{c_1}\right)}} - \frac{b_1\hat{\gamma}}{2} = 0,$$

Let $F = \sqrt{-\ln\left(\frac{p_B}{c_1}\right)}$, and use $A = 1 + a_1\hat{\gamma}$ and $B = b_1\hat{\gamma}$, the above expression is simplified to

$$AF - \frac{1}{4F} + \frac{b_1\hat{\gamma}}{2} = 0, \tag{A.20}$$

$$AF^2 + \frac{b_1\hat{\gamma}F}{2} - \frac{1}{4} = 0, \tag{A.21}$$

Based on quadratic formula, the critical points (see Theorem 1 in Step II ) are

$$F_{1,2} = \frac{1}{4A}\left[-B \pm \sqrt{B^2 + 4A}\right], \tag{A.22}$$

and the corresponding BER estimate is expressed as

$$\hat{p}_{B_{1,2}} = c_1 \exp[-(F_{1,2})^2]. \tag{A.23}$$

## Step II: Evaluation of critical points $F_1$ and $F_2$

### Theorem 1

Definition of critical points: $x_a$ is a critical point of the function $f(x)$ if $f(x_a)$ exists and if either of the following are true: i)$f'(x_a) = 0$, or, ii) $f'(x_a)$ is not defined or f(x) is not differentiable [72].

In the context of the MAP function, since $I_{MAPeq}\left(\hat{p}_{B_{1,2}}\right)$ exists and $I_{MAPeq}\left(\hat{p}_{B_{1,2}}\right) = 0$, $\hat{p}_{B_{1,2}}$ (alternatively $F_{1,2}$) are clearly the critical points of the MAP function.

The next step is to define the closed range of the MAP function and verify if the critical points fall within the range of interest. The range is determined by the practical BER value in the range $p_B = [0, c_1]$. The corresponding range for $F \triangleq \sqrt{-\ln(p_B/c_1)}$ will be $F = [\infty, 0]$. Note that $F$ is a positive integer.

In (A.22), $F_{1,2}$ is expressed in terms of $A$ and $B$. Recall that

$$A = 1 + a_1\hat{\gamma} \tag{A.24}$$

$$= 1 + \frac{1}{1-\rho}\left(\frac{-(M-1)}{\sigma c_2}\frac{1}{\Gamma}\right)\hat{\gamma}, \tag{A.25}$$

$$B = b_1\hat{\gamma} \tag{A.26}$$

$$= \frac{2\sqrt{\rho}}{1-\rho}\left(\sqrt{\frac{M-1}{\sigma c_2}}\sqrt{\frac{1}{\Gamma\hat{\Gamma}}}\right)\hat{\gamma}. \tag{A.27}$$

For a given value of BERT, $\rho$ and $\Gamma$, and that $\frac{-\sigma c_2}{M-1} = \ln(\text{BERT})$, $a_1$ (c.f. A.18) and $b_1$ (c.f. A.19) are negative and positive constants respectively. $A$ and $B$ are therefore expressed as a function of $\hat{\gamma}$. This implies that computation of critical points $F_1$ and $F_2$ have to be verified across the entire range of possible $\hat{\gamma}$ values, which is $\hat{\gamma} \in [0, \infty]$.

To determine the range of $F_{1,2}$ for all $\hat{\gamma}$, it is equivalent to evaluate the limit of $F_{1,2}$ as $\hat{\gamma}$ approaches $0^+$ and $\infty$. Since $F_{1,2}$ is expressed as a function of $A$ and

$B$, the limit of $A$ and $B$ shall be first identified.

$$\lim_{\hat{\gamma}\to 0^+} A(\hat{\gamma}) = \lim_{\hat{\gamma}\to 0^+} 1 + a_1\hat{\gamma} = 1, \tag{A.28}$$

$$\lim_{\hat{\gamma}\to \infty} A(\hat{\gamma}) = \lim_{\hat{\gamma}\to \infty} 1 + a_1\hat{\gamma} = -\infty, \tag{A.29}$$

and

$$\lim_{\hat{\gamma}\to 0^+} B(\hat{\gamma}) = \lim_{\hat{\gamma}\to 0^+} b_1\hat{\gamma} = 0, \tag{A.30}$$

$$\lim_{\hat{\gamma}\to \infty} B(\hat{\gamma}) = \lim_{\hat{\gamma}\to \infty} b_1\hat{\gamma} = \infty. \tag{A.31}$$

Subsequently, the limit of $F_1$ as $\hat{\gamma}$ approaches $0^+$ is

$$\lim_{\hat{\gamma}\to 0^+} F_1(\hat{\gamma}) = \lim_{\hat{\gamma}\to 0^+} \frac{1}{4A}\left[-B + \sqrt{B^2 + 4A}\right] \tag{A.32}$$

$$= \frac{1}{4}\left[-0 + \sqrt{0^2 + 4}\right] = 0.5. \tag{A.33}$$

The limit of $F_1$ as $\hat{\gamma}$ approaches $\infty$ is

$$\lim_{\hat{\gamma}\to \infty} F_1(\hat{\gamma}) = \lim_{\hat{\gamma}\to \infty} \frac{1}{4A}\left[-B + \sqrt{B^2 + 4A}\right] \tag{A.34}$$

$$= \lim_{\hat{\gamma}\to \infty} \frac{-B}{4A} + \sqrt{\frac{B^2}{16A^2} + \frac{1}{4A}} \tag{A.35}$$

$$= \lim_{\hat{\gamma}\to \infty} \frac{-B}{4A} + \sqrt{\lim_{\hat{\gamma}\to \infty} \frac{B^2}{16A^2} + 0} \tag{A.36}$$

$$= \lim_{\hat{\gamma}\to \infty} \left(\frac{-B}{4A} + \frac{B}{4A}\right) = 0. \tag{A.37}$$

Note that in order to avoid any indeterminate solution, the above expression is re-arranged before substitution of the respective limits for $A$ and $B$.

Next, the limit of $F_2$ as $\hat{\gamma}$ approaches $0^+$ is

$$\lim_{\hat{\gamma}\to 0^+} F_2(\hat{\gamma}) = \lim_{\hat{\gamma}\to 0^+} \frac{1}{4A}\left[-B - \sqrt{B^2 + 4A}\right] \tag{A.38}$$

$$= \frac{1}{4}\left[0 - \sqrt{0^2 + 4}\right] = -0.5. \tag{A.39}$$

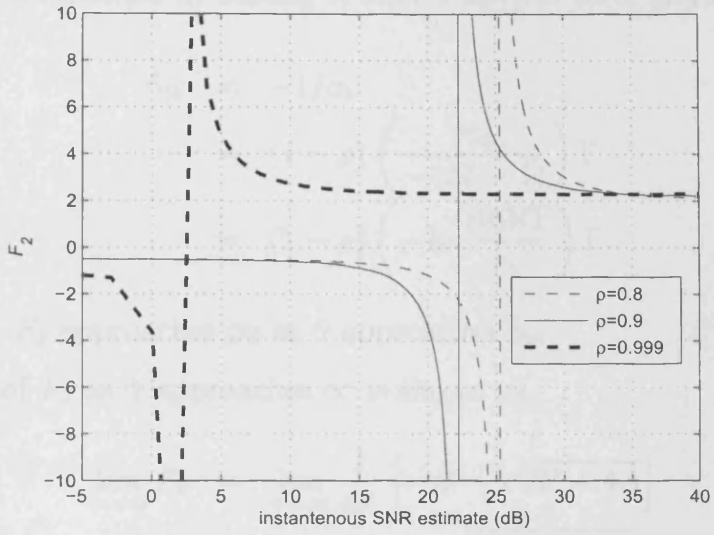


Figure A.1: $F_2$ versus instantaneous SNR estimate $\hat{\gamma}$; for the VRVP-MQAM-CSI system at $\Gamma = \hat{\Gamma} = 25$ dB, BER target$= 10^{-3}$, and $\rho = 0.8, 0.9, \sim 1$.

Note that this is an invalid solution since this falls in the negative $F$ domain. This provides further insight into the response of $F_2$ as a function of $\hat{\gamma}$. A numerical evaluation of $F_2$ as a function $\hat{\gamma}$, as shown in Figure A.1, clearly reveals that $F_2$ is discontinued at a particular $\hat{\gamma}$ value and becomes negative below this $\hat{\gamma}$ value. Let $\hat{\gamma}_{th}$ define the location where this discontinuity occurred. For a rational function like $F_2$, expression for $\hat{\gamma}_{th}$ can be obtained if the denominator term, $A$, is set to zero. That is

$$F_2'|_{A=0} = \frac{1}{4A}\left[-B - \sqrt{B^2 + 4A}\right]\Big|_{A=0} \tag{A.40}$$

$$= \infty. \tag{A.41}$$

Therefore $\hat{\gamma}_{th}$ is obtained by setting $A \triangleq (1 + a_1\hat{\gamma})$ to zero, and thus

$$\begin{aligned}
\hat{\gamma}_{th} &= -1/a_1 && \text{(A.42)}\\
&= (1-\rho)\left(\frac{\sigma c_2}{-(M-1)}\right)\Gamma && \text{(A.43)}\\
&= (1-\rho)\left(-\ln\frac{\text{BERT}}{c_1}\right)\Gamma. && \text{(A.44)}
\end{aligned}$$

Subsequently, $F_2$ approaches $\infty$ as $\hat{\gamma}$ approaches $\hat{\gamma}_{th}$.

The limit of $F_2$ as $\hat{\gamma}$ approaches $\infty$ is shown as,

$$\begin{aligned}
\lim_{\hat{\gamma}\to\infty} F_2 &= \lim_{\hat{\gamma}\to\infty}\frac{1}{4A}\left[-B-\sqrt{B^2+4A}\right] && \text{(A.45)}\\
&= \lim_{\hat{\gamma}\to\infty}\frac{-B}{4A}-\sqrt{\frac{B^2}{16A^2}+\frac{1}{4A}} && \text{(A.46)}\\
&= \lim_{\hat{\gamma}\to\infty}\frac{-B}{4A}-\sqrt{\lim_{\hat{\gamma}\to\infty}\frac{B^2}{16A^2}+0} && \text{(A.47)}\\
&= \lim_{\hat{\gamma}\to\infty}\left(\frac{-B}{4A}-\frac{B}{4A}\right) && \text{(A.48)}\\
&= \lim_{\hat{\gamma}\to\infty}\frac{-B}{2A} && \text{(A.49)}\\
&= \lim_{\hat{\gamma}\to\infty}\sqrt{\frac{\rho\frac{-\sigma c_2}{M-1}\frac{\Gamma}{\hat{\Gamma}}}{\left((1-\rho)\frac{\sigma c_2}{M-1}\frac{\Gamma}{\hat{\gamma}}-1\right)^2}} && \text{(A.50)}\\
&= \sqrt{\frac{\sigma c_2}{M-1}} && \text{(A.51)}\\
&= \vartheta. && \text{(A.52)}
\end{aligned}$$

Note that since the ratio $\frac{B}{A}|_{\hat{\gamma}=\infty} = \frac{-\infty}{\infty}$ is indeterminate in (A.49), expressions $A$ (A.25) and $B$ (A.27) are to be substituted into (A.49). After several algebraic operations, (A.50) is obtained and a value $\vartheta$ is obtained. Note that when $F_2$ approaches $\vartheta$, the corresponding BER estimate $\hat{p}_B$ approaches BERT. This suggests that in all cases, the BER estimate approaches BERT at a higher $\hat{\gamma}$.

Finally, the appropriate range for $F_{1,2}$ is summarized as follow,

$$F_1 = [0.5, 0] \quad \text{for} \quad \hat{\gamma} \in [0, \infty], \tag{A.53}$$

$$F_2 = [\infty, \vartheta] \quad \text{for} \quad \hat{\gamma} \in [\hat{\gamma}_{th}, \infty], \tag{A.54}$$

where $\vartheta$ and $\hat{\gamma}_{th}$ are positive integers.

## Step III: Classification of local maxima and minima

The next step is to determine if $F_1$ and $F_2$ produce the maximum and/or minimum values of the MAP function. Two tests are commonly used, the first derivative test and the second derivative test, given as below [73, 74].

**Theorem 2**

Definition of first derivative test: Given a function $f(x)$,

- if $f'(x) > 0$ on an open interval extending left from $x_a$ and $f'(x) < 0$ on an open interval extending right from $x_a$, then the function has a local maximum at $x_a$.

- If $f'(x) < 0$ on an open interval extending left from $x_a$ and $f'(x) > 0$ on an open interval extending right from $x_a$, then the function has a local minimum at $x_a$.

- If $f'(x)$ has the same sign on both an open interval extending left from $x_a$ and an open interval extending right from $x_a$, then the function does not have a local maxima or minimum.

**Theorem 3**

Definition of second derivative test:

- If the second derivative of a function $f''(x_a) < 0$, $x_a$ is a local maximum.

- If the second derivative of a function $f''(x_a) > 0$, $x_a$ is a local minimum.

- If the second derivative of a function $f''(x_a) = 0$, $x_a$ can be local maximum, local minimum or neither.

The verification based on the first derivative test clearly required numerical evaluation of function $f(.)$ at and around the critical points. It is apparent that to use the first derivative test on the MAP function $I_{MAPeq}$ is tedious. This is because the MAP function has to be evaluated around critical points $\hat{p}_B = \{c_1 \exp(-F_1^2), c_1 \exp(-F_2^2)\}$ not for one time but for a large number of times as the critical points are dependent upon SNR estimate $\hat{\gamma}$. On the other hand, the second derivative test requires numerical evaluation of $f'(x_a)$ at the critical points. This suggest that the second derivative test requires lesser effort in the context of the work here.

The second derivative of the MAP function is

$$\frac{\partial''\left(I_{MAP_{eq}}\right)}{\partial'' p_B} = \frac{1}{4p_B\left[-\ln\left(\frac{p_B}{c_1}\right)\right]^2} - \frac{B}{4p_B\left[-\ln\left(\frac{p_B}{c_1}\right)\right]^{3/2}} \tag{A.55}$$

$$= \frac{1}{4p_B\left[F\right]^4} - \frac{B}{4p_B\left[F\right]^3} \tag{A.56}$$

$$= \frac{1}{4p_B\left[F\right]^3}\left(\frac{1}{F} - B\right). \tag{A.57}$$

Clearly it is observed that the term $(\frac{1}{F} - B)$ is sufficient for the second derivative test. That is, if $(\frac{1}{F_a} - B) < 0$, the critical point $F_a$ is a local maxima and if $(\frac{1}{F_a} - B) > 0$, $F_a$ is a local minima. The numerical evaluation for $(\frac{1}{F} - B)$ with $F_a = \{F_1, F_2\}$ throughout the valid $\hat{\gamma}$ range can be easily computed. For illustration, the results for a system setting of $\Gamma = 25$dB, BERT $= 0.001$ and $\rho = 0.9$ are computed and shown in Figure A.2. The results clearly confirm that $F_2$ is the local maximum point and $F_1$ is the local minimum point of the MAP function.

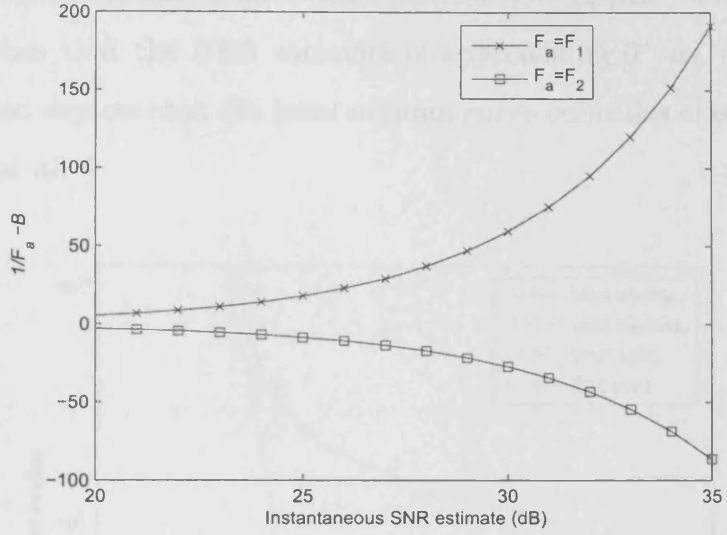


Figure A.2: Plot of function $(1/F - B)$ as a functon of $\hat{\gamma}$ for $F_1$ and $F_2$, at settings $\Gamma = 25$ dB, $\rho = 0.9$ and BERT $= 0.001$.

## Classification of absolute maxima and minima

For a closed interval, absolute maxima can occur at both endpoints and critical points. In the context here, the valid range for BER the estimate is $\hat{p}_B = [0, c_1]$ and it is necessary to verify that the absolute maximum of the MAP functions does not occur at the endpoints.

This can be easily verified by numerical evaluation of the function $I_{MAPeq}$ at the endpoints $\hat{p}_B = \{0, c_1\}$ and at the local maxima $\hat{p}_B = c_1 \exp(-F_2^2)$. For illustration, Figure A.3 shows the numerical plot of the MAP function versus SNR estimate $\hat{\gamma}$ at system setting $\Gamma = 25$ dB, $\rho = 0.9$ and BERT $= 0.001$. The legend 'local minima' and 'local maxima' refer to $\hat{p}_B = c_1 \exp(-F_1^2)$ and $\hat{p}_B = c_1 \exp(-F_2^2)$ respectively and 'Start point' and 'End point' refer to $\hat{p}_B = 0$ and $\hat{p}_B = c_1$ respectively. The plot confirms that $\hat{p}_B = c_1 \exp(-F_2^2)$ is also the absolute maximum and is valid throughout the range $\hat{\gamma} \in [\hat{\gamma}_{th}, \infty]$. It is noted

that both the 'local maxima' and 'Start point' curves appear to converge at lower $\hat{\gamma}$. This implies that the BER estimate is approaching $0^+$ as $\hat{\gamma}$ becomes lower. The figure also depicts that the local minima curve coincides closely with the end point curve at all $\hat{\gamma}$.

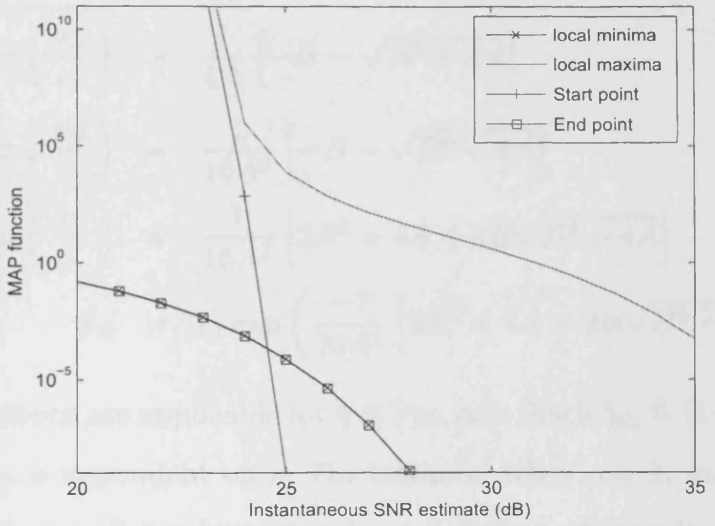


Figure A.3: Evaluation of MAP function at critical points (local maxima and minima), start and end points, with $\Gamma = 25$ dB, $\rho = 0.9$ and BERT $= 0.001$.

## Expressions for BER estimates

Having verified $F_2$ as the maximum of the MAP function, the exact BER estimate expression $\hat{p}_B$ can be obtained as

$$F_2 = \frac{1}{4A}\left[-B - \sqrt{B^2+4A}\right] \tag{A.58}$$

$$\sqrt{-\ln\left(\frac{p_B}{c_1}\right)} = \frac{1}{4A}\left[-B - \sqrt{B^2+4A}\right] \tag{A.59}$$

$$-\ln\left(\frac{p_B}{c_1}\right) = \frac{1}{16A^2}\left[-B - \sqrt{B^2+4A}\right]^2 \tag{A.60}$$

$$-\ln\left(\frac{p_B}{c_1}\right) = \frac{1}{16A^2}\left[2B^2+4A+2B\sqrt{B^2+4A}\right] \tag{A.61}$$

$$\hat{p}_B = c_1 \exp\left(\frac{-1}{16A^2}\left[2B^2+4A+2B\sqrt{B^2+4A}\right]\right). \tag{A.62}$$

Recall the solutions are applicable for $\hat{\gamma} \in [\hat{\gamma}_{th}, \infty]$. Since $\hat{\gamma}_{th} \triangleq (1-\rho)(-\ln\frac{\text{BERT}}{c_1})\Gamma$ (c.f. A.44), $\hat{\gamma}_{th}$ is dependent on $\rho$. For instance, when $\rho = 1$, expressions (A.58-A.62) will apply for all $\hat{\gamma}$ values since $\hat{\gamma}_{th} = 0$, but as $\rho$ becomes $< 1$, the solution will be applicable at a higher $\hat{\gamma}$ value.

In the context of the spectral efficiency optimization problem, expression (A.62) is a cumbersome expression to work on. Therefore the aim is to simplify the BER estimate expression. Since the BER estimate expression consists of polynomial terms of $A$ and $B$, it will be appropriated to compare these terms.

The first step is to express $A$ and $B$ as a function of $\hat{\gamma}_{th}$. Let $A_{th}$ and $B_{th}$

denote $A$ and $B$ respectively at $\hat{\gamma}_{th}$ . Therefore at $\hat{\gamma} = \hat{\gamma}_{th}$,

$$B_{th}^2 = (b_1\hat{\gamma}_{th})^2; \quad A_{th} = 1 + a_1\hat{\gamma}_{th}, \tag{A.63}$$

$$B_{th}^2 = \left(b_1\frac{-1}{a_1}\right)^2; \quad A_{th} = 1 + a_1\frac{-1}{a_1}, \tag{A.64}$$

$$B_{th}^2 = 4\rho\frac{\sigma c_2}{M-1}\frac{\Gamma}{\hat{\Gamma}}; \quad A_{th} = 0, \tag{A.65}$$

$$B_{th}^2 = 4\rho\left[-\ln\left(\frac{\text{BERT}}{c_1}\right)\right]\frac{\Gamma}{\hat{\Gamma}}; \quad A_{th} = 0, \tag{A.66}$$

$$B_{th}^2 = 4\left[-\ln\left(\frac{\text{BERT}}{c_1}\right)\right]; \quad A_{th} = 0; \quad (\hat{\Gamma} = \rho\Gamma), \tag{A.67}$$

Next, compare $B^2$ and $A$ at $\hat{\gamma} > \hat{\gamma}_{th}$. Define $\hat{\gamma}_H \triangleq H\hat{\gamma}_{th}$, where $H > 1$ is a scaling integer. Denote $A$ and $B$ at $\hat{\gamma}_H$ as $A_H$ and $B_H$ respectively,

$$B_H^2 = (b_1\hat{\gamma}_H)^2; \quad A_H = 1 + a_1\hat{\gamma}_H, \tag{A.68}$$

$$B_H^2 = \left(b_1\frac{-H}{a_1}\right)^2; \quad A_H = 1 + a_1\frac{-H}{a_1}, \tag{A.69}$$

$$B_H^2 = H^2 4\rho\frac{\sigma c_2}{M-1}\frac{\Gamma}{\hat{\Gamma}}; \quad A_{th} = 1 - H, \tag{A.70}$$

$$B_H^2 = H^2 4\rho\left[-\ln\left(\frac{\text{BERT}}{c_1}\right)\right]\frac{\Gamma}{\hat{\Gamma}}; \quad A_H = 1 - H, \tag{A.71}$$

$$B_H^2 = H^2 4\left[-\ln\left(\frac{\text{BERT}}{c_1}\right)\right]; \quad A_H = 1 - H; \quad (\hat{\Gamma} = \rho\Gamma), \tag{A.72}$$

From (A.67) and (A.72), it is noted that $B^2 > A$ at $\hat{\gamma} = \hat{\gamma}_{th}$ and $B^2 >> A$ as $\hat{\gamma} > \hat{\gamma}_{th}$. Therefore, when based on a higher SNR estimate (i.e $\hat{\gamma} > \hat{\gamma}_{th}$), the $A_H$ term is essentially insignificant in comparison to the $B_H$ term. Subsequently, the corresponding BER estimate expression can be approximated as

$$\hat{p}_B = c_1 \exp\left(\frac{-1}{16A^2}\left[2B^2 + 4A + 2B\sqrt{B^2 + 4A}\right]\right), \tag{A.73}$$

$$\approx c_1 \exp\left(\frac{-1}{16A^2}\left[2B^2 + 2B\sqrt{B^2}\right]\right), \tag{A.74}$$

$$= c_1 \exp\left(\frac{-B^2}{4A^2}\right). \tag{A.75}$$

Finally, with the substitution of functions $A$ (A.25) and $B$ (A.27), and after some algebraic operations, the BER estimate can be approximated as

$$\hat{p}_B \approx c_1 \exp\left(\frac{\rho \frac{-\sigma c_2}{M-1}\frac{\Gamma}{\hat{\Gamma}}}{\left((1-\rho)\frac{\sigma c_2}{M-1}\frac{\Gamma}{\hat{\gamma}}-1\right)^2}\right). \tag{A.76}$$

## Numerical evaluation of the BER estimate

This section evaluates the impact of an imperfect channel estimate on the BER of the VRVP-MQAM system using the exact and approximate $\hat{p}_B$ expressions (A.73, A.75). The error introduced from the approximate $\hat{p}_B$ expression (A.75) will also be discussed.

All numerical results are computed based on the system settings $\Gamma = 25$ dB, BERT $= 0.001$ and $\hat{\Gamma} = \rho\Gamma$, where $\rho = 0.8, 0.9, 1$. First, numerical results using the exact instantaneous $\hat{p}_B$ expression (A.73) versus instantaneous SNR estimate $\hat{\gamma}$ is shown in Figure A.4. The figure illustrates the impact of imperfect channel estimate on the instantaneous BER performance. When the channel is perfectly estimated ($\rho = 1$), the instantaneous BER always attains the BER requirement BERT. However, when the channel is inaccurately estimated ($\rho < 1$), the instantaneous BER estimate approaches BERT only at a higher $\hat{\gamma}$ value.

Next, the approximate instantaneous BER expression is compared with the exact BER. Figure A.5 shows that the approximate BER estimate matches closely to the exact BER estimate. In Figure A.6, the BER error based on $p_{Berror} \triangleq \hat{p}_{B,\text{exact}} - \hat{p}_{B,\text{approx}}$ is evaluated. The figure shows that the error introduced is $< 2 \times 10^{-5}$, which is insignificant for the rate and power variations.

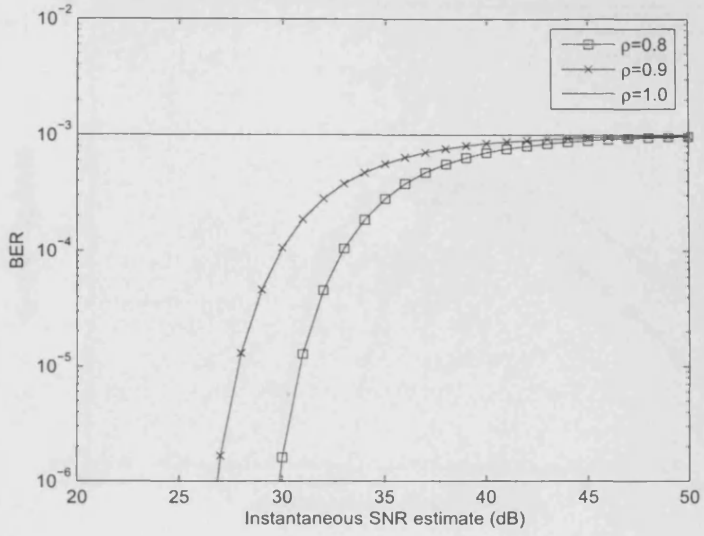


Figure A.4: Instantaneous BER estimate $p_{B\text{exact}}$ versus instantaneous SNR estimate $\hat{\gamma}$ for $\rho = \{0.8, 0.9, 1.0\}$.

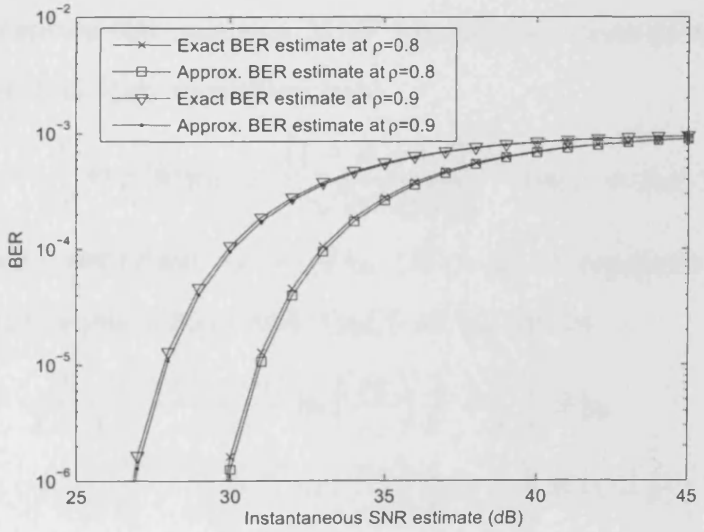


Figure A.5: Comparisons of instantaneous BER estimate based on exact BER estimate expression and approximate BER estimate expression.

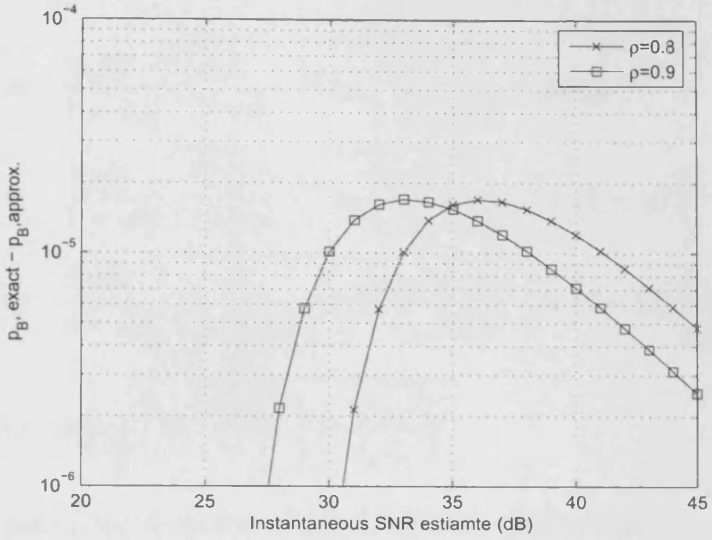


Figure A.6: BER error due to approximation.

## Verification of $I_{MAPeq}$ based on $\hat{\gamma}_{th}$

Since the BER estimate expression is applicable when $\hat{\gamma} > \hat{\gamma}_{th}$, it will be appropriate to express the resulting MAP function in terms of $\hat{\gamma}_{th}$. Consider the complete MAP function, re-written here

$$I_{MAP} = \frac{1}{p_B} \exp\left(b\left(p_B\right)\hat{\gamma}\right) \frac{\left(1+\Delta+\epsilon\sqrt{2\pi}\right)}{\sqrt{2\pi b\left(p_B\right)\hat{\gamma}}} \exp\left(-a\left(p_B\right)\hat{\gamma}\right). \tag{A.77}$$

Using the earlier definition $\hat{\gamma}_H = H\hat{\gamma}_{th}$ $(H > 1)$ to represent $\hat{\gamma}$ in the higher region, the expressions $a(p_B)\hat{\gamma}$ and $b(p_B)\hat{\gamma}$ at $\hat{\gamma}_{th}$ will be

$$\begin{aligned}
a(p_B)\hat{\gamma}_H &= \frac{1}{1-\rho}\left(\frac{-\left(M-1\right)}{\sigma c_2}\ln\left(\frac{p_B}{c_1}\right)\frac{1}{\Gamma}+\frac{1}{\hat{\Gamma}}\right)H\hat{\gamma}_{th} \\
&= \frac{1}{1-\rho}\left(\frac{-\left(M-1\right)}{\sigma c_2}\ln\left(\frac{p_B}{c_1}\right)\frac{1}{\Gamma}+\frac{1}{\hat{\Gamma}}\right)H\left(1-\rho\right)\left(-\ln\frac{\mathrm{BERT}}{c_1}\right)\Gamma \\
&= \frac{1}{1-\rho}\left(\frac{1}{\ln\left(\frac{\mathrm{BERT}}{c_1}\right)}\ln\left(\frac{p_B}{c_1}\right)\frac{1}{\Gamma}+\frac{1}{\hat{\Gamma}}\right)H\left(1-\rho\right)\left(-\ln\frac{\mathrm{BERT}}{c_1}\right)\Gamma \\
&= \left[-\ln\left(\frac{p_B}{c_1}\right)+\frac{\Gamma}{\hat{\Gamma}}\left(-\ln\frac{\mathrm{BERT}}{c_1}\right)\right]H
\end{aligned} \tag{A.78}$$

and

$$
\begin{aligned}
b\left(p_B\right)\hat{\gamma}_H &= \frac{2\sqrt{\rho}}{1-\rho}\sqrt{\frac{-\left(M-1\right)}{\sigma c_2}\ln\left(\frac{p_B}{c_1}\right)\frac{1}{\Gamma\hat{\Gamma}}} \quad H\hat{\gamma}_{th} \\
&= \frac{2\sqrt{\rho}}{1-\rho}\sqrt{\frac{-\left(M-1\right)}{\sigma c_2}\ln\left(\frac{p_B}{c_1}\right)\frac{1}{\Gamma\hat{\Gamma}}} \quad H\left(1-\rho\right)\left(-\ln\frac{\mathrm{BERT}}{c_1}\right)\Gamma \\
&= \frac{2\sqrt{\rho}}{1-\rho}\sqrt{\frac{1}{\left(\ln\frac{\mathrm{BERT}}{c_1}\right)}\ln\left(\frac{p_B}{c_1}\right)\frac{1}{\Gamma\hat{\Gamma}}} \quad H\left(1-\rho\right)\left(-\ln\frac{\mathrm{BERT}}{c_1}\right)\Gamma \\
&= 2H\sqrt{\left(\ln\frac{\mathrm{BERT}}{c_1}\right)\ln\left(\frac{p_B}{c_1}\right)}. \qquad \text{(A.79)}
\end{aligned}
$$

Next, the polynomial terms in (A.13) are re-written as,

$$
\begin{aligned}
\Delta &= \frac{g_1}{b(p_B)\hat{\gamma}_H} + \frac{g_2}{\left(b(p_B)\hat{\gamma}_H\right)^2} + \ldots + \frac{g_8}{\left(b(p_B)\hat{\gamma}_H\right)^8} \qquad \text{(A.80)} \\
&= \sum_{n=1}^{8}\frac{g_n}{\left(2H\sqrt{\left(\ln\frac{\mathrm{BERT}}{c_1}\right)\ln\left(\frac{p_B}{c_1}\right)}\right)^n}. \qquad \text{(A.81)}
\end{aligned}
$$

By substituting (A.78), (A.79) and (A.81) into the MAP function (A.77),

$$
\begin{aligned}
I_{MAP} &= \frac{1}{p_B}\exp\left(b\left(p_B\right)\hat{\gamma}_H\right)\frac{\left(1+\Delta+\epsilon\sqrt{2\pi}\right)}{\sqrt{2\pi b\left(p_B\right)\hat{\gamma}_H}}\exp\left(-a\left(p_B\right)\hat{\gamma}_H\right) \\
&= \frac{1}{p_B}\exp\left(2H\sqrt{\left(\ln\frac{\mathrm{BERT}}{c_1}\right)\ln\left(\frac{p_B}{c_1}\right)}\right) \cdot \\
&\quad \frac{1+\Delta+\epsilon\sqrt{2\pi}}{\sqrt{2\pi}\left(2H\sqrt{\left(\ln\frac{\mathrm{BERT}}{c_1}\right)\ln\left(\frac{p_B}{c_1}\right)}\right)^{1/2}} \cdot \\
&\quad \exp\left(-\left[-\ln\left(\frac{p_B}{c_1}\right)+\frac{\Gamma}{\hat{\Gamma}}\left(-\ln\frac{\mathrm{BERT}}{c_1}\right)\right]H\right) \qquad \text{(A.82)}
\end{aligned}
$$

Through the associated terms in $\Delta$, $I_{MAP}$ can also be defined with polynomial terms

$$
I_{MAP} = \sum_{n=0}^{9}\Lambda_n, \qquad \text{(A.83)}
$$

where

$$\Lambda_n = \frac{1}{p_B}\exp\left(2H\sqrt{\left(\ln\frac{\text{BERT}}{c_1}\right)\ln\left(\frac{p_B}{c_1}\right)}\right) \cdot \frac{g_n}{\sqrt{2\pi}\left(2H\sqrt{\left(\ln\frac{\text{BERT}}{c_1}\right)\ln\left(\frac{p_B}{c_1}\right)}\right)^{n+1/2}} \cdot \exp\left(-\left[-\ln\left(\frac{p_B}{c_1}\right)+\frac{\Gamma}{\hat{\Gamma}}\left(-\ln\frac{\text{BERT}}{c_1}\right)\right]H\right), \quad \text{(A.84)}$$

$g_0 = 1$ and $g_9 = \epsilon$. It can be clearly seen that $\Lambda_0 = I_{MAPeq}$ of (A.16), and $\Lambda_{1..8}$ are the remaining terms of the MAP function associated with the polynomial terms in $\Delta$.

The MAP function (A.83) that is expressed in terms of $\Lambda_n$ and $H$ is a convenient form to use. The aim is to evaluate the appropriateness of truncating the polynomial terms in $\Delta$, and show that BER can still be accurately estimated from $\Lambda_0 = I_{MAPeq}$. It is suffice to compare only the first few lower polynomial terms of $\Lambda_n$, and for low $H$ values, as higher polynomial terms or higher $H$ value clearly resulted in substantially lower contribution to the MAP function. For illustration, Figures (A.7) and (A.8) show the numerical results for MAP function $I_{MAPeq} = \Lambda_0$, and $I_{MAPeq2} = \Lambda_0 + \Lambda_1 + \Lambda_2$ for $H = \{2, 4\}$. That is, the two figures evaluate results at $\hat{\gamma} = \hat{\gamma}_{th} + \{3, 6\}$ dB. The figures demonstrate that $\Lambda_1 + \Lambda_2$ is not sensitive to the maxima of the cost function and confirm that BER can be accurately estimated from $\Lambda_0 = I_{MAPeq}$. It is also obvious from the two figures that as $H < 2$, $\hat{p}_B$ approaches to literately zero and is not useful. This is in support to the claim (as stated in S ection 5.3.1, paragraph after (5.22)) that the derived BER expression is applicable for $\hat{\gamma} > \gamma_{th}$ as when $\hat{\gamma} \leq \gamma_{th}$ there is no reliable BER estimate available.

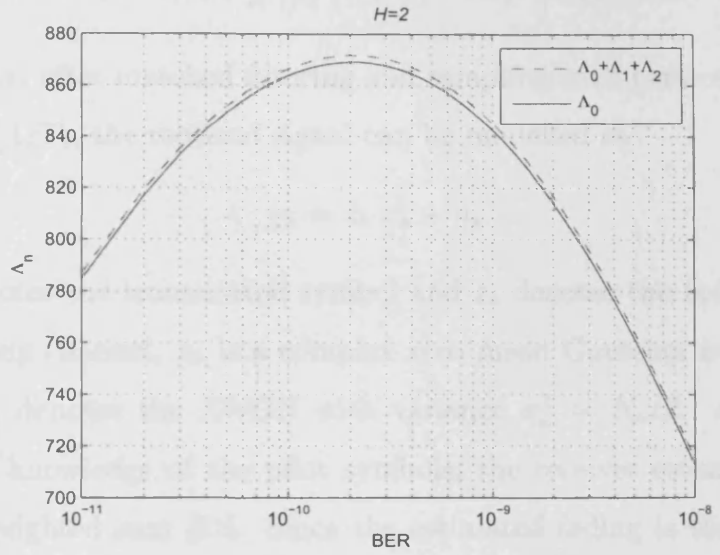


Figure A.7: Comparisons of functions $I_{MAPeq} = \Lambda_0$ and $(\Lambda_0 + \Lambda_1 + \Lambda_2)$. At BER target= $10^{-3}$ and $H = 2$.

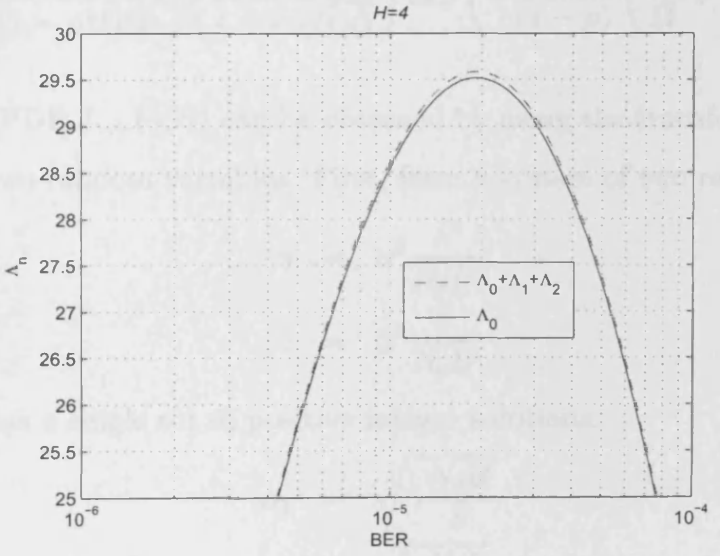


Figure A.8: Comparisons of functions $I_{MAPeq} = \Lambda_0$ and $(\Lambda_0 + \Lambda_1 + \Lambda_2)$, at BER target= $10^{-3}$, and $H = 4$.

## A.4 Proof of the $f_{\gamma,\hat{\gamma}}(\gamma,\hat{\gamma})$ expression

At the receiver, after matched filtering and sampling with perfect symbol timing at the rate of $1/T_s$, the received signal can be modelled as

$$y_k = z_k\, x_k + n_k \tag{A.85}$$

where $x_k$ denotes the transmitted symbol and $z_k$ denotes the fading gain. For a Rayleigh fading channel, $z_k$ is a complex zero mean Gaussian random variable. The value $n_k$ denotes the AWGN with variance $\sigma_n^2 = N_o/2$. At the receiver, based on the knowledge of the pilot symbols, the receiver estimates the fading based on a weighted sum [51]. Since the estimated fading is the weighted sum of zero-mean complex Gaussian random variables, it is also a zero-mean complex Gaussian random variable. Therefore the amplitude of the channel gain $\alpha$ and its estimate obey a bivariate Rayleigh distribution [51]

$$f_{\alpha,\hat{\alpha}}(\alpha,\hat{\alpha}) = \frac{4\alpha\hat{\alpha}}{(1-\rho)\,\Omega\hat{\Omega}} I_0\left(\frac{2\sqrt{\rho}}{1-\rho}\frac{\alpha\hat{\alpha}}{\sqrt{\Omega\hat{\Omega}}}\right)\exp\left(-\frac{1}{(1-\rho)}\left(\frac{\alpha^2}{\Omega}+\frac{\hat{\alpha}^2}{\hat{\Omega}}\right)\right) u(\gamma)\,u(\hat{\gamma})\,. \tag{A.86}$$

The joint PDF $f_{\gamma,\hat{\gamma}}(\gamma,\hat{\gamma})$ can be obtained by using the transformation of two functions of two random variables. First, form a system of two random variables

$$\gamma = \alpha^2\frac{\bar{S}}{N_oB} \tag{A.87}$$

$$\hat{\gamma} = \hat{\alpha}^2\frac{\bar{S}}{N_oB} \tag{A.88}$$

The system has a single set of positive integer solutions:

$$\alpha_1 = \sqrt{\gamma\frac{N_oB}{\bar{S}}} \tag{A.89}$$

$$\hat{\alpha}_2 = \sqrt{\hat{\gamma}\frac{N_oB}{\bar{S}}} \tag{A.90}$$

where $\alpha_1$ and $\alpha_2$ are the particular realizations of RVs $\gamma$ and $\hat{\gamma}$ respectively. Subsequently, $f_{\alpha,\hat{\alpha}}(\alpha,\hat{\alpha})$ is obtained from

$$f_{\gamma,\hat{\gamma}}(\alpha,\hat{\alpha}) = \frac{f_{\alpha,\hat{\alpha}}(\alpha_1,\hat{\alpha}_2)}{|J(\alpha_1,\hat{\alpha}_1)|}, \tag{A.91}$$

where

$$J(\alpha_1,\hat{\alpha}_1) = \begin{vmatrix} \frac{\partial\gamma}{\partial\alpha} & \frac{\partial\gamma}{\partial\hat{\alpha}} \\ \frac{\partial\hat{\gamma}}{\partial\alpha} & \frac{\partial\hat{\gamma}}{\partial\hat{\alpha}} \end{vmatrix} \tag{A.92}$$

$$= \begin{vmatrix} 2\alpha\frac{\bar{S}}{N_oB} & 0 \\ 0 & 2\hat{\alpha}\frac{\bar{S}}{N_oB} \end{vmatrix} \tag{A.93}$$

$$= 4\alpha\hat{\alpha}\left(\frac{\bar{S}}{N_oB}\right)^2 \tag{A.94}$$

is the Jacobian of the transformation of (A.87) and (A.89), and $f_{\alpha,\hat{\alpha}}(\gamma,\hat{\gamma})$ is obtained by substituting $\alpha = \alpha_1$ and $\hat{\alpha} = \hat{\alpha}_1$ into the joint PDF $f_{\alpha,\hat{\alpha}}(\alpha,\hat{\alpha})$. Note that in (A.86), $\Omega = E\{\alpha^2\}$, thus

$$\Gamma = E\{\gamma\} = \frac{\bar{S}}{N_oB}E\{\alpha^2\} = \frac{\bar{S}}{N_oB}\Omega. \tag{A.95}$$

Similarly, $\hat{\Omega} = E\{\hat{\alpha}^2\}$, and thus

$$\hat{\Gamma} = E\{\hat{\gamma}\} = \frac{\bar{S}}{N_oB}E\{\hat{\alpha}^2\} = \frac{\bar{S}}{N_oB}\hat{\Omega}. \tag{A.96}$$

Using (A.95) and (A.96) in (A.86), the final form of (A.91) is obtained as

$$f_{\gamma,\hat{\gamma}}(\gamma,\hat{\gamma}) = \frac{1}{(1-\rho)\Gamma\hat{\Gamma}} I_0\left(\frac{2\sqrt{\rho}}{1-\rho}\sqrt{\frac{\gamma\hat{\gamma}}{\Gamma\hat{\Gamma}}}\right)\exp\left(-\frac{1}{(1-\rho)}\left(\frac{\gamma}{\Gamma}+\frac{\hat{\gamma}}{\hat{\Gamma}}\right)\right)u(\gamma)\,u(\hat{\gamma}). \tag{A.97}$$

## A.5 Proof of the SNR cutoff threshold, i.e. $\hat{\gamma}_0 = \hat{\gamma}_{th} + \chi$

To satisfy the following two conditions, i) a positive transmit power $S(\hat{\gamma}) \geq 0$ and ii) for $k_{\hat{p}_B} \geq 1$, the SNR cutoff threshold can be obtained based on the MQAM

constellation size $M \geq 2$. That is,

$$M(\hat{\gamma}) = \frac{K\hat{\Gamma}}{\rho\Gamma}\left\{\frac{c_2}{K}\frac{\Gamma}{\hat{\gamma}}(1-\rho)-1\right\}^2 \hat{\gamma}U \geq 2. \tag{A.98}$$

Subsequently, the expression for $\hat{\gamma}_0$ is obtained from the solution of

$$\frac{K\hat{\Gamma}}{\rho\Gamma}\left\{\frac{c_2}{K}\frac{\Gamma}{\hat{\gamma}}(1-\rho)-1\right\}^2 \hat{\gamma}U - 2 = 0. \tag{A.99}$$

Based on quadratic formula, the roots are obtained as

$$\gamma_{th} \pm \frac{\Gamma}{2KU\hat{\Gamma}}\left[2\rho + 2\sqrt{\rho\left(2Uc_2\hat{\Gamma} - 2Uc_2\hat{\Gamma}\rho + \rho\right)}\right], \tag{A.100}$$

where $\gamma_{th} = (1-\rho)\left(-\ln\left(\frac{\text{BERT}}{c_2}\right)\right)$ (see (A.44)). Since realistic $\hat{p}_B$ values exist for the range $\hat{\gamma} > \hat{\gamma}_{th}$, the SNR cutoff threshold takes only the solution,

$$\hat{\gamma}_0 = \gamma_{th} + \frac{\Gamma}{2KU\hat{\Gamma}}\left[2\rho + 2\sqrt{\rho\left(2Uc_2\hat{\Gamma} - 2Uc_2\hat{\Gamma}\rho + \rho\right)}\right] \tag{A.101}$$

$$= \gamma_{th} + \chi. \tag{A.102}$$

# Appendix B

# Appendix: Proofs for the Derivations in Chapter 7

## B.1 The PDF of $p_B$, i.e. $f_{p_B}(p_B)$

The closed form expression for $f_{p_B,\hat{\gamma}}(p_B,\hat{\gamma})$ has been derived (in Section A.1) as

$$f_{p_B,\hat{\gamma}}(p_B,\hat{\gamma}) = c(p_B)\, I_0(b(p_B)\hat{\gamma}) \exp(-a(p_B)\hat{\gamma}), \tag{B.1}$$

where

$$a(p_B) = \frac{1}{1-\rho}\left(\frac{-(M-1)}{\sigma c_2}\ln\left(\frac{p_B}{c_1}\right)\frac{1}{\Gamma} + \frac{1}{\hat{\Gamma}}\right), \tag{B.2}$$

$$b(p_B) = \frac{2\sqrt{\rho}}{1-\rho}\sqrt{\frac{-(M-1)}{\sigma c_2}\ln\left(\frac{p_B}{c_1}\right)\frac{1}{\Gamma\hat{\Gamma}}}, \tag{B.3}$$

$$c(p_B) = \frac{(M-1)\hat{\gamma}}{p_B c_2 \sigma (1-\rho)\Gamma\hat{\Gamma}}. \tag{B.4}$$

Subsequently, the marginal PDF $f_{p_B}(p_B)$ can be written as

$$f_{p_B}(p_B) = \int_0^\infty f_{p_B,\hat{\gamma}}(p_B,\hat{\gamma})\, d\hat{\gamma} \tag{B.5}$$

$$= \int_0^\infty c(p_B)\, I_0(b(p_B)\hat{\gamma}) \exp(-a(p_B)\hat{\gamma}))d\hat{\gamma}. \tag{B.6}$$

The integration is solved based on the following definite integrals [39, eqn. (6.611.4)]

$$\int_0^\infty I_\upsilon(\beta x)\exp(-\delta x)dx = \frac{\beta^{-\upsilon}[\delta - \sqrt{\delta^2-\beta^2}]^\upsilon}{\sqrt{\delta^2-\beta^2}}, \qquad [\mathrm{Re}\{\upsilon\} > -1, , \mathrm{Re}\{\delta\} > |\mathrm{Re}\{\beta\}|]. \tag{B.7}$$

In the context here $\upsilon = 0$ and $a(p_B) > b(p_B)$, thus

$$\int_0^\infty I_0\left(b\left(p_B\right)\hat{\gamma}\right)\exp\left(-a\left(p_B\right)\hat{\gamma}\right)d\hat{\gamma} = \frac{1}{\sqrt{a\left(p_B\right)^2 - b\left(p_B\right)^2}}, \tag{B.8}$$

$$\int_0^\infty \hat{\gamma} I_0\left(b\left(p_B\right)\hat{\gamma}\right)\exp\left(-a\left(p_B\right)\hat{\gamma}\right)d\hat{\gamma} = \frac{a\left(p_B\right)}{a\left(p_B\right)^2 - b\left(p_B\right)^{2^{3/2}}}. \tag{B.9}$$

Using (B.9), $f_{p_B}(p_B)$ in (B.6) is obtained as,

$$f_{p_B}\left(p_B\right) = \frac{(M-1)}{p_B c_2 \sigma (1-\rho)\Gamma\hat{\Gamma}} \frac{a\left(p_B\right)}{\left[a\left(p_B\right)^2 - b\left(p_B\right)^2\right]^{3/2}}. \tag{B.10}$$

## B.2 The ML function

With the $f_{p_B,\hat{\gamma}}(p_B,\hat{\gamma})$ and $f_{p_B}(p_B)$ functions known, the conditional PDF $f_{\hat{\gamma}|p_B}(\hat{\gamma}|p_B)$ is therefore

$$f_{\hat{\gamma}|p_B}\left(\hat{\gamma}|p_B\right) = \frac{f_{p_B,\hat{\gamma}}\left(p_B,\hat{\gamma}\right)}{f_{p_B}\left(p_B\right)} \tag{B.11}$$

$$= \hat{\gamma} I_0\left(b\left(p_B\right)\hat{\gamma}\right)\exp\left(-a\left(p_B\right)\hat{\gamma}\right)\frac{\left[a\left(p_B\right)^2 - b\left(p_B\right)^2\right]^{3/2}}{a\left(p_B\right)}. \tag{B.12}$$

The ML function $l(p_B)$ is also the function $f_{\hat{\gamma}|p_B}(\hat{\gamma}|p_B)$ expressed as a function of $p_B$. The ML function is further simplified by using the approximation,

$$I_0(p_B) \approx \frac{\exp(b\left(p_B\right)\hat{\gamma})}{\sqrt{2\pi b\left(p_B\right)\hat{\gamma}}}, \tag{B.13}$$

which is based on a higher $\hat{\gamma}$, and has been proven in Section A.2. Finally, the equivalent ML function is expressed as

$$l_{eq}\left(p_B\right) = \hat{\gamma}\frac{\exp\left(b\left(p_B\right)\hat{\gamma}\right)}{\sqrt{2\pi b\left(p_B\right)\hat{\gamma}}}\exp\left(-a\left(p_B\right)\hat{\gamma}\right)\frac{\left[a\left(p_B\right)^2 - b\left(p_B\right)^2\right]^{3/2}}{a\left(p_B\right)}. \tag{B.14}$$

Note that the first $\hat{\gamma}$ term in (B.14) can be removed as it is not a function of $p_B$.

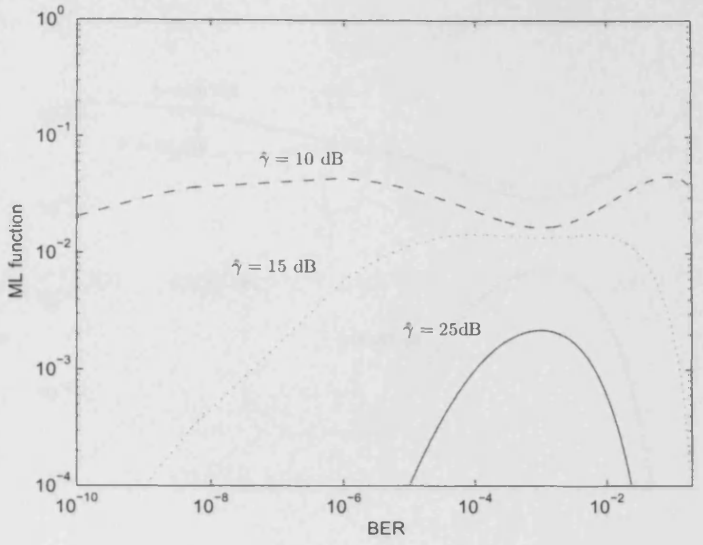


Figure B.1: ML curves for $\hat{\gamma} = (10, 15, 20)$ dB, at $\rho = 0.9$, $\Gamma = 15$ dB, $\hat{\Gamma} = \rho\Gamma$ and BER target$= 10^{-3}$.

## B.3 The BER estimate $\hat{p}_B$

The BER estimate expression is found from the solution to $\frac{\partial l_{eq}(p_B)}{p_B} = 0$. Due to the high non linearity of the ML function, an unique closed form solution is not obtainable for all $\hat{\gamma}$ values. Exploiting the numerical evaluation of the ML function, it is noted that at high $\hat{\gamma}$ a dominant maximum mode exists. Whereas, at low $\hat{\gamma}$, there appears to be more than one maximum modes, but none of these modes is dominant. That is, these modes seem to have approximately the same likelihood of occurrence across the BER estimate range. For illustration, numerical results of some discrete cases of low and high $\hat{\gamma}$ values are shown in Figure B.1 and Figure B.2.

In fact, at higher $\hat{\gamma}$, the maximum mode can be uniquely defined by the ML

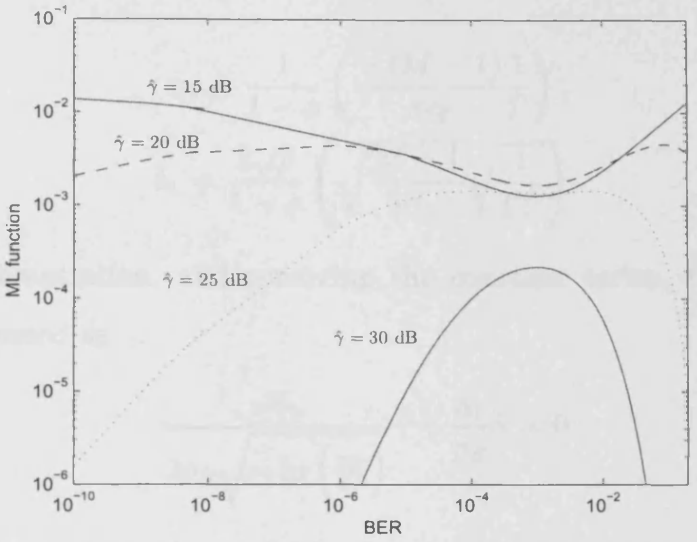


Figure B.2: ML curves for $\hat{\gamma} = (15, 20, 25, 30)$ dB, at $\rho = 0.9$, $\Gamma = 25$ dB, $\hat{\Gamma} = \rho\Gamma$ and BER target$= 10^{-3}$.

function. That is, if the ML function (B.14) is arranged in this form,

$$l_{eq}(p_B) = \hat{\gamma} \underbrace{\exp\left(b(p_B)\hat{\gamma}\right)\exp\left(-a(p_B)\hat{\gamma}\right)}_{\text{term A}} \underbrace{\frac{\left[a(p_B)^2 - b(p_B)^2\right]^{3/2}}{a(p_B)\sqrt{2\pi b(p_B)\hat{\gamma}}}}_{\text{term B}}, \quad \text{(B.15)}$$

term A is the dominant term for the maximum mode of the ML function, while term B is a relatively uniform function across $p_B$. It is also clear that the first $\hat{\gamma}$ term in (B.15) does not contribute to the maximum mode.

In cases of higher SNR $\hat{\gamma}$, the BER estimate $\hat{p}_B$ can be obtained by obtaining the solution of

$$\frac{\partial(\text{term A})}{\partial p_B} = 0. \quad \text{(B.16)}$$

The differentiation is solved based on the natural logarithm of term A, after omitting the constant terms,

$$\ln(\text{term A}) \Rightarrow b_1\sqrt{-\ln\left(\frac{p_B}{c_1}\right)\hat{\gamma}} - \left(a_1 \ln\frac{p_B}{c_1} + a_2\right)\hat{\gamma}, \quad \text{(B.17)}$$

where

$$a_1 = \frac{1}{1-\rho}\left(\frac{-(M-1)}{\sigma c_2}\frac{1}{\Gamma}\right), \tag{B.18}$$

$$b_1 = \frac{2\sqrt{\rho}}{1-\rho}\left(\sqrt{\frac{M-1}{\sigma c_2}}\sqrt{\frac{1}{\Gamma\hat{\Gamma}}}\right). \tag{B.19}$$

After the differentiation, and removing the constant terms, the final form of (B.16) is expressed as

$$\frac{-b_1}{2p_B\sqrt{-\ln\left(\frac{p_B}{c_1}\right)}}\hat{\gamma} + \frac{a_1}{p_B}\hat{\gamma} = 0. \tag{B.20}$$

The BER estimate $\hat{p}_B$ is obtained by solving the quadratic function (B.20). The solution is

$$\hat{p}_B = c_1 \exp\left(-\frac{b_1^2}{4a_1^2}\right). \tag{B.21}$$

With the expressions $b_1$ and $a_1$ substituted into (B.21), the final form for the BER estimate is obtained as

$$\hat{p}_B = c_1 \exp\left(\frac{-c_2\sigma}{M-1}\frac{\rho\Gamma}{\hat{\Gamma}}\right). \tag{B.22}$$

# Bibliography

[1] E. Biglieri, J. Proakis, and S. Shamai, "Fading channels: information-theoretic and communications aspects," *IEEE Transactions on Information Theory*, vol. 44, pp. 2619 – 2692, Oct. 1998.

[2] A. J. Goldsmith and P. P. Varaiya, "Capacity of fading channels with channel side information," *IEEE Transactions on Information Theory*, vol. 43, pp. 1986– 1992, Nov. 1997.

[3] M.-S. Alouini and A. J. Goldsmith, "Capacity of Rayleigh fading channels under different adaptive transmission and diversity-combining techniques," *IEEE Transactions on Vehicular Technology*, vol. 48, pp. 1165 – 1181, Jul. 1999.

[4] A. J. Goldsmith and S. Chua, "Variable-rate variable-power MQAM for fading channels," *IEEE Transactions on Communications*, vol. 45, pp. 1218 –1230, Oct. 1997.

[5] S. Chung and A. J. Goldsmith, "Degrees of freedom in adaptive modulation: A unified view," *IEEE Transactions on Communications*, vol. 49, pp. 1561–1571, Sep. 2001.

[6] J. F. Paris, M. C. Aguayo-Torres, and J. T. Entrambasaguas, "Impact of channel estimation error on adaptive modulation performance in flat fading," *IEEE Transactions on Communications*, vol. 52, pp. 716 –720, May 2004.

[7] D. L. Goeckel, "Adaptive coding for time-varying channels using outdated fading estimates," *IEEE Transactions on Communications*, vol. 47, pp. 844 – 855, Jun. 1999.

[8] S. Falahati, A. Svensson, T. Ekman, and M. Sternad, "Adaptive modulation systems for predicted wireless channels," *IEEE Transactions on Communications*, vol. 52, pp. 307 – 316, Feb. 2004.

[9] X. Cai and G. B. Giannakis, "Adaptive PSAM accounting for channel estimation and prediction errors," *IEEE Transactions on Wireless Communications*, vol. 4, pp. 246 – 256, Jan. 2005.

[10] A. Duel-Hallen, S. Hu, and H. Hallen, "Long-range prediction of fading signals," *IEEE Signal Processing Magazine*, vol. 17, pp. 62 – 75, May 2000.

[11] P. S. Kumar, R. D. Yates, and J. Holtzman, "Power control based on bit error rate measurements," *Military Communications Conference Proceedings*, vol. 2, pp. 617 – 620, Nov. 1995.

[12] C. W. Sung, K. K. Leung, and W. S. Wong, "Adaptive fixed-step power control algorithm based on link quality measure," *IEEE Global Telecommunications Conference*, vol. 4, pp. 2103 – 2108, Nov. 1998.

[13] H. Holma and A. Toskala, *WCDMA For UMTS*. John Wiley and Sons, 2001.

[14] M. Shikh-Bahaei, "Joint optimization of 'transmission rate' and 'outer-loop SNR target' adaptation over fading channels," *IEEE Transactions on Communications*, Mar. 2007.

[15] L. T. Ong, A. Olfat, and M. Shikh-Bahaei, "Joint SNR target and rate adaptation based on bit error rate estimation," *IEEE Int. Symp. Wireless Communication Systems*, pp. 470–474, Sep. 2005.

[16] J. Pons and J. Dunlop, "Bit error rate based link adaptation for GSM," *International Symposium on Personal, Indoor and Mobile Radio Communications*, vol. 3, pp. 1530–1534, Sep. 1998.

[17] A. Paulraj, R. Nabar, and D. Gore, *Introduction to Space-Time Wireless Communications*. Cambridge University Press, 2003.

[18] B. Vucetic and J. Yuan, *Space-Time Coding*. John Wiley and Sons Ltd, 2003.

[19] G. Foschini and M. Gans, "On limits of wireless communications in a fading environment when using multiple antennas," *Wireless Personal Communications*, vol. 6, pp. 311 – 335, Mar. 1998.

[20] E. Telatar, "Capacity of multi-antenna Gaussian channels," *European Transactions on Telecommunications*, vol. 10, pp. 585 – 595, Nov.-Dec. 1999.

[21] A. Goldsmith, S. A. Jafar, N. Jindal, and S. Vishwanath, "Capacity of limits of MIMO channels," *IEEE Journal on Selected Areas in Communications*, vol. 21, p. 684, Jun. 2003.

[22] S. K. Jayaweera and H. V. Poor, "Capacity of multiple-antenna systems with both receiver and transmitter channel state information," *IEEE Transactions on Information Theory*, vol. 49, pp. 2697 – 2709, Oct. 2003.

[23] Z. Zhou, B. Vucetic, M. Dohler, and Y. Li, "MIMO systems with adaptive modulation," *IEEE Transactions on Vehicular Technology*, vol. 54, pp. 1828 – 1842, Sep. 2005.

[24] G. E. Oien, H. Holm, and K. J. Hole, "Impact of channel prediction on adaptive coded modulation performance in Rayleigh fading," *IEEE Transactions on Vehicular Technology*, vol. 53, pp. 758 – 769, May 2004.

[25] S. Zhou and G. B. Giannakis, "How accurate channel prediction needs to be for transmit-beamforming with adaptive modulation over Rayleigh MIMO channels?," *IEEE Transactions on Wireless Communications*, vol. 3, pp. 1285 – 1294, Jul. 2004.

[26] Z. Zhou and B. Vucetic, "Design of adaptive modulation using imperfect CSI in MIMO systems," *Electronics Letters*, vol. 40, pp. 1073 – 1075, Aug. 2004.

[27] G. Lebrun, J. Gao, and M. Faulkner, "MIMO transmission over a time-varying channel using SVD," *IEEE Transactions on Wireless Communications*, vol. 4, pp. 757 – 764, Mar. 2005.

[28] A. Narula, M. J. Lopez, M. D. Trott, and G. W. Wornell, "Efficient use of side information in multiple-antenna data transmission over fading channels," *IEEE Journal on selected areas in Communications*, vol. 16, pp. 1423–1436, Oct. 1998.

[29] S. Zhou and G. B. Giannakis, "Adaptive modulation for multiantenna transmissions with channel mean feedback," *IEEE Transactions on Wireless Communications*, vol. 3, pp. 1626 – 1636, Sep. 2004.

[30] A. M. G. Kuo and and R. Prasad, "QoS and resource allocation in 3rd-generation wireless networks," *IEEE Communications Magazine*, vol. 39, p. 115, Feb. 2001.

[31] M.-S. Alouini, X. Tang, and A. J. Goldsmith, "Adaptive modulation scheme for simultaneous voice and data transmission over fading channels," *IEEE Journal on Selected Areas in Communications*, vol. 17, pp. 837 – 850, May 1999.

[32] Y. C. Liang, R. Zhang, and J. M. Cioffi, "Transmit optimization for MIMO-OFDM with delay-constrained and no-delay-constrained traffic," *IEEE Transactions on Signal processing*, vol. 54, pp. 3190–3199, Aug. 2006.

[33] L. T. Ong and S. Lambotharan, "Variable rate variable power MIMO system for integrated voice and data services," *IEEE International Conference on Communication Systems*, pp. 1–5, Oct. 2006.

[34] T. S. Rappaport, *Wireless Communications Principles and Practice.* Prentice Hall, 1996.

[35] M. Hata, "Empirical formula for propagation channel," *IEEE Transactions on Vehicular Technology*, vol. 29, pp. 317–325, Aug. 1980.

[36] R. H. Clarke, "A statistical theory of mobile-radio reception," *Bell Systems Technical Journal*, vol. 47, pp. 957–1000, 1968.

[37] A. Papoulis and S. U. Pillai, *Probability, Random Variables and Stochastic Processes.* Mc Graw Hill, fourth ed., 2002.

[38] S. O. Rice, "Mathematical analysis of random noise," *Bell System Technical Journal*, vol. 24, pp. 46 – 156, Jul. 1944.

[39] I. S. Gradshteyn and I. M. Ryzhik, *Table of Integrals, Series and Products.* London, UK Academic, 2000.

[40] M. Nakagami, *The m-distribution- A general formula of intensity distribution of rapid fading.* Pergamon Press, Oxford, England, 1960.

[41] R. Steele, *Mobile Radio Communications.* IEEE Press, 1992.

[42] C. E. Shannon, "A mathematical theory of communication," *Bell System Technical Journal*, vol. 27, pp. 623–656, Oct. 1948.

[43] J. G. Proakis, *Digital Communications.* McGraw-Hill, 2001.

[44] M.-S. Alouini and A. Goldsmith, "Capacity of Nakagami multipath fading channels," *IEEE Vehicular Technology Conference*, vol. 1, pp. 358 – 362, May 1997.

[45] M. Abramowitz and I. A. Stegun, *Handbook of Mathematical Functions with Formulas, Graphs, and Mathematical Tables, National Bureau of Standards Applied Mathematics Series 55, U.S.* Government Printing Office, 1972.

[46] S. Sampei, *Applications of Digital Wireless Technologies to Global Wireless Communications.* Prentice Hall, 1997.

[47] M.-S. Alouini and A. Goldsmith, "Adaptive M-QAM modulation over Nakagami fading channels," *IEEE Global Communication Conference*, pp. 218 – 223, Nov. 1997.

[48] C. H. Lim and J. M. Cioffi, "Performance of the adaptive rate MQAM with On/Off power control," *IEEE Communications Letters*, vol. 5, pp. 16 – 18, Jan. 2001.

[49] S. Hu, A. Duel-Hallen, and H. Hallen, "Adaptive modulation using long range prediction for flat Rayleigh fading channels," *IEEE Int. Symp. Information Theory*, vol. 2, p. 159, Jun. 1997.

[50] J. K. Cavers, "An analysis of pilot symbol assisted modulation for Rayleigh fading channels," *IEEE Trans. Veh. Technol.*, vol. 40, pp. 686 – 693, Nov. 1991.

[51] X. Tang, M.-S. Alouini, and A. J. Goldsmith, "Effect of channel estimation error on M-QAM BER performance in Rayleigh fading," *IEEE Transactions on Communications*, vol. 47, pp. 1856 – 1864, Dec. 1999.

[52] H. Holm, *Adaptive Coded Modulation Performance and Channel Estimation Tools for Flat Fading Channels.* PhD thesis, Norwegian University of Science and Technology, 2002.

[53] R. Steele and L. Hanzo, *Mobile Radio Communications.* John Wiley and Sons Ltd, 2nd ed., 2000.

[54] Y. S. Kim, C. J. Kim, G. Y. Jeong, Y. J. Bang, H. K. Park, and S. S. Choi, "New Rayleigh fading channel estimator based on PSAM channel sounding technique," *IEEE Int. Conf. Commun.*, pp. 1518–1520, 1997.

[55] H. Meyr, M. Moeneclaey, and S. A. Fechtel, *Digital Communication Receivers:Synchronization, Channel Estimation, and Signal Processing.* Wiley Series in Telecommunications and Signal Processing, 1998.

[56] S. M. Kay, *Fundamentals of Statistical Signal Processing, Estimation Theory.* Prentice Hall, 1993.

[57] W. C. Jakes, *Microwave Mobile Communications.* New York: Wiley, 1974.

[58] L. T. Ong, M. Shikh-Bahaei, and J. A. Chambers, "Variable rate and variable power MQAM system based on Bayesian Bit Error Rate and channel estimation techniques," *IEEE Transactions on Communications*, accepted subject to revision, Sep. 2006.

[59] H. L. V. Trees, *Detection, Estimation, and Modulation Theory, Part I.* John Wiley and Sons, 2001.

[60] P. Dent, G. Bottomley, and T. Croft, "Jakes fading model revisited," *Electronics Letters*, vol. 29, pp. 1162 – 1163, Jun. 1993.

[61] M. Shikh-Bahaei and M. Mouna-Kingue, "Joint optimisation of outer-loop power control and rate adaptation over fading channels," *IEEE Vehicular Technology Conference*, vol. 3, pp. 2205–2209, Sep. 2004.

[62] L. T. Ong and S. Lambotharan, "Adaptive rate and power allocation for integrated voice and data services in MIMO systems," *IEEE Transactions on Communications*, submitted for possible publication. Feb. 2007.

[63] G. Bremer and K. D. Ko, "Simultaneous voice and data on the general switched telephone network using framed QADM," *IEEE Communications Magazine*, vol. 34, pp. 58 – 63, Dec. 1996.

[64] K. Zhang and K. Pahlavan, "Integrated voice/data system for mobile indoor radio networks," *IEEE Transactions on Vehicular Technology*, vol. 39, pp. 75 – 82, Feb. 1990.

[65] A. Fluked, K. Pulmotor, and G. Wu, "Analysis of an integrated voice and data transmission system using packet reservation multiple access," *IEEE Transactions on Vehicular Technology*, vol. 43, pp. 289 – 297, May 1994.

[66] M.-S. Alouini, X. Tang, and A. J. Goldsmith, "Adaptive modulation scheme for simultaneous voice and data transmission over fading channels," *IEEE Journal on Selected Areas in Communications*, vol. 17. pp. 837 – 850, May 1999.

[67] A. Edelman, *Eigenvalues and Condition Numbers of Random Matrices. PhD Thesis.* Department of Mathematics, Massachusetts Institute of Technology, Cambridge MA, 1989.

[68] M. Dohler, *Virtual Antenna Arrays. PhD Thesis.* King's College London, UK, 2003.

[69] P. A. Dight, R. K. Mallei, and S. S. Jaguar, "Analysis of Transmit Receive Diversity in Rayleigh Fading," *IEEE Transactions on Communications*, vol. 51, pp. 694 – 703, Apr. 2003.

[70] C. M. Paella, A. and M. Win, "Performance of MIMO MRC in correlated Rayleigh fading environments," *IEEE Vehicular Technology Conference*, vol. 3, pp. 1633 – 1637, Jun. 2005.

[71] J. Zander and S.-L. Kim, *Radio Resource management for wireless networks.* Artech House Publishers, 2001.

[72] E. W. Weisstein, "Critical point." MathWorld-A Wolfram Web Resource. http://mathworld.wolfram.com/CriticalPoint.html.

[73] E. W. Weisstein, "First derivative test." MathWorld-A Wolfram Web Resource. http://mathworld.wolfram.com/FirstDrivativeTest.html.

[74] E. W. Weisstein, "Second derivative test." MathWorld-A Wolfram Web Resource. http://mathworld.wolfram.com/SecondDrivativeTest.html.



CARDIFF UNIVERSITY PRIFYSGOL CAERDYDD